

Development of an artificial silk protein on the basis of a lacewing egg stalk protein

Dissertation

zur Erlangung des akademischen Grades

Doktor der Naturwissenschaften

An der Bayreuther Graduiertenschule für Mathematik und
Naturwissenschaften

der Universität Bayreuth

vorgelegt von

Diplom Biologe

Felix Bauer

Bayreuth, Mai 2013

Die vorliegende Arbeit wurde in der Zeit von Juli / 2008 bis November /2013 in Bayreuth am Lehrstuhl Biomaterialien unter Betreuung von Herrn Professor Dr. Thomas Scheibel angefertigt.

Vollständiger Abdruck der von der Bayreuther Graduiertenschule für Mathematik und Naturwissenschaften (BayNAT) der Universität Bayreuth genehmigten Dissertation zur Erlangung des akademischen Grades Doktor der Naturwissenschaften (Dr.rer. nat.)

Dissertation eingereicht am: 17.05.2013

Zulassung durch das Leitungsgremium: 10.06.2013

Wissenschaftliches Kolloquium: 14.11.2013

Amtierender Direktor: Prof. Dr. Franz Xaver Schmid

Prüfungsausschuss:

Prof. Dr. Thomas Scheibel (Erstgutachter)

PD Dr. Stefan Geimer (Zweitgutachter)

Prof. Dr. Andreas Fery (Vorsitz)

Prof. Dr. Birgitta Wöhrl

CONTENT

| | |
|--|-----------|
| 1. SUMMARY | 1 |
| 2. ZUSAMMENFASSUNG | 3 |
| 3. INTRODUCTION..... | 7 |
| 3.1. Silk | 7 |
| 3.1.1. Structure | 8 |
| 3.1.2. Myriapoda silk | 9 |
| 3.1.3. Spider silk | 10 |
| 3.1.4. Insect silk | 11 |
| 3.1.4.1. Caddisfly silk | 12 |
| 3.1.4.2. Lacewing silk..... | 13 |
| 3.1.4.2.1. Cocoon silk | 14 |
| 3.1.4.2.2. Egg stalk silk | 14 |
| 3.1.4.2.3. Production of lacewing egg stalks | 15 |
| 3.1.4.2.4. The colleterial gland | 17 |
| 3.1.4.2.5. Protein sequences/dope composition | 18 |
| 3.1.4.2.6. Mechanics of lacewing egg stalks | 18 |
| 3.1.4.2.7. Structure | 19 |
| 3.2. Recombinant production of silk proteins | 20 |
| 3.3. Technical processing of silk proteins | 21 |
| 3.4. Aims of the work | 24 |
| 4. OVERVIEW OF THE THESIS INCLUDING UNPUBLISHED DATA | 25 |
| 4.1. Mechanical analysis of natural lacewing egg stalks and fibres of caddisflies | 25 |
| 4.2. Structural analysis of lacewing egg stalk silk | 26 |
| 4.3. Silk gland analysis of lacewings | 28 |
| 4.4. Biotechnological production of N[AS] ₈ C, an artificial lacewing egg stalk protein | 30 |
| 4.5. Fibre/stalk formation and analysis | 33 |
| 4.6. Further processing of a recombinant lacewing protein | 37 |
| 4.6.1. Films | 37 |
| 4.6.2. Capsules | 39 |

| | |
|--|-----------|
| 4.6.3. Hydrogels and foams..... | 40 |
| 4.7. Cell culture on structured films | 42 |
| 4.8. Individual contributions to joined publications | 46 |
| 5. LITERATURE | 47 |
| 6. LIST OF ABBREVIATIONS..... | 63 |
| 7. DEPENDENCE OF MECHANICAL PROPERTIES OF LACEWING EGG STALKS ON RELATIVE HUMIDITY..... | 65 |
| 8. ARTIFICIAL EGG STALKS MADE OF A RECOMBINANTLY PRODUCED SILK PROTEIN | 75 |
| 9. CONTROLLABLE CELL ADHESION, GROWTH AND ORIENTATION ON LAYERED SILK PROTEIN FILMS | 83 |
| 10. LIST OF PUBLICATIONS AND PATENTS..... | 91 |
| 11. ACKNOWLEDGEMENT | 93 |
| 12. ERKLÄRUNG:..... | 95 |

1. Summary

Silks are widely used in textile industry as clothing and furnishings due to their tensile strength, smoothness, soft texture, lustre, and drape. Most commonly silk of the mulberry silkworm *Bombyx mori* (*B. mori*) is used in such applications, however, silks evolved independently in many different arthropods for various purposes.¹ During evolution the different silks were optimised for their task-specific uses over millions of years, e.g. adopting different mechanical properties. The mechanical properties mainly derive from the protein secondary structure and its higher order arrangement in silk fibres. Spider silk, for example, is known for its tensile properties surpassing nylon, Kevlar®, silkworm silk, and high-tensile steel.²⁻⁵ Beyond their mechanical properties, some silks are also reported to be biocompatible and non-immunogenic.⁶ One beneficial feature of silk proteins is the possibility to process them into various morphologies.^{7,8}

Several of these silk features make them interesting for material scientists, intending to produce silks with tuneable properties depending on the desired application, ranging from technical ones such as high performance fibres to medical ones such as drug delivery.

This thesis deals with the characterisation and reproduction of a less explored silk, the lacewing egg stalk silk. Mechanical testing revealed a strong dependence on the relative humidity. In the dry state at 30% relative humidity, the stalks are quite rigid and break at an elongation of 2% whereas at 70% and 100% relative humidity they elongate up to 434%. This extension is accompanied by a secondary structure change from cross- β to parallel- β . The cross- β structure in unstretched stalks provides bending stiffness and rigidity to the stalk, and this bending stiffness gets lost when the stalks are stretched. In this thesis a model is proposed which explains these differences at various relative humidity on the molecular level, wherein changes in the strength of hydrogen bonds upon exposure to water (a hydrogen bond donor/acceptor) in combination with multiple disulphide cross-links (which are not affected by water) act together and are responsible for this behaviour.

Based on consensus sequences of published sequence data (derived from MalXB2 an egg stalk protein of *Mallada signata* (*M. signata*)),⁹ an engineered egg stalk protein named N[AS]₈C was recombinantly produced.

To produce an artificial stalk, a droplet of a solution of purified N[AS]₈C was placed on a substrate, and tweezers were used to pull out a fibre. After drying, and post treatment, the properties of the artificial stalks were investigated in comparison to the natural ones. Mechanical testing revealed similar behaviour at 30% relative humidity, but at 70% and 100% relative humidity the artificial stalks were not as extensible as the natural ones. This corresponds to the fact, that no cross- β structure was formed, and, therefore, no rearrangement into parallel- β structure was possible.

Subsequently, N[AS]₈C was processed into non-fibrous morphologies. It was possible to produce capsules, hydrogels, foams, and films. The foams show an interesting micro and nano structure which differs from that of recombinant spider silk. The cavities are filled with a mesh of nano fibres building a 3D scaffold.

Films are a morphology with potential for application in cell culture. Fibroblast attachment on N[AS]₈C films is quite poor. Therefore, we tried to induce guided fibroblast growth on patterned protein films. A first layer of the films was cast from ntag^{Cys}C16-c(RGDfK), an engineered spider silk protein coupled with the integrin recognition motif RGD to provide a protein layer to which fibroblasts attached well. The second protein layer was produced using a PDMS (polydimethylsiloxane) template and N[AS]₈C. Fibroblasts grown on these films adhere only to the RGD modified spider silk and not to the N[AS]₈C areas. A second feature of such films is to orient the fibroblasts on films with alternating lines of the two proteins. Such films might be useful for tissue engineering to control cell adhesion and get a structured cell pattern. This is essential for many tissues such as bones, muscles, and epithelia tissue. The low cell adhesion properties of N[AS]₈C films might be interesting for coatings for applications where cell adhesion is not desired such as stents or catheters.

2. Zusammenfassung

Seide ist wegen ihrer Reißfestigkeit, Glätte, weichen Textur, ihres Glanzes und ihres Faltenwurfs ein in der Textilindustrie weit verbreitetes Material für Kleidungsstücke und Einrichtungsgegenstände. Meist wird für solche Anwendungen die Seide des Maulbeerspinners *Bombyx mori* (*B. mori*) verwendet. Seiden entwickelten sich unabhängig in vielen Arthropoden und werden zu verschiedensten Zwecken verwendet.¹ Für diese wurden sie seit Millionen von Jahren durch die Evolution optimiert. Zum Beispiel haben Seiden unterschiedliche mechanische Eigenschaften entwickelt, welche hauptsächlich von der Sekundärstruktur der Proteine und ihrer übergeordneten Anordnung in den Seidenfäden abhängen. Spinnenseide ist beispielsweise bekannt für ihre Zugdehnungseigenschaften, welche die von Nylon, Kevlar®, Seidenspinnerseide und hochfestem Stahl überragen.²⁻⁵ Darüber hinaus gelten viele Seiden als biokompatibel und nicht immunogen.⁶ Eine weitere nützliche Eigenschaft von Seidenproteinen ist deren Verarbeitbarkeit in viele verschiedene Morphologien.^{7,8}

Viele dieser Eigenschaften machen Seiden interessant für Materialforscher, welche Seide mit gezielt beeinflussbaren Eigenschaften, abhängig von der erwünschten Anwendung, produzieren wollen. Denkbare Anwendungen reichen von Hochleistungsfasern für technische Anwendungen bis zu medizinischen Anwendungen, wie gezielte Pharmakotherapie.

Diese Dissertation beschäftigt sich mit der Charakterisierung und der rekombinanten Herstellung eines wenig erforschten Seidenproteins aus Florfliegen Eierstielen. Mechanische Tests an Florfliegen Eierstielen zeigten eine starke Abhängigkeit der Dehnbarkeit von der Luftfeuchtigkeit. Im trockenen Zustand bei 30% relativer Luftfeuchtigkeit sind die Stiele biegesteif und brechen bei einer Dehnung von 2%, wohingegen sie bei 70% und 100% relativer Luftfeuchtigkeit bis zu ca. 430% dehnbar sind. Diese Dehnung korreliert mit einer Sekundärstrukturänderung von *cross*- β zu *parallel*- β . Die *cross*- β Struktur in ungestreckten Stielen wird für deren Biegesteifigkeit verantwortlich gemacht. Diese Biegesteifigkeit geht verloren, wenn die Stiele gestreckt werden. In dieser Arbeit wird ein Modell vorgeschlagen, welches die Unterschiede bei verschiedener Luftfeuchtigkeit auf molekularer Ebene erklärt. Verantwortlich für dieses Verhalten sind Änderungen in der Bindungsenergie von

Wasserstoffbrückenbindungen durch die Anwesenheit von Wasser (Wasserstoffbrücken Donor/Akzeptor) im Zusammenspiel mit Disulfidbindungen, die nicht durch das Wasser beeinflusst werden.

Basierend auf Konsensussequenzen des veröffentlichten Eierstiel Proteins MalXB2 wurde das Protein N[AS]₈C, eine künstlich konstruierte Variante des Proteins, biotechnologisch hergestellt.⁹

Um einen künstlichen Stiel zu produzieren wurde ein Tropfen einer Lösung von gereinigtem N[AS]₈C auf einen Untergrund aufgebracht und anschließend aus dem Tropfen mithilfe einer Pinzette Fäden gezogen. Nach dem Trocknen und Nachbehandeln der Fäden wurden die Eigenschaften der künstlichen sowie der natürlichen Stiele untersucht. Mechanische Analysen zeigten ähnliche Eigenschaften der natürlichen und künstlichen Eierstiele bei 30% relativer Luftfeuchtigkeit, wohingegen die künstlichen Stiele bei 70% und 100% weniger dehnbar waren als die natürlichen. Dies stimmt mit der Tatsache überein, dass in den künstlichen Stielen keine *cross-β* Struktur gebildet wurde und somit keine Umformung von *cross-β* zu *parallel-β* stattfinden konnte.

In einem weiteren Schritt wurde N[AS]₈C in weitere Morphologien verarbeitet. Es war möglich Kapseln, Hydrogele, Schäume und Filme herzustellen. Die Schäume zeigen eine interessante Mikro- und Nano-Strukturierung, die sich von Spinnenseiden-Schäumen unterscheidet. Die Poren sind von Nano-Fasern durchzogen, die ein 3D Netzwerk bilden. Diese Schäume könnten für weitere Untersuchungen und Anwendungen als Filtermaterial oder Zellkultur-Gerüst interessant sein.

Eine Morphologie mit Potential zur Anwendung in der Zellkultur sind Filme. Da Fibroblasten schlecht auf Filmen aus N[AS]₈C adhären, wurde versucht, Fibroblasten gezielt auf einem gemusterten Film wachsen zu lassen. Die Grundschicht wurde aus ntag^{Cys}C16-c(RGDfK), einer technisch erzeugten Variante eines Spinnenseidenproteins, an welches die Integrin-Erkennungssequenz RGD gekoppelt ist, gegossen. Aufgrund dieser Erkennungssequenz adhären Fibroblasten gut auf diesen Filmen. Eine zweite Schicht aus N[AS]₈C wurde mithilfe einer PDMS (Polydimethylsiloxan) Maske aufgebracht. Fibroblasten adhären auf solchen gemusterten Filmen nur auf den ntag^{Cys}C16-c(RGDfK) und nicht auf den mit N[AS]₈C bedeckten Bereichen. Eine weitere Besonderheit dieser Filme ist die

Möglichkeit, durch Applikation des zweiten Films in Streifenform, Fibroblasten ausgerichtet wachsen zu lassen. Solche Filme könnten für „*Tissue engineering*“ genutzt werden, um Zelladhäsion zu kontrollieren und eine strukturierte Zellausrichtung zu erhalten. Dies ist essentiell für viele natürliche Gewebe wie Knochen, Muskeln, und Epithelgewebe. Des Weiteren könnten die schwachen Zelladhäsions-Eigenschaften von N[AS]₈C Filmen für Beschichtungen, bei denen Zelladhäsion nicht erwünscht ist, wie beispielsweise Stents oder Kathetern, interessant sein.

3. Introduction

3.1. Silk

Silks are structural proteins that are produced by arthropods.^{10, 11} They have been used by humans for a long time because of their good mechanical properties and biocompatibility.¹²⁻¹⁴ Fishermen in Polynesia used nets composed of spider silk spun in bamboo frames for fishing, and silk has also been used as wound dressings.¹⁵

The term silk was defined by Craig: “Silks are fibrous proteins containing highly repetitive sequences of amino acids and are stored in the animal as a liquid and configure into fibres when sheared or “spun” at secretion. This definition excludes keratin and collagen.”¹⁰

Table 1: Natural silks are used for a variety of functions.

| Function of silk | Examples of species | References |
|---------------------------|--|------------|
| Dragline/lifeline | Caddisfly larvae and spiders | 16, 17 |
| Cocoon/protective shelter | Weevils, Lepidoptera, lacewings, and caddisfly larvae | 18-21 17 |
| Structural support | Lacewing egg stalks | 18 |
| Dispersal | Newly hatched spiderlings | 22 |
| Foraging | Spiders, caddisfly larvae, and glowworm larvae threads | 16, 18, 20 |
| Reproduction | Thysanoptera and Myriapoda | 16, 18 |

Silks comprise a high percentage of the amino acids glycine, serine, and alanine, which are all small, non-essential amino acids and have an intermediate hydrophobicity.^{1, 10} Even though silks have many different functions (lifelines, protective shelters, structural supports, reproduction, foraging, and dispersal)^{11, 16, 18, 22-25} (Table 1) they are all characterised by a distinct crystallinity which confers the intriguing mechanical properties of silk fibres.²⁶⁻²⁸ The crystallinity is achieved by the tight packing of secondary structures of protein such as α -helices or β -strands into larger assemblies such as coiled coils, parallel- β structures or cross- β structures (Figure 1).²⁹

3.1.1. Structure

Coiled coil silks are composed of proteins with an α -helical (Figure 1 A) structure. Up to five α -helices are wound around each other achieving a more stable packing. The α -helices are composed of a seven amino acid repeat with hydrophobic amino acids at position one and four and have a low glycine content.¹ The helical structure is stabilized by hydrogen bonds between the protein backbone. The hydrophobic side chains are exposed on one side of the helix making it amphipathic. To form a coiled coil structure the hydrophobic patches of two helices lay together to shield the interface from the surrounding water.^{30, 31} Silks with α -helical structures have a low tensile strength but a high elasticity. They are produced by some insects (honey bees, ants, wasps, fleas, and lacewings (cocoon)) and spiders for certain types of silks.^{21, 28, 32-36}

Silks with β -sheet structures can form parallel- β and cross- β structures, differing in their backbone orientation corresponding to the fibre axis. β -sheets comprise β -strands with every second amino acid facing the opposite side of the strand. The amino acids on each side have similar spacing and hydrophobicity to enable a dense packing of β -strands. A hydrogen bond network perpendicular to the side chain packing exists between the N-H groups of the backbone of one strand and the C=O groups of an adjacent strand's backbone. This results in one hydrogen bond per amino acid on each side. The β -strands in parallel- β structures may be arranged in a parallel, anti-parallel, or even in a mixed manner to each other as described for tussock moth silk where the protein backbones lie parallel to the silk fibre axis (Figure 1 B and C).^{10, 29, 37} Warwicker classified all parallel- β structure silks into five groups depending on their packing distances.³⁸

These silks with sheets parallel to the fibre axis are the most common and well-studied and are produced by spiders and insects. They include the major ampullate-, minor ampullate-, aciniform-, and tubulliform silk from spiders, and silks from insects such as caddisfly-, butterfly-, moth- (such as *B. mori*, which produces the silk used commonly for textiles),^{20, 39-44} *Kahaono Montana* Evans-,^{45, 46} and sawfly silk^{26, 28}. In nature they are used for a variety of purposes, for example as a dragline/lifeline, capture spiral, egg case, cocoon, net, and for case building.

Silk with sheets perpendicular to the fibre axis are comparatively rare in nature. They are related to parallel- β structure silk, but the backbones of the β -strands are arranged perpendicular to the fibre axis (Figure 1 D).⁴⁷ The strands of all known cross- β silks are arranged in an antiparallel manner. Upon stretching the structure transforms to a parallel- β structure.²⁶ Such conversion is due to the fact that the protein chain forms a hairpin structure. Due to steric reasons there is a glycine in each turn.⁹ Cross- β silks are produced by water beetles (Hydrophilidae), plant eating beetles (*Hypera*), lacewings (in four of six neuropteran families), and glow worm larvae (*Arachnocampa luminosa*).^{9, 21, 27, 28, 48, 49}

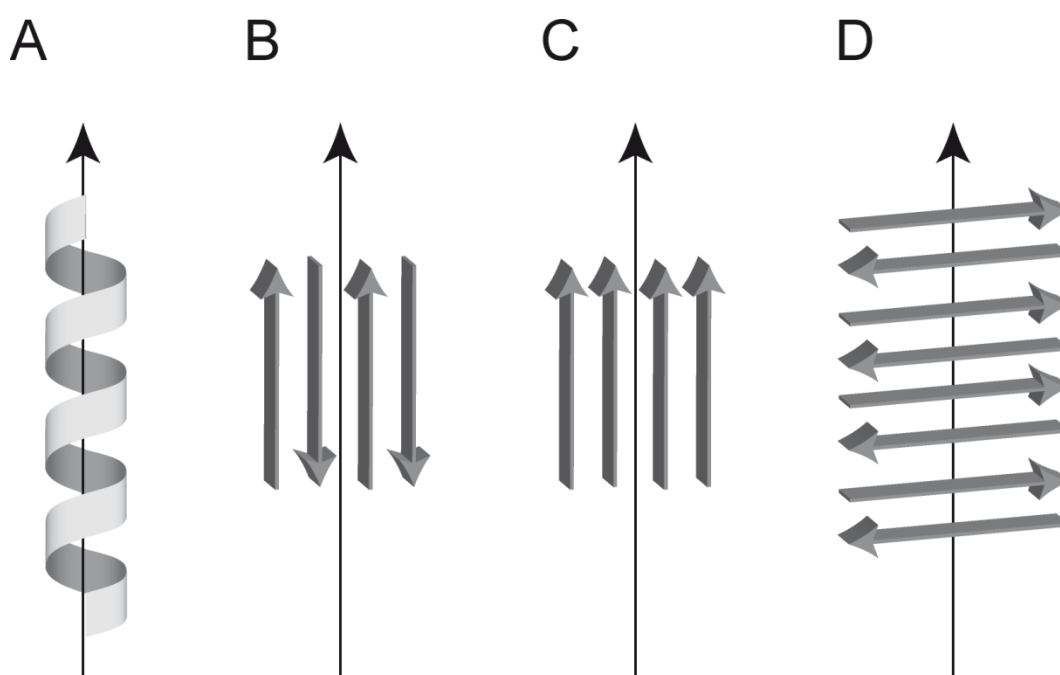


Figure 1: Schematic picture of different common protein secondary structures present in silks: **A:** α -helix; **B:** parallel- β structure with β -strands antiparallel to each other; **C:** parallel- β structure with β -strands parallel to each other; **D:** cross- β structure; black arrows indicate the fibre axis.

3.1.2. Myriapoda silk

Myriapoda are an example of silk producing arthropods, but little is known about their silk. Male centipedes produce a small silken web to deposit a sperm package from where it is picked up by the females.^{10, 50} Their silk proteins are produced in the accessory gland.

3.1.3. Spider silk

Spiders can produce up to seven different silk types for different purposes.²³ They are all secreted by different glands, from where their names derive from (aciniform silk, cylindrical/tubuliform silk, aggregate silk, pyriform silk, flagelliform silk, minor ampullate silk, and major ampullate silk).^{51, 52}

Major ampullate silk is the most studied spider silk because of its high tensile strength and extensibility, yielding a high toughness (*Araneus diadematus* (*A. diadematus*) for example 160 MJ/m³) depending on the species.⁵³ It is used as the main support and as radii of an orb web. These silk fibres have diameters ranging from 1 µm to 20 µm (depending on the species) and have a core-shell structure.⁷ In case of major ampullate silk the core comprises two protein classes (major ampullate spidroin 1 and 2) significantly differing in their proline content. This core structure is coated with glycoproteins and lipids.^{51, 54}

The central domain of the proteins are block copolymer-like sequences with polyalanine blocks forming stacked β-sheets that are responsible for the high tensile strength of the fibres.⁵⁵ Other blocks show GGX repeats forming 3₁₀-helices or a GPGXX motif forming β-turn spirals, both leading to elasticity of the fibre. These blocks are repeated multiple times within each core domain. The carboxy- and amino-terminal regions are highly conserved and non-repetitive. These regions are 5-helix bundles and are critically involved in initiating fibre assembly.⁵⁶⁻⁵⁸

One disadvantage of spider silk in comparison to *B. mori* silk is its low natural availability, due to the cannibalistic behaviour of spiders,⁵⁹ making it impossible to farm them on a large scale. It is relatively straightforward to obtain amounts that are sufficient for scientific purposes but not for industrial applications. The design of artificial proteins based on spider silk motifs, full length proteins and their recombinant production is necessary for both basic analyses of single motifs as well as putative applications.

3.1.4. Insect silk

Sutherland and co-workers grouped insect silk into 23 types according to silk gland type, silk protein molecular structure, and phylogenetic relationship of silk-producing species.¹ This shows the wide variation and multiple evolution events during silk development. The silks are produced from different gland types such as labial, malpighian or dermal glands.⁶⁰

The most studied silk producing animal is the mulberry silk worm (*B. mori*). Its silk has been used for thousands of years for textiles. For commercial silk production, the silkworm larvae are fed with fresh mulberry leaves until pupation which takes place after approximately one month. After completion, the cocoons are harvested and the larvae are killed with hot water.⁶¹⁻⁶⁴ The silk fibres have to be degummed to remove the glue-like sericin fibre coating before it can be used as a textile.⁶⁵⁻⁶⁹ *B. mori* silk fibres are composed of three proteins. Heavy chain fibroin (ca. 350 kDa) is linked to a light chain fibroin by a disulphide bond. Six of these heavy chain-light chain complexes interact with P25, the third protein present, by hydrophobic interactions.^{40, 70, 71} All three proteins are secreted in the salivary glands of the larvae. Due to the fact that there are two salivary glands joining each other directly before the spinneret, two so called brins form a double filament. The double filament is finally coated by sericin, glue-like serine-rich proteins which hold the filaments together. The resulting coated double filament is called bave.⁷²⁻⁷⁶ The silks of Trichoptera are listed in the same group.¹

Many silk producing species are found in the order of Hymenoptera producing six of the 23 silk types classified by Sutherland *et al.*¹ One type of silk is produced by bees, ants, and wasps. Their silk is produced in the labial gland of larvae and comprises four proteins (30-50 kDa) which adopt an α -helical structure and form a tetrameric coiled coil structure.^{35, 77} The production of spinning dope from recombinant proteins based on these natural proteins showed the importance of having all four proteins to achieve a stable highly concentrated silk solution.⁷⁷

Another order of silk producing insects is the Neuroptera. One of the two silk types in this order is produced by the larvae of lacewings and antlions and has an α -

helical structure, and these silks are used for building cocoons.^{21, 28, 49} The second type is a cross- β silk, which is used in egg stalks and is secreted by the colleterial gland.

3.1.4.1. Caddisfly silk

Caddisfly larvae are commonly used by ecologists to investigate the water quality of rivers and lakes. They are listed in the insect order Trichoptera and are Holometabola, which means they undergo metamorphosis with larvae and adults showing a totally different habitus. The adult flies attach their eggs under water or close above the water surface. The larvae depend on water as habitats where they undergo five to seven larval stages. The larvae feed on algae, leaves, and small water insects, depending on their species and are divided into two groups the eruciform (casemaking) and the campodeiform (free-living and net spinning) larvae (see Figure 2).⁷⁸ The eruciform larvae build round cases by gluing together various materials such as stones, sand, or small organic material by the use of a silken thread. The net spinning campodeiform larvae use silk to build small nets to catch small water insects and build a silken retreat to hide from predators (see Figure 2).⁷⁸ Larvae of both groups use silk to pupate in a cocoon.⁷⁹ Caddisfly silk is produced in the labial glands which are homologue to the labial glands of butterflies and therefore the silk morphology and composition is comparable to lepidopteran silk. Two flattened ribbon like fibres are glued together by sericin-like glue.⁸⁰ The silk is composed of homologues of heavy chain and light chain fibroins but no P25 was detected so far.^{20, 81} The caddisfly heavy chain fibroin has some differences to those of Lepidoptera, showing a high content of bulky and basic amino acid residues, a low alanine content, and a repeating motif containing phosphorylated serines which could provide crosslinking by Ca^{2+} -ions.⁸² An additional protein, Nf-1, with a high content of cysteine is thought to crosslink the proteins by disulphide bonds, providing water insolubility to the fibres.^{83, 84}

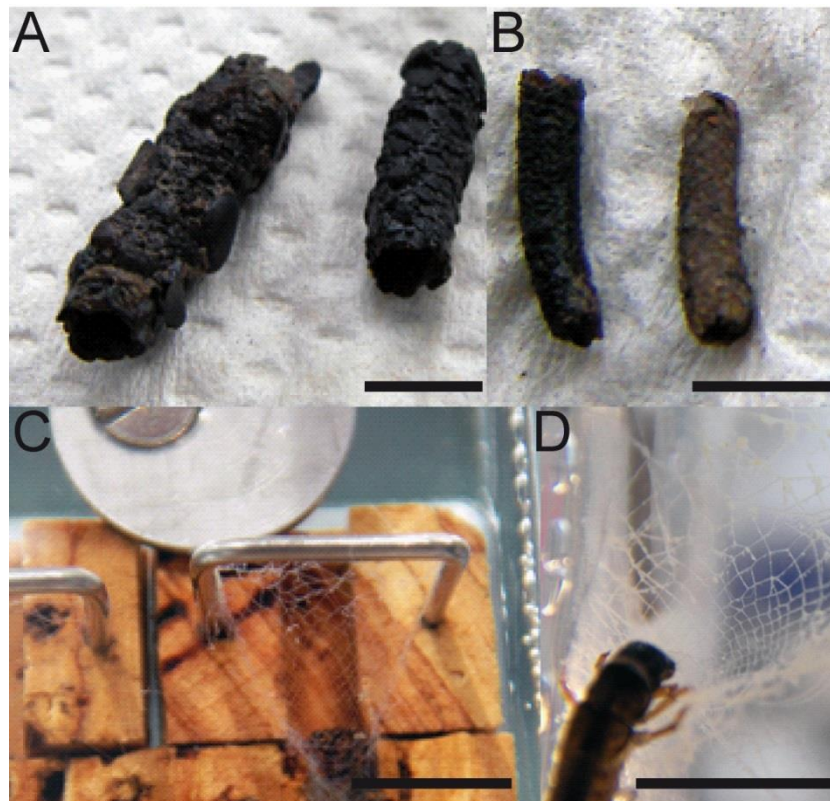


Figure 2: A and B: Caddisfly cases built from little stones; C and D: Caddisfly nets spun in an artificial surrounding. Scale bars: 0.7 cm.

3.1.4.2. Lacewing silk

Green lacewing larvae are known for eating aphids which they are bred for commercially. Lacewings such as *Chrysopa carnea* (*C. carnea*) (Neuroptera: Chrysopidae) are Holometabola. Normally insects are known to produce only one silk type, but lacewings produce two.⁹ The larvae (Figure 3 C) produce a cocoon before metamorphosis (Figure 3 D), while adult females (Figure 3 A) use a second type for a silken stalk to protect their eggs from predators (Figure 3 B).⁸⁵⁻⁸⁷

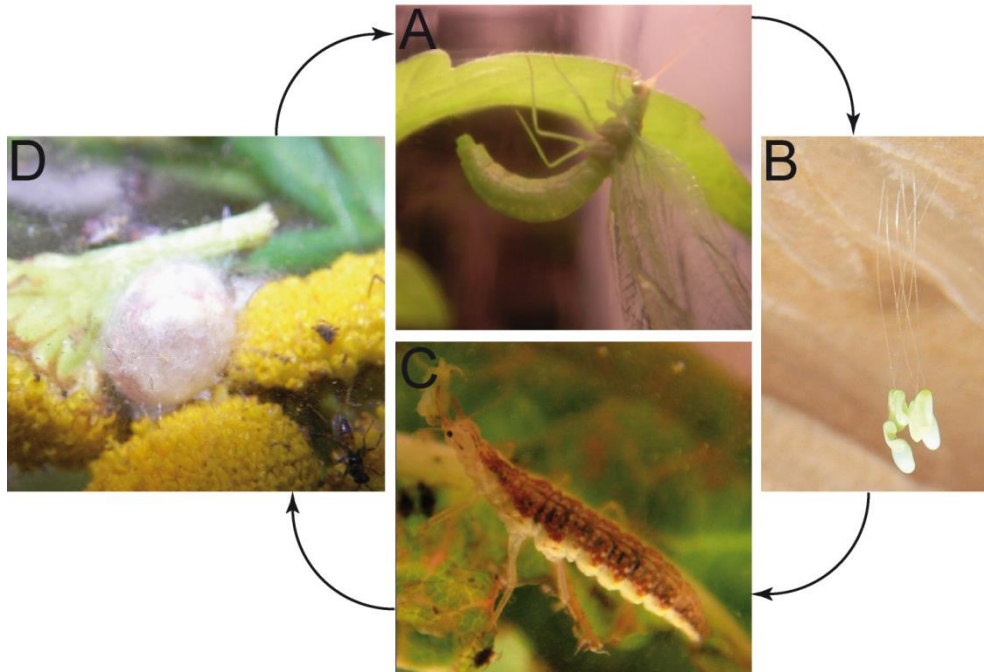


Figure 3: Lifecycle of lacewings comprising an adult lacewing (A), eggs on stalks (B), larva (C), and pupated larva (D).

3.1.4.2.1. Cocoon silk

The cocoon of lacewing larvae comprises two layers.^{21, 28, 88} First the larva secretes a silken thread from the malphigian tubules and deposits a loosely woven cocoon. Later the larva deposits an inner layer of lipids to protect itself from water loss during metamorphosis. The silken threads have diameters of about 2 μm , are composed of one protein which is 49 kDa in size, and are rich in alanine.²¹ The protein adopts an α -helical structure but surprisingly it does not assemble into coiled coils as other α -helical silks do.²¹

3.1.4.2.2. Egg stalk silk

Female lacewings attach their eggs to silken stalks to protect the eggs from predators such as ants or their own larvae.⁸⁷ The stalk is drawn from a secreted protein droplet produced in the colleterial gland. An amino acid composition analysis revealed high levels of serine (41%), glycine (24%) and alanine (20%).⁸⁹ Investigations

of a c-DNA library of the lacewing (*Mallada signata* (*M. signata*)) colleterial gland yielded clones encoding two proteins: MalXB1 (86 kDa) and MalXB2 (55 kDa), both containing a highly repetitive central structure (over 70%) which has a 16 amino acid periodicity.⁹ It was proposed that eight amino acid long β -strands fold into a regular antiparallel cross- β structure which is stacked in fibre- and side chain-direction. This structure converts into a parallel- β structure upon stretching.^{47, 90}

Further the stalks of some lacewing species such as *Ceraeochrysa smithi* are reported to be coated by droplets containing fatty acids, an ester, and various straight-chain aldehydes. This fluid was shown to protect the eggs from predators such as ants.⁸⁶

3.1.4.2.3. Production of lacewing egg stalks

The production of egg stalks seems to be quite simple compared to the complex spinning mechanisms of spiders where shear forces, pH change, and ion exchange play important roles.^{54, 91-100} The female lacewing first taps her abdomen a few times on the surface (Figure 4 A-C), deposits a droplet of spinning solution from the colleterial gland on a surface (Figure 4 D), dips the end of an egg into the solution, and raises its abdomen to draw a fibre between the droplet and the egg (Figure 4 E-G).⁶⁰ The fly stays in this position for 10 (~10% RH) to 35 seconds (~70% RH) to let the stalk dry and finally leaves.¹⁰¹

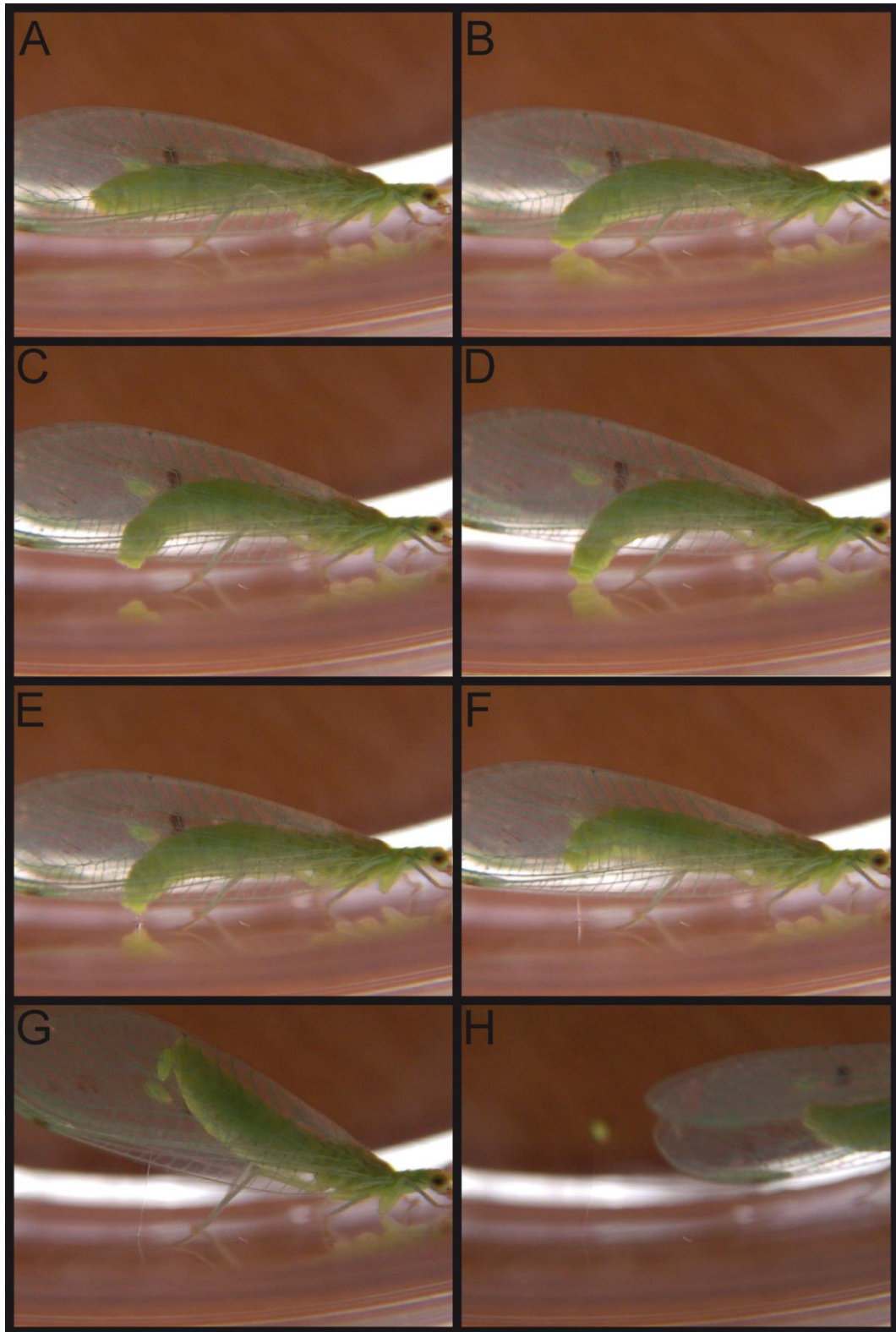


Figure 4: Lacewing producing an egg stalk: A-C: The lacewing taps its abdomen several times on the substrate; D: A droplet of dope is deposited on the surface and the egg is pressed into the droplet; E-G: The abdomen is pulled away from the substrate and a stalk is drawn. G: The fly holds its abdomen up until the stalk is hardened (approximately 10-35 seconds depending on the relative humidity); H: The stalk is finished.

3.1.4.2.4. The colleterial gland

The origin of the lacewing egg stalk proteins is the colleterial gland of female lacewings which is located in the dorsal region of the sixth to eighth body segment and has a sac-like shape. The exit of the gland joins the fallopian tube (Figure 5).¹⁰²

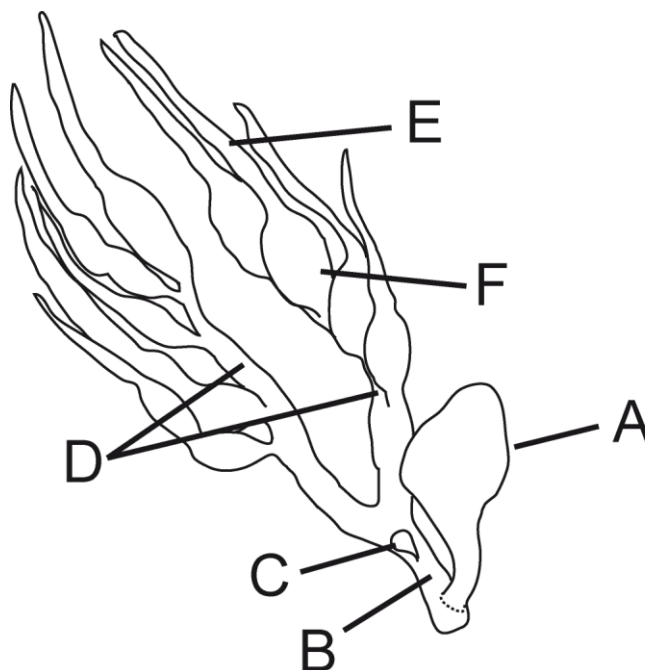


Figure 5: Schematic organisation of the female lacewings genitals. A: Colleterial gland; B: Fallopian tube; C: *Receptaculum seminis*; D: Paired ovary; E: Ovarioles; F: Egg.

Lucas and Rudall showed by transmission electron microscopy that secretion of the colleterial gland of *Chrysopa flava*, which was diluted with water, comprised fibrillar structures. These structures did not solubilise during dilution.²⁶ The fibrils are an assembly of around 20-30 molecules in side chain direction (about 13 nm) and have a thickness of approximately 2.5 nm which is the thickness of the fold of eight amino acids proposed by Geddes *et al.* and lengths of about 670 nm.^{26, 47} This preassembly in the spinning dope has been discussed to be a key requirement for a cross- β structure in the stalk.²⁶

3.1.4.2.5. Protein sequences/dope composition

Egg stalks of *M. signata* are composed of at least two proteins. The underlying c-DNA was extracted from a c-DNA library of colleterial gland cells.⁹ The two genes encoding the proteins (MalXB1 and MalXB2) are found to be expressed in a ratio of 7:1.⁹ Both proteins consist of a highly repetitive core domain with a repeat of 16 amino acids flanked by non-repetitive terminal domains. MalXB1 additionally has a non-repetitive central domain. MalXB1 is negatively charged with 17 acidic and 9 basic amino acid residues, whereas MalXB2 is positively charged with 11 acidic and 31 basic amino acids.

An interesting fact is the presence of seven (MalXB1) and five (MalXB2) cysteine residues, which are mostly situated in the non-repetitive terminal domains.

3.1.4.2.6. Mechanics of lacewing egg stalks

Mechanical tests on egg stalks were undertaken by Hepburn *et al.* (*C. carnea*) and Weisman *et al.* (*M. signata*).^{9, 103} Stress strain measurements at 65% relative humidity revealed extensibilities of ~249% and 381% and a tensile strength of ~375 MPa and 310 MPa. Measurements under water showed higher extensibility (502%/~560%) while strength was reduced (186 MPa/~250 MPa). Weisman *et al.* measured the lateral stiffness of egg stalks by scanning probe microscopy. Due to the lack of some physical constants of the system the modulus is reported in relation to *B. mori* silk. The measurements revealed 70% higher modulus values for the egg stalks. For the calculation of the bending stiffness, where the shape of a cross section is taken into account, the egg stalks have three times higher values (round shape of the stalks in comparison to the trilobal shape of *B. mori* silk).⁹ The high extensibility and high lateral stiffness might be related to the cross- β structure and disulphide cross linking.

3.1.4.2.7. Structure

The secondary structure of egg stalk proteins was investigated by Parker and Rudall.⁹⁰ X-ray diffraction patterns showed cross- β structure with β -strands running perpendicular to the fibre axis, and were excitingly the first detected natural protein with this structure.^{9, 90} 1968 Geddes *et al.* proposed a structural model to explain the X-ray diffraction pattern.⁴⁷ The stalk is built up by 25 Å thick micelles being separated by variable sized inter micelle spacing of 15 ± 4 Å (Figure 6). The longest dimension of the micelle is oriented parallel to the fibre axis. The β -strands are predicted to have a length of eight amino acids whereof the first two and last two amino acids form a β -turn. In each turn one of the two central amino acids has to be a glycine.⁴⁷ This prediction was confirmed by Weisman *et al.* for MalXB1 and MalXB2 where one glycine residue is found per turn in the repetitive domain. They further found that charged (Lysine) and bigger (>124 g/mol) amino acids are situated in the central turn regions.⁹ In MalXB2 two of the four central positions of the β -strands are alanine residues.

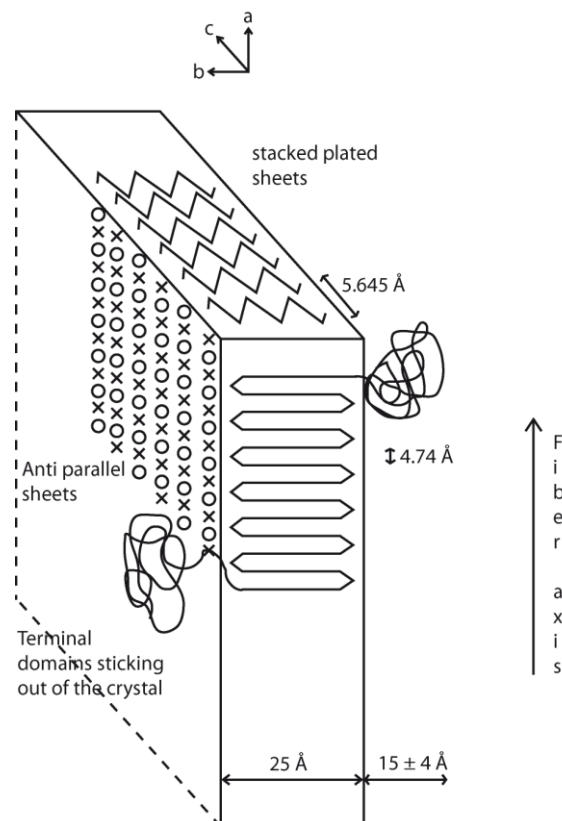


Figure 6: Cross- β micelle of a lacewing egg stalk.

3.2. Recombinant production of silk proteins

In contrast to spiders it is possible to farm lacewings which are utilised on a commercial scale as a biological pest control.¹⁰⁴ To obtain lacewing silk either flies have to be killed, the silk gland dissected, and the protein extracted, or single egg stalks have to be harvested, the eggs removed, the stalks solubilised, followed by extraction of the proteins. Both are time consuming and do not lead to large quantities of protein. Furthermore, both methods yield an undefined mixture of the proteins and other molecules such as the relatively low molecular weight egg defence molecules mentioned before, which are present in the stalk.

Recombinant production of lacewing silk proteins in host organisms such as bacteria or yeasts is a possibility to obtain reasonable quantities of pure proteins with consistent quality, which is an essential requirement for the use of the proteins in industrial applications. An advantage is that single domains of the proteins can be produced, and their contribution to the assembly of the protein can be analysed. Another advantage of recombinant silk production is the possibility to alter the properties of the proteins. For example, the substitution of poly-alanine rich modules (crystalline leading to stiffness and strength) for coiled coil forming modules (more extensible) might lead to a more elastic fibre after spinning of the protein. Addition of signal peptides such as the integrin recognition motive RGD or cell penetrating peptides to silk proteins leads to new functions of the proteins such as improved cell adhesion.¹⁰⁵⁻¹⁰⁷

Commonly reported problems occurring during the recombinant production of silk proteins are low yields and truncated versions of the proteins. The reasons therefor are the size of silk proteins (protein yield decreases at protein sizes above 100 kDa in *Escherichia coli* (*E. coli*)),¹⁰⁸ and their highly repetitive character (leads to undesirable recombination).

Various attempts have been made to overcome these problems, for example optimisation of the gene sequence (less repetitive genes due to codon variation/adaption of the codon usage of the host organism), host engineering (changes in the metabolism of the host organism), and a modular approach leading to shortened versions of the proteins.¹⁰⁸⁻¹¹⁵

Many companies such as AMSilk GmbH (Germany), BASF AG (Germany), Commonwealth Scientific and Industrial Research Organization (Australia), and Spiber AB (Sweden) are interested in recombinant production of silk proteins for industrial applications.

3.3. Technical processing of silk proteins

One particularly attractive feature of silk proteins is the possibility to produce different morphologies in addition to fibres. For other silk proteins, the production of fibres, particles, capsules, hydrogels, foams, films, and coatings has been reported, with possible applications ranging from drug delivery to high tech textiles. Allergan Inc. (USA), AMSilk GmbH (Germany), Commonwealth Scientific and Industrial Research Organization (Australia), Ekteino Laboratories Inc. (USA), Neurotex Ltd. (England), Orthox Ltd. (England), Oxford Biomaterials Ltd. (England), Spiber AB (Sweden), Spintec Engineering GmbH (Germany), Suturox Ltd. (England), and Vaxess Technologies Inc. (USA) work on processing silk proteins into marketable products such as conduits for nerve regeneration, coatings for breast implants, sutures, meniscal cartilage-, bone-, joint repair, and thermo stable vaccines. In this thesis some of the mentioned morphologies have been produced out of recombinant lacewing silk, and are therefore introduced briefly.

Fibres

For the processing of silk proteins (recombinant as well as regenerated natural silk) into fibres there are a few techniques such as hand drawing, wet spinning,¹¹⁶⁻¹²⁵ microfluidic spinning,^{92, 126} or electro spinning.¹²⁷⁻¹³¹ In this thesis the fibres were hand drawn.

Hand drawing fibres requires a highly concentrated protein solution which can be either aqueous or non-aqueous (Hexafluoroisopropanol (HFIP) or Hexafluoroacetone trihydrate (HFA) have been used). To produce a fibre, a droplet of silk solution is deposited on a surface and a fibre is pulled out of the droplet by using tweezers, and subsequently

the fibre is allowed to dry. This technique was used to produce fibres of silk from *B. mori*,¹³² *Nephila clavipes*,¹³³ and engineered spider silk.^{91, 134}

The produced fibres can be post treated to increase the protein β -sheet content which renders the fibres water insoluble. This can be achieved by the use of cosmotropic salt solutions, ethanol, methanol, isopropanol, heat, water vapour, or high pressure. The β -sheet crystals in the fibres can be aligned by post stretching of the produced fibres. This improves their mechanical properties.^{135, 136}

Capsules

Capsules are thin membranes enveloping an aqueous compartment which might include organs, bacteria, dyes, chemicals, enzymes, and drugs. Technically, capsules can be generated by once or multiple times coating a solid core, which is subsequently solubilised and washed off.¹³⁷ By deposition of multiple silk layers the molecular weight cut-off of such capsules might be tuned.¹³⁷ A technique which was used in this thesis is based on the amphiphilic character of silk proteins to induce self-assembly at the interface between an aqueous and an organic phase in an emulsion.^{138, 139} Capsules can be used as delivery platforms for cells, enzymes, nanoparticles, genes, and drugs due to their ability to reduce the diffusion of drugs, protect enzymes from proteases, and stabilize proteins.^{140, 141}

Hydrogels

Hydrogels consist of a polymer network that absorbs significant amounts of water but does not dissolve therein. A hydrogel can be generated by physical or chemical connectivity such as crosslinking of the polymer chains. Self-assembling systems for example silks can form hydrogels due to fibril formation. This has been shown for silk proteins such as *B. mori* fibroins^{109, 142-152} and spider silk proteins for instance natural and engineered *A. diadematus* silk proteins.^{93, 109, 151, 152} Hydrogels have a porous structure and elastic properties comparable to human tissues, which makes them suitable as scaffold for tissue engineering.

Foams

Foams are porous three dimensional structures with solid walls surrounding air filled cavities. They can be produced by different techniques such as gas foaming, salt leaching, and freeze drying.¹⁵³⁻¹⁶² Foams can be used as scaffolds for tissue engineering and as filter material.

Here the foams were generated by freeze drying of hydrogels. This technique uses the ability of silk proteins to form hydrogels. After spontaneous or alcohol induced gelation the hydrogels are frozen. The freezing temperature, protein concentration, and (if applied) the alcohol concentration have an influence on the secondary structure of the protein, the shape of the sponge, the pore size, and the mechanical properties. By directional ice freezing, laminar silk scaffolds could be produced.¹⁶³

Films

One method to produce films and coatings out of silk proteins is casting of a protein solution on a substrate followed by solvent evaporation. Other techniques to deposit a silk protein layer are dip coating, where the substrate is dipped into a protein solution which is allowed to dry after lifting the substrate out of the solution and spray coating.^{164, 165} Silk films are used in biomedical applications such as biocompatible carrier for drug delivery or wound dressings. Many investigations concentrate on tissue engineering of bone, cartilage, as well as cornea.¹⁶⁵⁻¹⁷¹

In this thesis films were generated by casting. The film thickness is depending on the concentration, and the volume of the protein solution. The secondary structure of such films is dependent on the protein, the solvent,¹⁷²⁻¹⁷⁶ and the substrate they are cast on.

Such films may, depending on the protein solvent, require post treatment to render them insoluble in water. This happens due to secondary structure changes of the proteins from an α -helical to a β -sheet rich structure. There are various possibilities to change the secondary structure of the silk proteins in films such as treatment with methanol, ethanol, isopropanol, water vapour, temperature annealing, stretching, storage/aging, cosmotropic salt solutions, and UV treatment.^{172-174, 177, 178}

For the use of silk films as material for optics, electronics, and aligned cell culture applications, it is necessary to generate a structured instead of smooth surface. Fabricating patterned films is possible by various techniques such as soft lithography, nanoimprinting, inkjet printing, and contact printing.¹⁷⁹⁻¹⁸² Often a template out of PDMS which is produced by casting on a lithographically fabricated silicon pattern is used to cast a film thereon, or lithographically produced templates are imprinted into a smooth film. Inkjet printing as well as contact printing uses another principle, where silk protein is printed or stamped on defined areas of a surface.

3.4. Aims of the work

Silks are envisioned as a raw material for a broad range of applications such as the use as biomaterials, wound dressings, drug delivery vehicles, or high performance fibres.^{8, 180, 183-185} For the development of a novel silk material, with defined properties, the connection between structure and function of natural silk proteins has to be understood in detail.

The aim of this work was to design and produce a silk protein, which can be processed into various morphologies to be used for different applications. To find a silk with interesting properties, silks deriving from different animals were mechanically analysed. Secondary structure analysis and sequence data of the underlying proteins of the silk was intended to understand structure-mechanical properties relationship of the silks. A synthetic gene could be designed comprising the important sequences. After expression of this gene in *E. coli*, a purification strategy for the resulting protein was developed. The processability of the protein into various morphologies such as fibres, films, capsules, hydrogels, and foams was subsequently investigated and compared to the natural material in the case of fibres.

4. Overview of the thesis including unpublished data

This dissertation contains three publications (chapters six to eight) spanning the analysis of silk materials, through recombinant production of a designed lacewing egg stalk protein, to processing of the artificial protein into materials.

4.1. Mechanical analysis of natural lacewing egg stalks and fibres of caddisflies

Fibres spun under water by caddisfly larvae and egg stalks produced by lacewings were mechanically analysed.

Final instar larvae of *Hydropsyche* sp. were bred in a vented beaker overnight at 4°C. The next day single fibres were removed carefully from the water. Afterwards the fibres were glued on plastic frames with a gauge length of 2 mm, and the diameter of the fibres was measured using a light microscope. Mechanical testing was conducted at different relative humidity (30%, 70%, and 100%, the later for lacewing (*C. carena*) egg stalks only), to analyse the influence of humidity on the mechanical properties of silk.¹⁸⁶

The caddisfly silk was more extensible at 30% relative humidity with 70% extensibility compared to 2% for the lacewing egg stalks (Table 2). In contrast at 70% relative humidity the egg stalks exceed the extensibility of caddisfly silk with 210%. The caddisfly silk has a higher tensile strength yielding 462 MPa (30% relative humidity) respectively 510 MPa (70% relative humidity) compared to the egg stalks with 68 MPa (30% relative humidity) to 232 MPa (70% relative humidity). The egg stalks are stiffer than the caddisfly silk by a factor of 1.57 (30% relative humidity) respectively 1.25 at 70% relative humidity, indicated by a higher Young's modulus. The toughness (energy which could be absorbed before breakage) which reflects a combination of extensibility and

strength is much higher for the caddisfly silk at 30% relative humidity whereas at 70% relative humidity the difference is less pronounced.

Table 2: Mechanical analyses of caddisfly silk and lacewing egg stalks at different relative humidity (RH).

| | RH [%] | Real stress [MPa] | Extensibility [%] | Young's Modulus [MPa] | Toughness [MJm ⁻³] |
|------------------------|--------|-------------------|-------------------|-----------------------|--------------------------------|
| <i>Hydropsyche Sp.</i> | 30 | 462 ± 193 | 70 | 3,683 ± 1,163 | 120 ± 71 |
| | 70 | 510 ± 205 | 114 | 2,532 ± 1,357 | 146 ± 67 |
| <i>Chrysopa carnea</i> | 30 | 68 ± 19 | 2 ± 1 | 5,777 ± 1,257 | 1 ± 1 |
| | 70 | 155 ± 75 | 210 ± 100 | 3,175 ± 1,015 | 87 ± 49 |
| | 100 | 232 ± 104 | 433 ± 127 | 1,285 ± 481 | 110 ± 43 |

Even though caddisfly silk has a higher strength and toughness than lacewing egg stalk silk, we decided to concentrate on the lacewing egg stalk silk because of the interesting secondary structure of the proteins involved and the bending stiffness of the stalks (Figure 13 B).

4.2. Structural analysis of lacewing egg stalk silk

The secondary structure of lacewing egg stalks was analysed by Raman spectroscopy. The cross- β structure present in unstretched egg stalks transforms into a parallel- β structure after stretching up to 500% at 70% and 100% relative humidity (Figure 7 A), but not at 30% relative humidity.

At the lower relative humidity the stalk ruptures at 2% strain and no structural changes could be observed. Scanning electron microscopic (SEM) images of partially stretched egg stalks show a sequential thinning and no homogeneous thinning over the entire length (Figure 7 B). Raman measurements at thinned parts (100% stretched stalks) revealed a partial rearrangement of the β -strands to parallel β sheets (Figure 7 A).

We developed a model explaining the differences between 30% and 100% relative humidity when hydrogen bonds between the β -strands rupture and the strands rearrange parallel to the fibre axis (Figure 8).

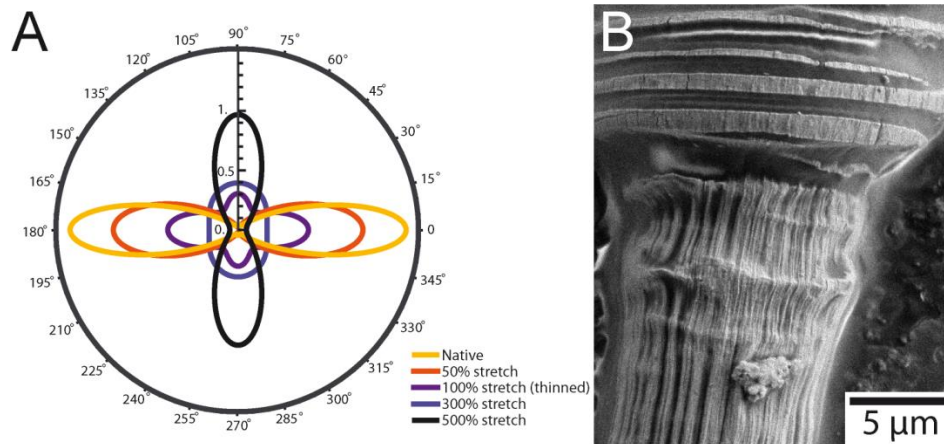


Figure 7: A: Orientation parameters and most probable distribution functions for amide I bands. The 0° of the polar plot coincides with the fibre direction; B: Scanning electron micrograph of a partially stretched lacewing egg stalk. Adapted with permission from *Biomacromolecules* (2012, 13, 3730-5). Copyright 2012 American Chemical Society.

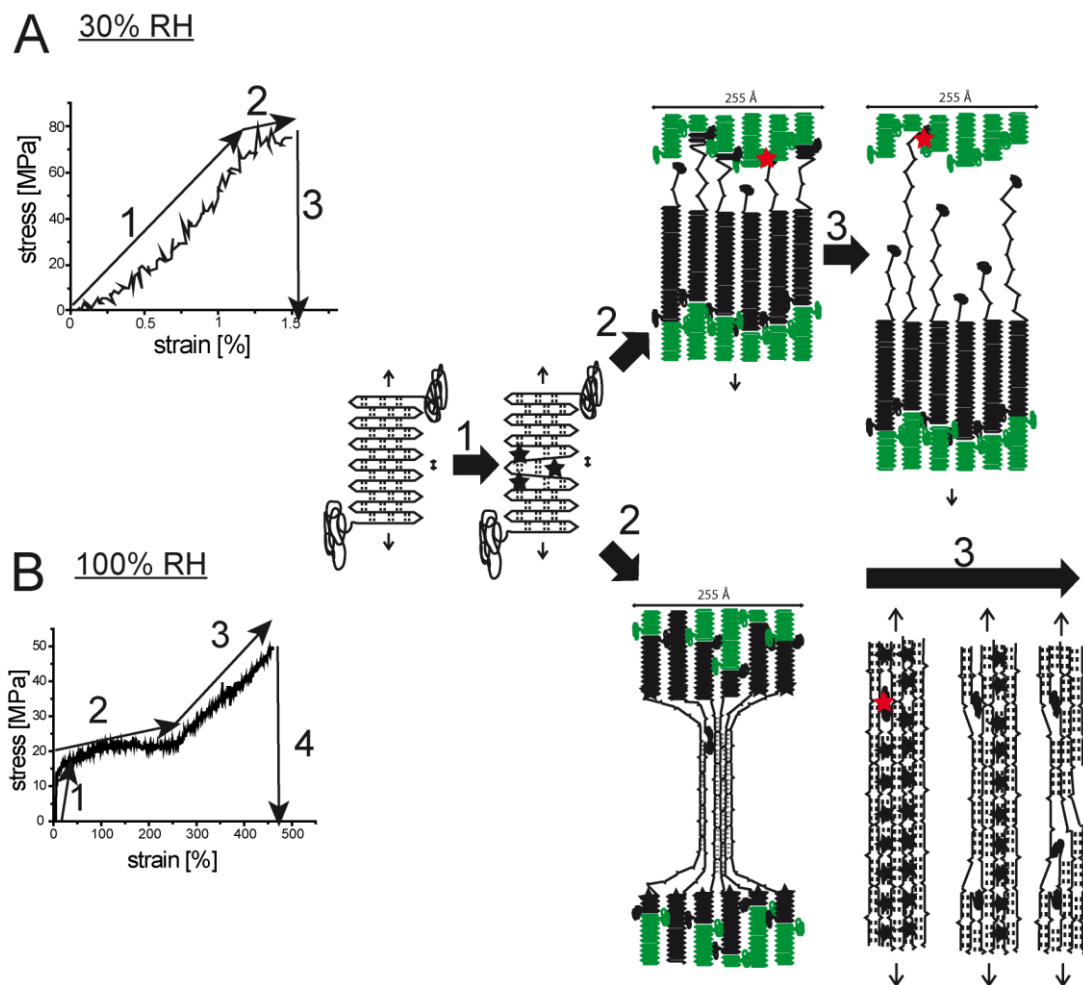


Figure 8: Schematic picture of stalk rupture at low and high relative humidity (RH). (Black stars: Hydrogen bonds break; red stars: disulphide bonds break; black protein backbone: involved in rearrangement; green protein backbone: unaffected). Reprinted with permission from *Biomacromolecules* (2012, 13, 3730-5). Copyright 2012 American Chemical Society.

After rearrangement of the strands at 100% relative humidity, new hydrogen bonds can be formed. This results in an extension of the stalk of up to 500%. Finally the β -strands start slipping on each other by a stick-slip mechanism described by Keten *et al.* before the stalk ruptures.¹⁸⁷ In contrast at 30% relative humidity the hydrogen bonds have higher bond energy due to the lack of interacting water molecules. Therefore, in one layer of the stalk the sum of hydrogen bonds has higher bond energy than the individual disulphide bonds which crosslink the proteins in the stalk. The disulphide bonds break and the stalk ruptures without breakage of the hydrogen bonds along the entire length of the stalk.

4.3. Silk gland analysis of lacewings

Colleterial glands of female *C. carnea* were dissected under a 95 mM sodium chloride (NaCl) solution and incubated three times in fixing buffer (100 mM HEPES (4-(2-hydroxyethyl)-1-piperazineethanesulfonic acid), 2.5% glutaraldehyde, 2% formaldehyde, pH 7.2) (one hour, two hours, 18 hours in the fridge respectively). Afterwards the glands were washed three times with wash buffer (100 mM HEPES, pH 7.2) followed by incubation in 1% osmium tetroxide (v/w in water) for one hour at 4 °C and three times washing in water. After embedding the glands in 1% agar they were dehydrated using increasing concentrations of ethanol (30%, 50%, 70%, 90%, and two times 100%). Ethanol was substituted by incubating the embedded gland in a 1:1 mixture of ethanol and propylene oxide (15 minutes), followed by incubation two times in pure propylene oxide (12 hours at -20°C). Finally the samples were embedded in glycid ether 100 using standard procedures. The samples were cut with a diamond knife equipped ultramicrotome into ultrathin sections, which were mounted on copper grids. After staining with uranyl acetate and lead citrate they were imaged using a transmission electron microscope (TEM).

Two to four cell layers were detected depending on the position in the gland. In general the gland cells contain many mitochondria and are filled with rough endoplasmic reticulum (Figure 9). In some cells vesicles with fibrillar structures are visible (Figure 9 D-F). The fibrils have diameters of about 5 nm and lengths of about 200 nm. This may be related to egg stalk proteins forming eight amino acid β -strands. Such a structure would have a thickness of 2.5 nm. Lucas and Rudall showed similar structures in diluted dope from a

Chrysopa flava colleterial gland.²⁶ Such a pre-structured silk solution might be critical to achieve a cross- β structure. The fibrils might be oriented by shear forces during the egg stalk production, and the cysteines might cross-link the fibrils to give a stable egg stalk structure (Figure 15).

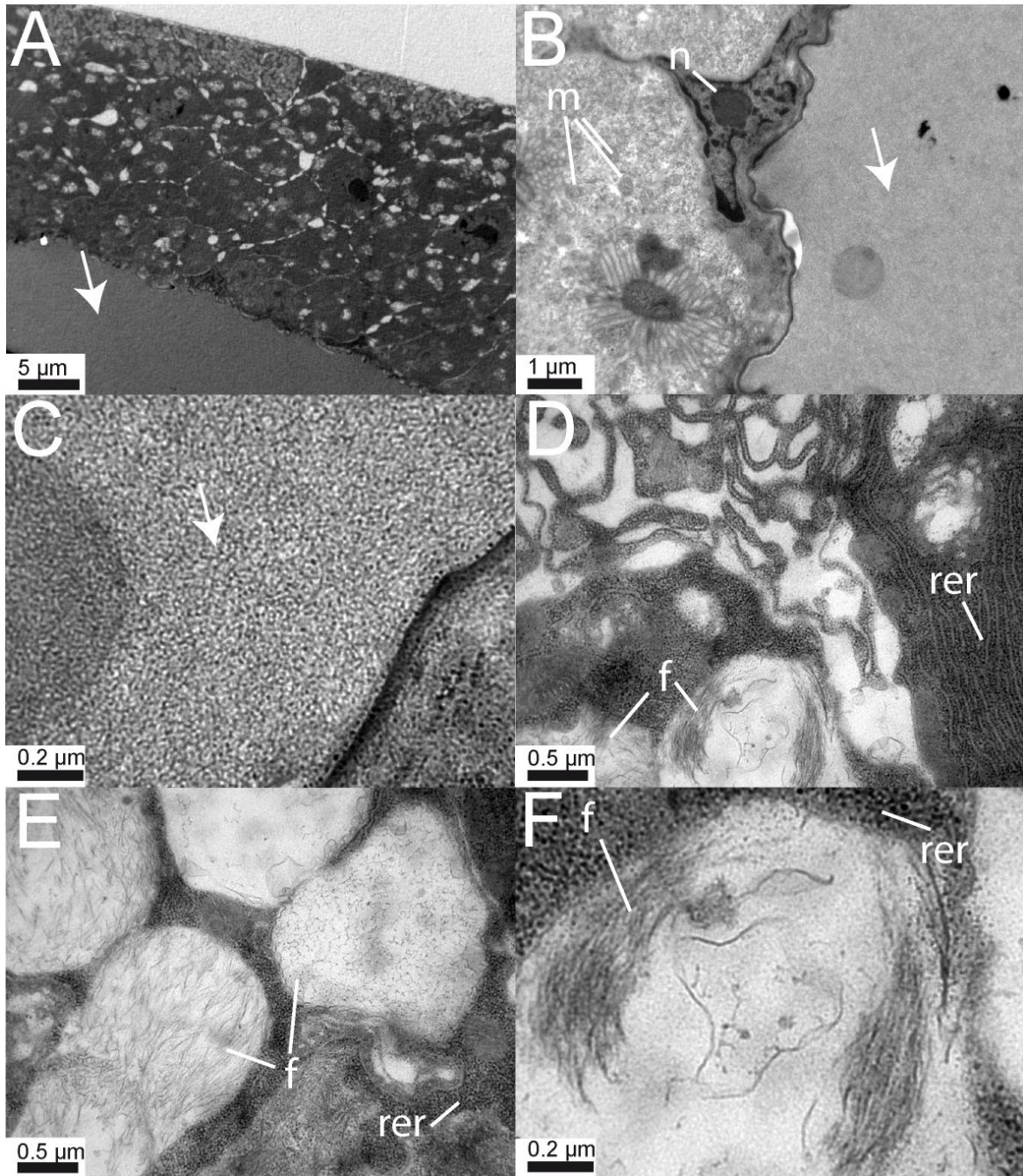


Figure 9: TEM images of cross sections of a lacewing colleterial gland; A: Silk gland tissue and silk dope (arrows); B: Cells with Nucleus (n), mitochondria (m), and silk dope; C: Inhomogeneity of the silk solution; D, E and F: Cells are filled with rough endoplasmic reticulum (rer) and protein filled vesicles with fibrillar structures (f).

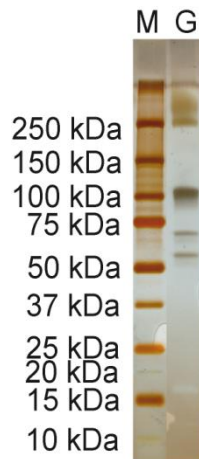


Figure 10: Silver stained SDS-page of silk solution stored in the colleterial gland of a female lacewing (*C. carnea*). M: protein marker; G: silk gland extract.

SDS-PAGE analysis of the silk dope of a female *C. carnea* revealed five distinct bands (Figure 10). Surprisingly this are three more than Weismann *et al.* gathered from their c-DNA library of *M. signata*.⁹ One reason for this might be the quality of their c-DNA library where only one clone encoding MalXB2 and seven clones encoding MalXB1 could be found.

4.4. Biotechnological production of N[AS]₈C, an artificial lacewing egg stalk protein

Due to the low availability of lacewing egg stalk protein from natural sources, it is an important step to produce the proteins in a different manner, for use in both basic research and technical processing.

Here we developed an artificial version of MalXB2, an egg stalk protein of *M. signata* and produced it recombinantly in *E. coli* bacteria.

MalXB2 consists of non-repetitive amino- and carboxy-terminal domains. These were used as modules N (amino-terminal module) and C (carboxy-terminal module) for the artificial Protein N[AS]₈C (Figure 11). To ensure a proper steric build-up of the protein (the terminal domains in the natural blueprint face to different sides of the cross-β sheets of the repetitive part (Figure 6)) the carboxy-terminal module starts with the last eight amino

acids of the repetitive part of MalXB2 (Figure 11). Detailed analysis of the amino acid sequence of the repetitive part of MalXB2 showed a repeat every 48 amino acids, which was called AS module and better fits to the original sequence than a 16 amino acid repeat proposed by Weismann *et al.*⁹ The starting of the 48 amino acid repeat was chosen to start with a glycine which is relevant for the use of a cloning strategy developed by Hümmerich.¹⁰⁹

The modules were translated to *E. coli* optimised nucleotide sequences and an additional nucleotide triplet (GGC) was added to the end of the N- and AS module (Due to the cloning technique. These nucleotides get lost during multimerisation/cloning). The cloning technique allows a seamless multimerisation of the AS modules and subsequent linkage of the N- and C module (Figure 11 C). As a length of the repetitive part we chose eight AS modules to mimic the original length.

Afterwards the N[AS]₈C nucleotide sequence was cloned into a pET 28a vector. *E. coli* BL21 (DE3) cells were transformed with the plasmid and were cultivated in a 2.5 L fermenter. After induction and expression of the artificial gene, the bacteria could be harvested and a purification strategy for the protein had to be developed. The bacteria were lysed by an urea/thiourea buffer followed by pH decrease to 4. Finally the protein was purified without the use of columns by fractionated ammonium sulphate precipitation, and after washing with water, lyophilised and stored at -20°C. Purity was tested by SDS-PAGE and mass spectrometry (Figure 12).

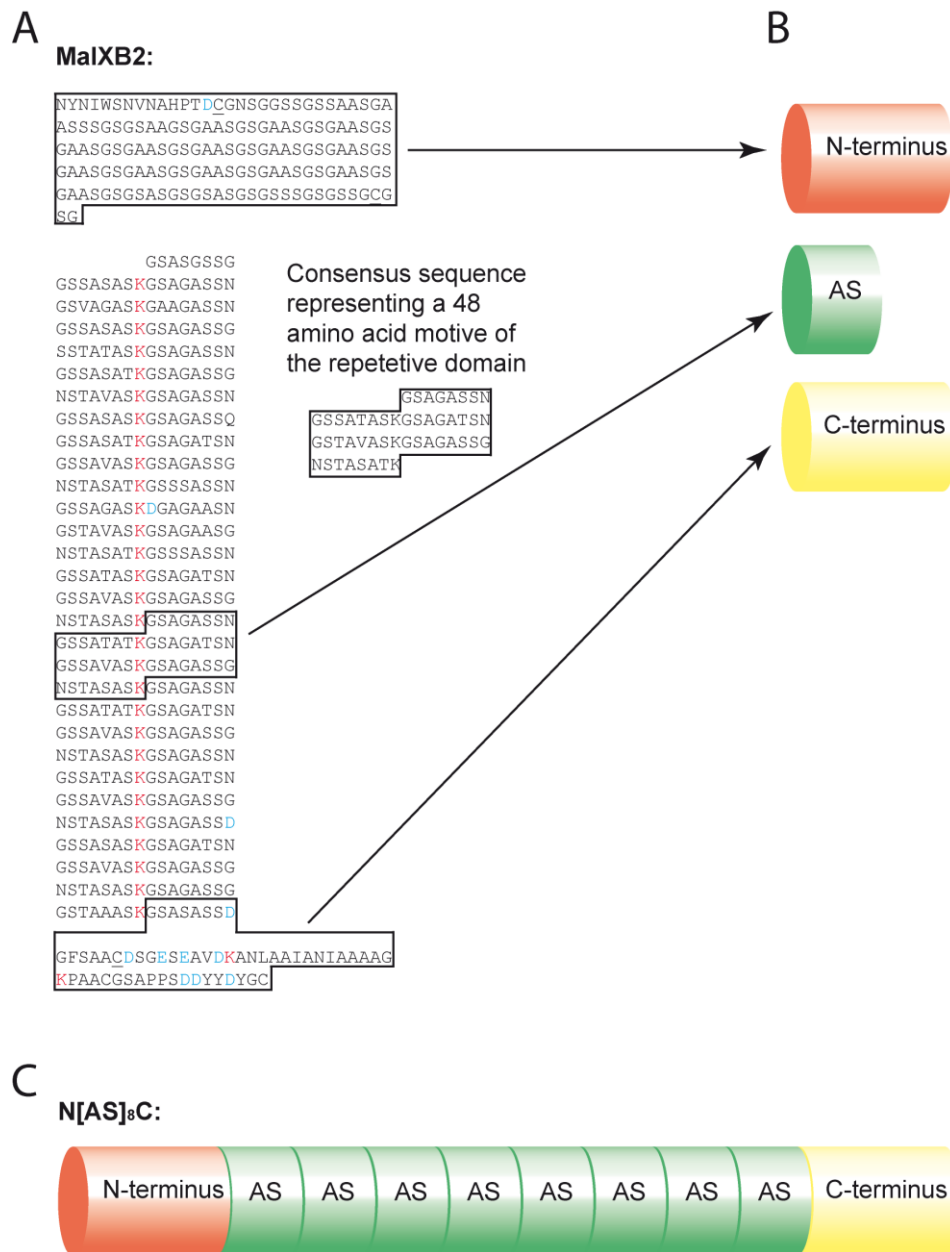


Figure 11: A: Sequence and organisation of MalXB2, a natural egg stalk protein; B: The three modules derived from MalXB2; C: Schematic build-up of an artificial lacewing egg stalk protein - N[AS]₈C.

The full length protein N[AS]₈C has a molecular weight of 53 kDa including detection and purifications tags and is comparable in size to the naturally occurring variant MalXB2 (55 kDa).

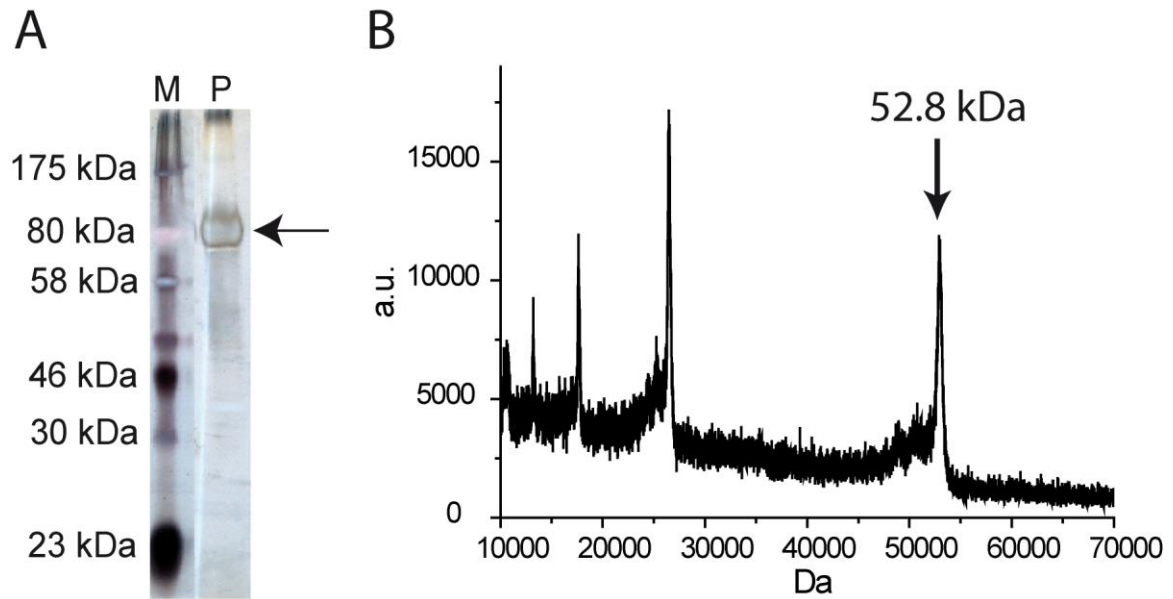


Figure 12: SDS-PAGE (A) and mass spectrometry (B) of N[AS]₈C. The lower molecular weight peaks are multiple charged N[AS]₈C molecules. Adapted with permission from *Angewandte Chemie International edition* (2012, 51, 6521-4). Copyright 2012 WILEY-VCH Verlag GmbH & Co. KGaA, Weinheim.

4.5. Fibre/stalk formation and analysis

To produce fibres out of N[AS]₈C, we used a process close to the natural one. Due to the low solubility of the protein in water we chose HFA as the solvent. The volatility of HFA is beneficial for fast drying of the generated fibres.

10% w/v of lyophilised N[AS]₈C was dissolved in HFA to produce a solution from which fibres could be spun. A small droplet (~1-2 μL) was pipetted on a surface. Now tweezers were dipped into the droplet, mimicking the lacewing egg stalk production, and were subsequently pulled out to draw a fibre. The end connected to the tweezers was transferred to a tinfoil support (Figure 13 A). After drying, the tinfoil support was moved closer to the droplet to reduce tension in the fibres and avoid rupture during post treatment. By applying 60°C and 70% relative humidity overnight the β-sheet content increased from 20% to 32% which is close to the values of natural egg stalks with 40% β-sheet content and the fibres turned water insoluble.

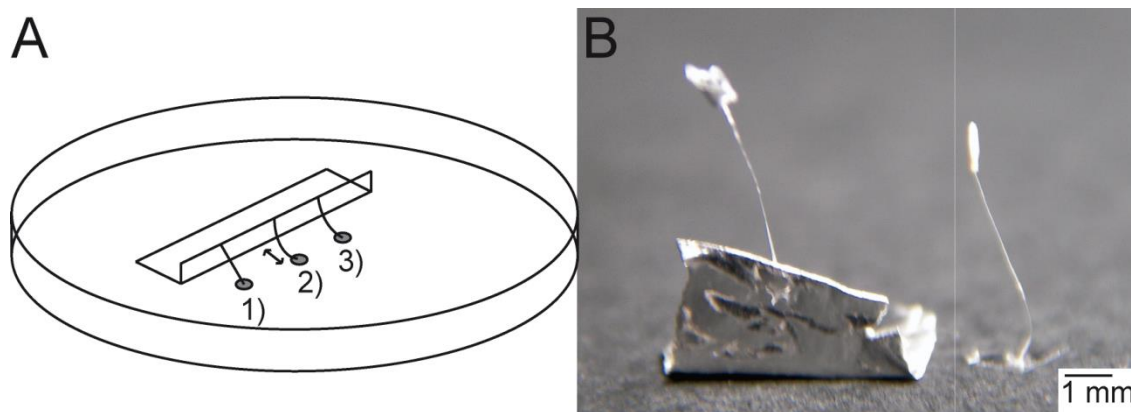


Figure 13: Comparison of natural and artificial stalks. A) schematic picture of the stalk production 1) stalk drawn from the dope to tinfoil using tweezers; 2) relaxation of the stalk by moving of the tinfoil; 3) the stalk contracts during post-treatment at 60°C and 70% relative humidity; B) picture of an artificial egg stalk with tinfoil on top (left) and a natural egg stalk with an egg on top (right). Reprinted with permission from *Angewandte Chemie International edition* (2012, 51, 6521-4). Copyright 2012 WILEY-VCH Verlag GmbH & Co. KGaA, Weinheim.

The artificial stalks are stiff, like the natural ones (Figure 13 B). Analysis of the artificial stalks showed similar mechanical properties to the natural ones at 30% relative humidity with 2% extensibility for the natural ones compared to 5% for the artificial ones (Table 3). Even the tensile strength is nearly equal with 55 MPa compared to 68 MPa for the natural stalks. Nevertheless there are differences at 70% relative humidity where the extensibility of the natural stalks of 210% could not be observed for the artificial ones.

Artificial stalks show, as well as the natural lacewing egg stalks, birefringence under a polarised microscope, meaning there are ordered structures in the stalk (Figure 14). Nevertheless, no cross- β structure could be detected by X-ray diffraction or by polarised FTIR (Fourier transform infrared spectroscopy) measurements. This might be a reason for the differences in mechanical properties at 70% relative humidity. In the absence of cross- β structure no transition to parallel- β structure is possible. This means the stalks will not be that extensible and the mechanical properties will differ.

Table 3: Tensile testing of natural (*C. carnea*) and artificial egg stalks. Experiments were carried out at 30% and 70% relative humidity at 22°C. Reprinted with permission from *Angewandte Chemie International edition* (2012, 51, 6521-4). Copyright 2012 WILEY-VCH Verlag GmbH & Co. KGaA, Weinheim.

| | Extensibility [%] | Strength σ_{\max} [MPa] | Young's modulus [MPa] | Toughness [MJ/m ³] |
|---|-------------------|--------------------------------|-----------------------|--------------------------------|
| Literature values (<i>M. signata</i> and <i>C. spec</i>) | | | | |
| 65% RH ⁹ | 381 | 310 | | |
| 65% RH ¹⁰³ | 249 | ~375 | | |
| Natural egg stalk | | | | |
| 30% RH | 2 ± 1 | 68 ± 19 | 5,777 ± 1,257 | 1.2 ± 0.72 |
| 70% RH | 210 ± 100 | 155 ± 75 | 3,175 ± 1,016 | 87 ± 49 |
| Artificial egg stalk | | | | |
| 30% RH | 5 ± 2 | 55 ± 14 | 2,330 ± 850 | 1.76 ± 0.9 |
| 70% RH | 6 ± 3 | 25 ± 11 | 1,012 ± 252 | 1.09 ± 0.59 |

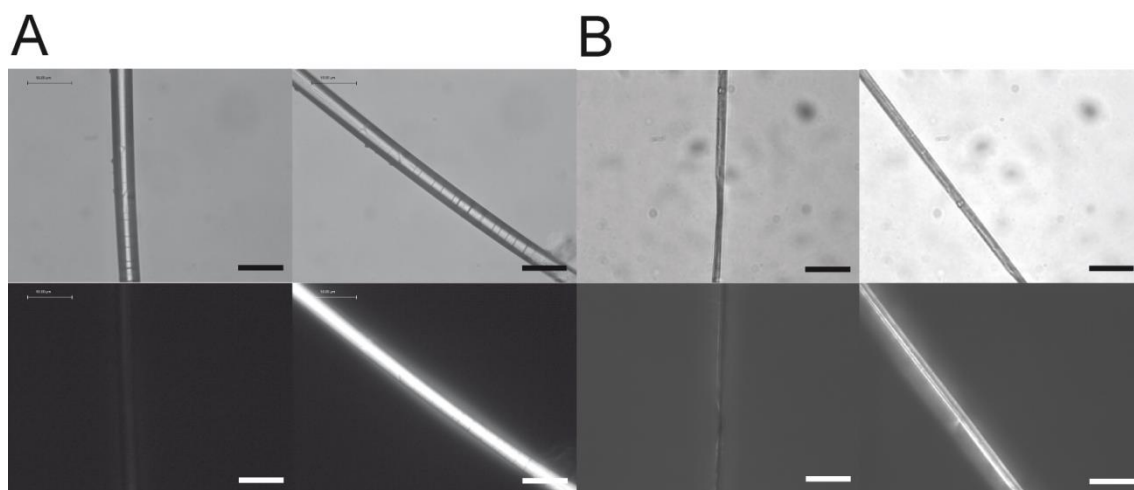


Figure 14: Comparison of birefringence of natural and artificial stalks. A) Microscopic pictures of a natural lacewing egg stalk. B) Microscopic pictures of an artificial egg stalk. Top: bright field; bottom: with crossed polarisers; scale bars: 50 μm . Reprinted with permission from *Angewandte Chemie International edition* (2012, 51, 6521-4). Copyright 2012 WILEY-VCH Verlag GmbH & Co. KGaA, Weinheim.

A possibility to solve this problem in the future is to use an aqueous spinning solution with pre-structured proteins, as seen for natural dope (Figure 9), which might orient due to shear forces during the production process and crosslink to each other by disulphide bonds (Figure 15).²⁶

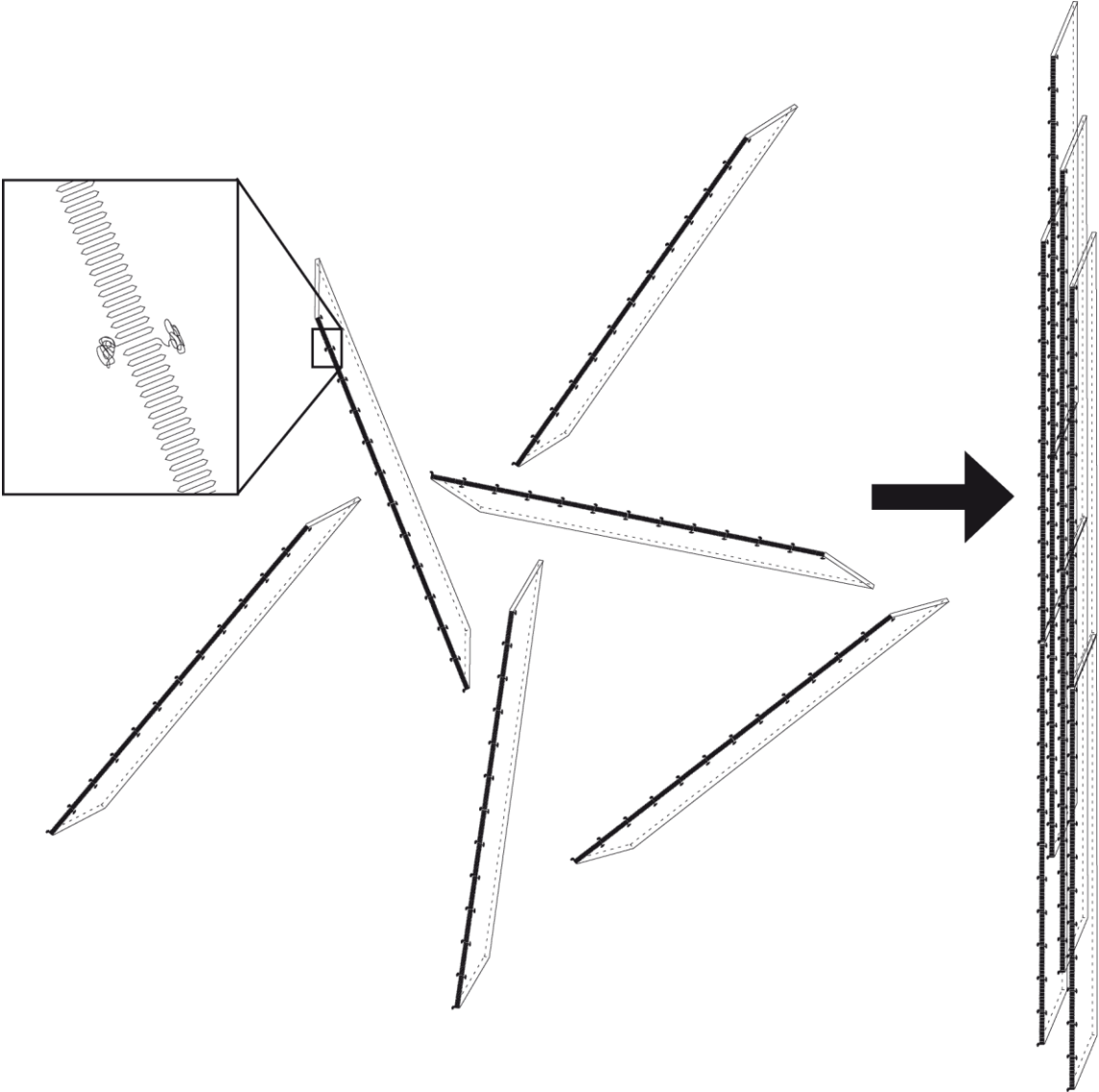


Figure 15: Model of a pre-structured silk solution which assembles upon shear forces.

4.6. Further processing of a recombinant lacewing protein

Next the processing of N[AS]₈C into different morphologies was tested as described for other silk proteins.

4.6.1. Films

In order to obtain films (Figure 16) 1% (w/v) N[AS]₈C was dissolved in HFA or formic acid. Both solutions were cast on polystyrene. After drying, the films were either peeled off the substrate or first post-treated by immersion in methanol or over-night treatment at 60°C and 50% relative humidity. Secondary structure was analysed using FTIR. For SEM the samples were glued on aluminium stubs and were sputter-coated with platinum. Images were obtained using a Zeiss 1530.

Table 4: Secondary structure of films cast from HFA and formic acid. The HFA films were post-treated with methanol or at 60°C and 50% RH overnight.

| | HFA | | | | Formic acid |
|---------------------------------------|---------|------------------------|------------------------|--------------|-------------|
| | As cast | Untreated after 4 days | 60°C 50% RH over night | MeOH treated | As cast |
| β sheets | 6% | 19% | 42% | 50% | 59% |
| Alpha-helices | 21% | 12% | 9% | 7% | 6% |
| Turns | 11% | 26% | 18% | 22% | 14% |
| Random coils | 58% | 39% | 23% | 20% | 20% |
| Side chains/ aggregated strands | 4% | 4% | 8% | 1% | 1% |

Films cast from formic acid (Figure 16 B, D, F) were more brittle than the ones from HFA, and water insoluble directly after drying. They had a β-sheet content of approximately 59% (Table 4). In contrast, films cast from HFA (Figure 16 A, C, E) were water soluble and, therefore, had to be post-treated. Without post-treatment they had a β-sheet content of 6% which increased due to aging to around 19% (after 4 days). Overnight heat treatment of the films at 60°C and 50% relative humidity led to a β-sheet content of around 42%. Slightly higher values could be obtained by treating the film with

methanol. Methanol treated films were stable in water. SEM images of methanol treated films show a smooth surface. The breaking edge of films cast from formic acid show a layered structure (Figure 16 F). This layers might be related to N[AS]₈C folding into band like sheets with a thickness of 2.5 nm (without terminal domains)/4 nm (with terminal domains), or multiples thereof, which one would expect from the structure of the natural proteins in an egg stalk (Figure 15 right part).

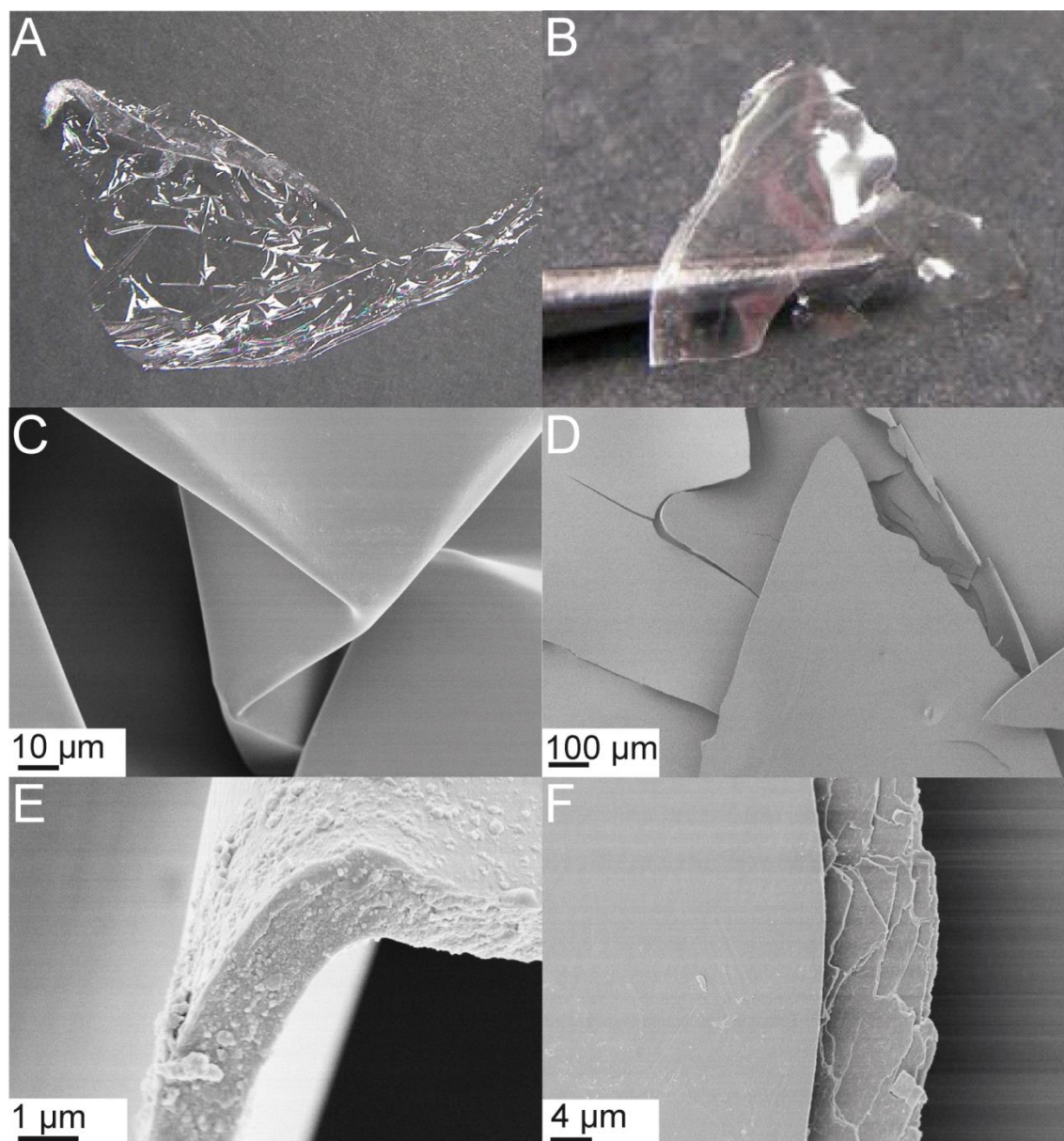


Figure 16: N[AS]₈C-films. A, C, and E are cast from HFA and treated with methanol; B, D, and F are cast from formic acid. C-F: Scanning electron microscopic pictures of film surfaces and breaking edges.

4.6.2. Capsules

Capsules could be produced by using protein self-assembly at a water-oil interface. This is caused by the amphiphilic character of N[AS]₈C as shown by a Kyte-Doolittle hydropathy plot (Figure 17).¹⁸⁸ Hydrophobic and hydrophilic patches are alternating in the N-terminal-, repetitive-, and the C-terminal domains.

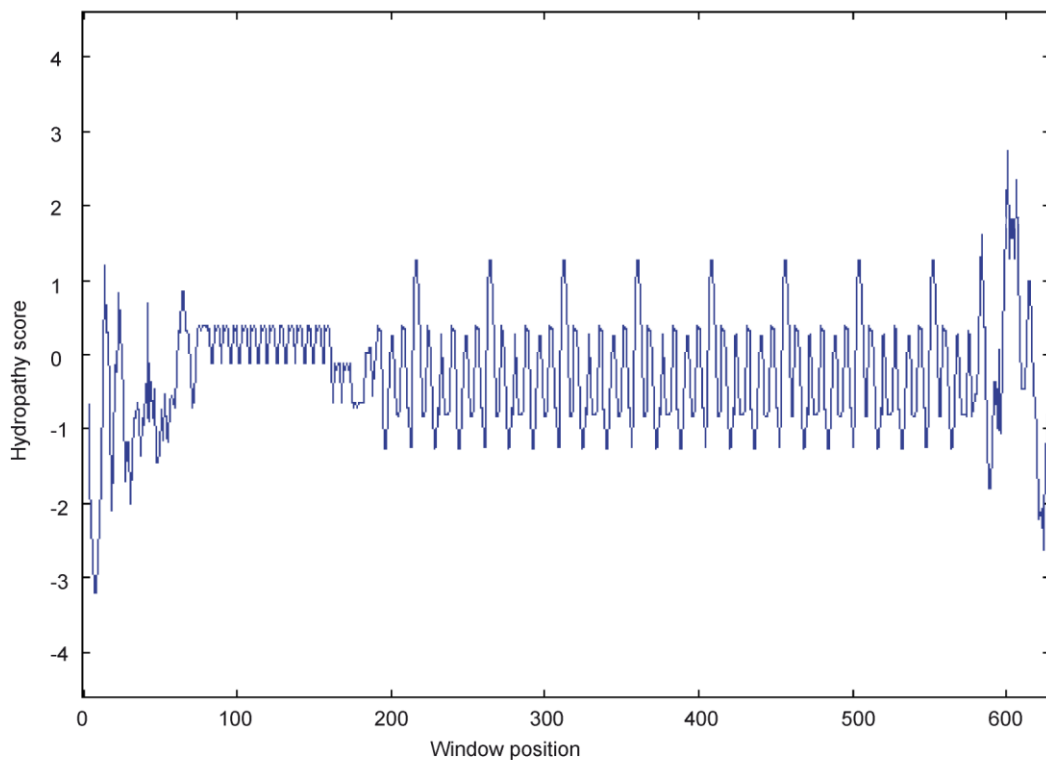


Figure 17: Kyte-Doolittle hydropathy plot of N[AS]₈C; Window size 5; Start position 1. Hydrophobic and Hydrophilic stretches are alternating (plotted by: <http://gcat.davidson.edu/DGPB/kd/kyte-doolittle.htm>. Which was created by Soren Johnson, Rachel Patton McCord and Lisa Robinson, and modified by Laurie Heyer.).¹⁸⁸

To produce capsules, 1.5 mg N[AS]₈C was dissolved in 1 mL of 6 M guanidinium thiocyanate solution. Afterwards the solution was dialysed against 10 mM Tris (2-Amino-2-(hydroxymethyl)-propan-1,3-diol)/HCl (hydrogen chloride); pH 7.5; 5 mM β-mercaptoethanol using a dialysis tube with a cut-off of 6-8 kD. 5 μL of this solution were transferred into 500 μL M100 silicon oil and subsequently were shaken for 45 s using a vortex. After emulsification (shaking), a protein layer builds at the oil-water interface of

the water droplets. To transfer the capsules in an aqueous environment the silicon oil was supplemented with 70% ethanol and the oil mixture was removed. Repeating this step several times led to oil free capsules which were washed with water afterwards. Finally the capsules were observed in a light microscope (see Figure 18).

The capsules shrunk during ethanol treatment due to osmosis and did not swell afterwards in water. This indicates a complete protein layer on the surface with semipermeable properties.

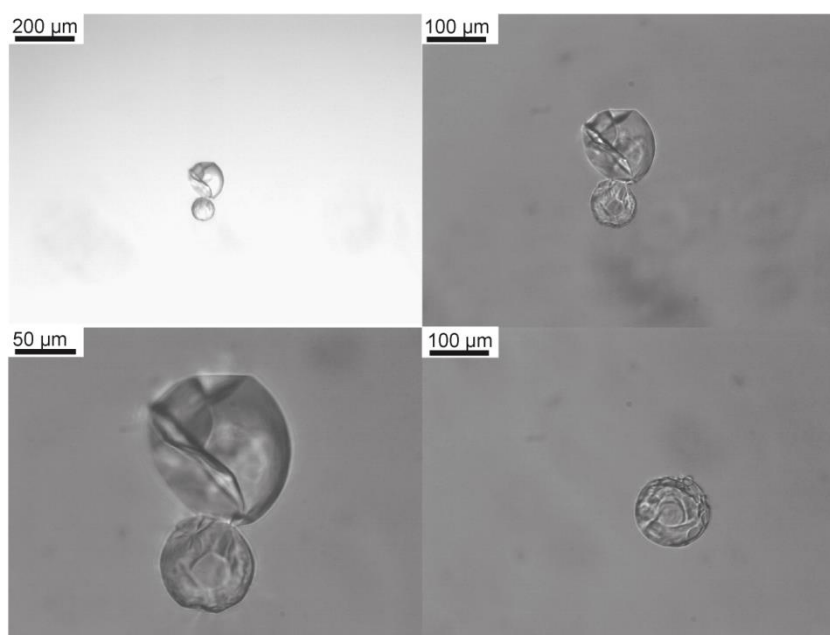


Figure 18: Capsules made of N[AS]₈C produced by interfacial polymerisation.

4.6.3. Hydrogels and foams

To produce hydrogels, 3% (w/v) N[AS]₈C was dissolved in 6 M guanidinium thiocyanate supplemented with 5 mM β-mercaptoethanol. During dialysis against 10 mM Tris/HCl pH 7.5 a hydrogel forms (Figure 19). Foams could be fabricated by freeze drying of such hydrogels. After freezing in liquid nitrogen the hydrogels were lyophilised resulting in foams. Samples of the foams were glued on aluminium stubs and were sputter-coated with platinum. Images were obtained using a Zeiss 1530.

The resulting hydrogel was stable in shape and did not start flowing for hours (Figure 18). The hydrogel formation is probably forced by a nucleation–aggregation

mechanism of nanofibrils in the solution which build a stable network. This formation is reported to be accelerated by increasing the temperature and can be slowed down by cooling.^{152, 189, 190}



Figure 19: Hydrogel of 3% (w/v) N[AS]₈C.

Freeze drying of a 3% N[AS]₈C hydrogel led to a stable foam like structure. SEM images revealed a pore size of 6 to 17 μm (Figure 20). Surprisingly the pores are filled with a 3D mesh of fibres on the nanometre scale with a pore size of 200–400 nm (Figure 20 B-D).

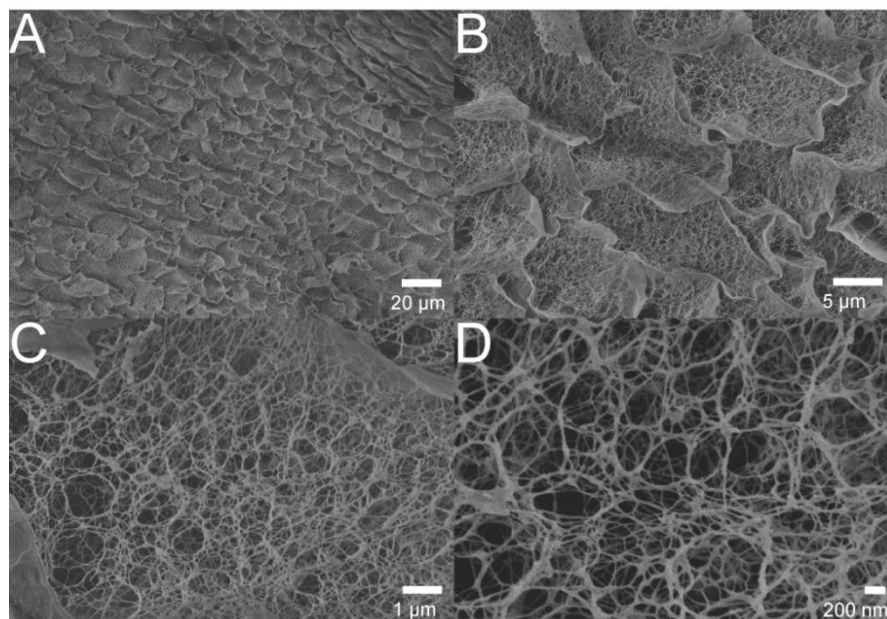


Figure 20: SEM images of a foam produced by freeze drying of a 3% (w/v) N[AS]₈C hydrogel.

These fibrous structures which are embedded in the stable porous scaffold might be suitable as a filter material or as a scaffold for tissue engineering.

4.7. Cell culture on structured films

Cell culture experiments of BALB/3T3 mouse fibroblasts as well as C2C12 mouse myoblasts on N[AS]₈C films cast from formic acid showed weak adhesion and proliferation (Figure 21 B and E). Most cells stayed round in shape and did not spread.

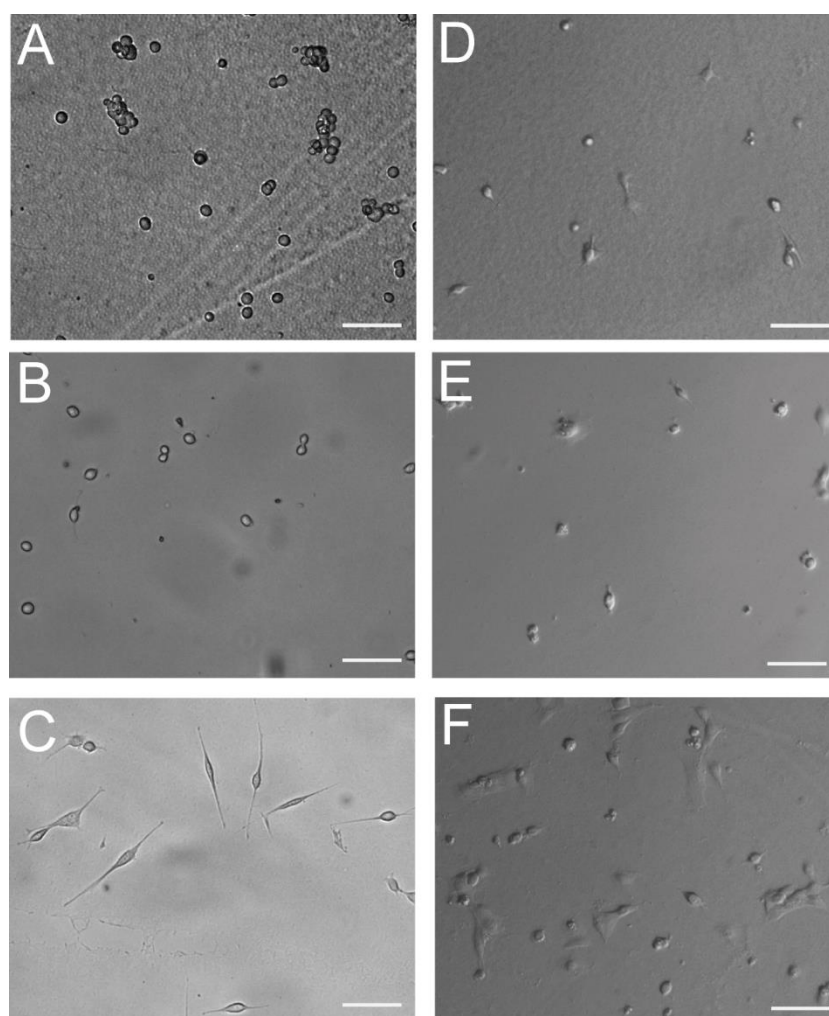


Figure 21: A-C: BALB/3T3 mouse fibroblasts cultured on films made of eADF4(C16) (A), N[AS]₈C (B), or ntag^{Cys}C16-c(RGDfK) (C) with a cell seeding density of 5000 cells/cm² after 24 hours of incubation. D-F: C2C12 myoblasts cultured on films made of eADF4(C16) (D), N[AS]₈C (E), or ntagCysC16-c(RGDfK) (F) with a cell seeding density of 5000 cells/cm² after 24 hours of incubation. Scale bars: 100 μm. Reproduced by permission of *The Royal Society of Chemistry*.

We intended to use this feature to create advanced films, with cell growth only on distinct areas and cell alignment which is crucial for many tissues in nature.

Therefore a layered, two protein film was created by first casting a film of ntag^{Cys}C16-c(RGDfK), an engineered, recombinant variant of a spider silk protein optimised for cell binding.¹⁰⁵ BALB/3T3 fibroblasts and C2C12 myoblasts adhered well to these films because of the integrin recognition motif RGD (Figure 21 C and F). After drying of the film a second layer out of N[AS]₈C was deposited by using a PDMS template (Figure 22). The second layer with a thickness of less than 1 µm did not cover the complete ntag^{Cys}C16-c(RGDfK) film, but small 20 µm wide strips were left without the second layer due to shielding from the PDMS template.

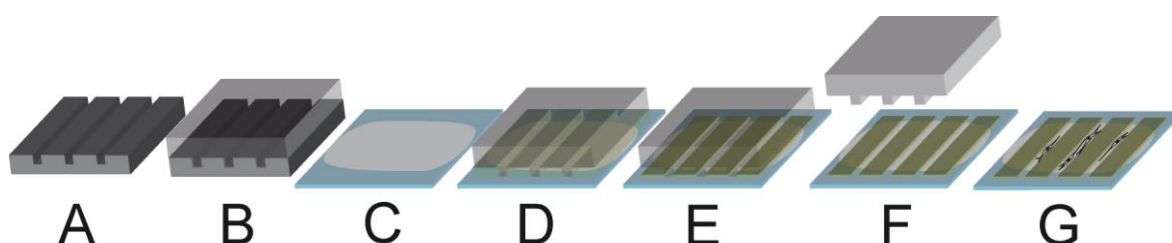


Figure 22: Production of patterned films (the ridges have a width of 50 µm and a height of less than 1 µm, whereas the grooves (i.e. spacings between the ridges) have a width of 20 µm): A: A silicon wafer was used as a template to process a PDMS stamp (B); C: A film was cast on a glass slide to form a ground layer; D: A PDMS stamp was placed on the ground layer protein film; E: A protein solution with a second protein was soaked into the channels of the PDMS stamp by capillary forces; F: After drying, the PDMS stamp was removed, leaving stripes of the second protein; G: Cells preferentially adhere and align on the ground layer but not on the ridges. Reproduced by permission of *The Royal Society of Chemistry*.

Table 5: Distribution of fibroblasts on patterned films consisting of two independent proteins. Most cells spread within the grooves. The first protein reflects the ground layer and the second the stripe material. Reproduced by permission of *The Royal Society of Chemistry*.

| | ntag ^{Cys} C16-c(RGDfK)/ N[AS] ₈ C | eADF4(C16)/ N[AS] ₈ C | eADF4(C16)/ eADF4(C16) |
|-------------------------------|---|-------------------------------------|---------------------------|
| Cells in the grooves | 85.5% | 78.8% | 63.2% |
| Cells per area in the grooves | 94.2% | 91.5% | 85.3% |

BALB/3T3 fibroblasts were cultured on such structured two protein films for 48 hours. Most cells adhered on the ntag^{Cys}C16-c(RGDfK) stripes and orient in the direction of the strip structure. Majority of the cells on the N[AS]₈C protein were round in shape and

non-adherent. 94% of the cells grew on the ntag^{Cys}C16-c(RGDfK) stripes (Table 5 and Figure 23).

Surprisingly fibroblasts grown on structured control films of unmodified eADF4(C16) with N[AS]₈C as a top layer and structured film only out of eADF4(C16) showed the same tendency of distribution with 92% respectively 85% of the fibroblasts in the grooves (Table 5 and Figure 23) but with much lower overall cell number on the solely eADF4(C16) films.

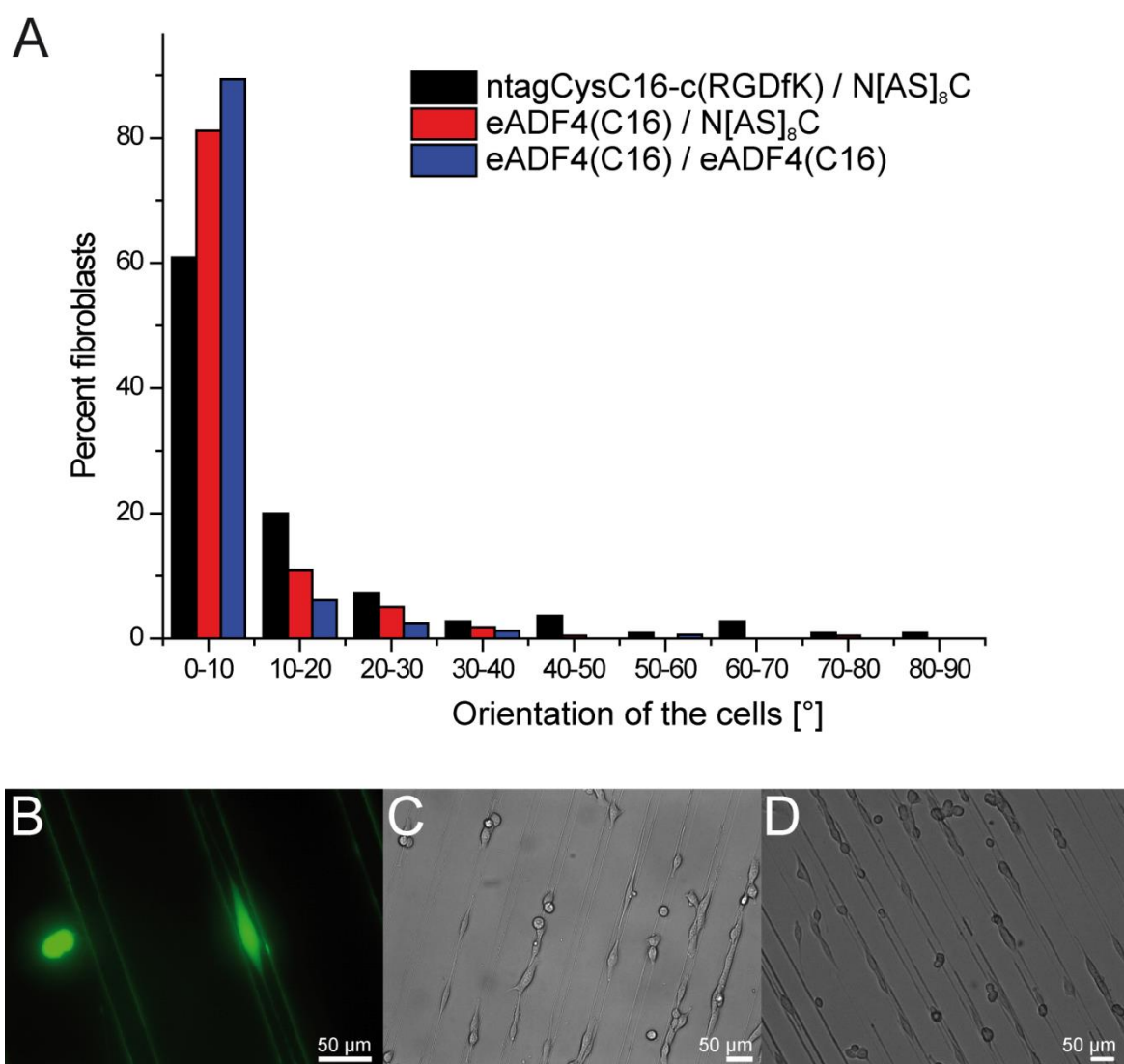


Figure 23: BALB/3T3 fibroblasts grown on structured films. A: Orientation of fibroblasts grown on patterned films made of different protein combinations (ground layer protein/ ridge protein) as depicted by the colour code after 48 hours of incubation; B: Fluorescence microscopy of calcein AM (Calcein acetoxymethyl ester) stained cells, grown on a film with ntag^{Cys}C16-c(RGDfK) as ground layer and N[AS]₈C as ridges; C and D: light microscopic image after 48 hours of incubation using ntag^{Cys}C16-c(RGDfK) as ground layer with N[AS]₈C as ridges (C) and eADF4(C16) as ground layer with N[AS]₈C as ridges (D). Adapted by permission of *The Royal Society of Chemistry*.

The orientation of the fibroblasts was most pronounced for films out of eADF4(C16) with 80.6% of the cells being oriented in an angle of $\pm 7.5^\circ$ to the structures axis whereas only 52.1% of the fibroblasts on ntag^{Cys}C16-c(RGDfK)/N[AS]₈C were in this range (Figure 23 A). This indicates the importance of the structure to orientate the cells while the materials/proteins properties influenced their location.

Even after 96 hours of cultivation the fibroblasts stayed mostly on the ntag^{Cys}C16-c(RGDfK) protein stripes and proliferated well to a high cell density (Figure 24 A). Such high cell densities are necessary for many tissue culture experiments, such as differentiation of myoblasts into myotubes.

C2C12 myoblasts showed the same tendency as the fibroblasts, but we were not able to count cells and measure their orientation to the scaffold due to their ability to form myotubes and higher cell density (Figure 24 B).

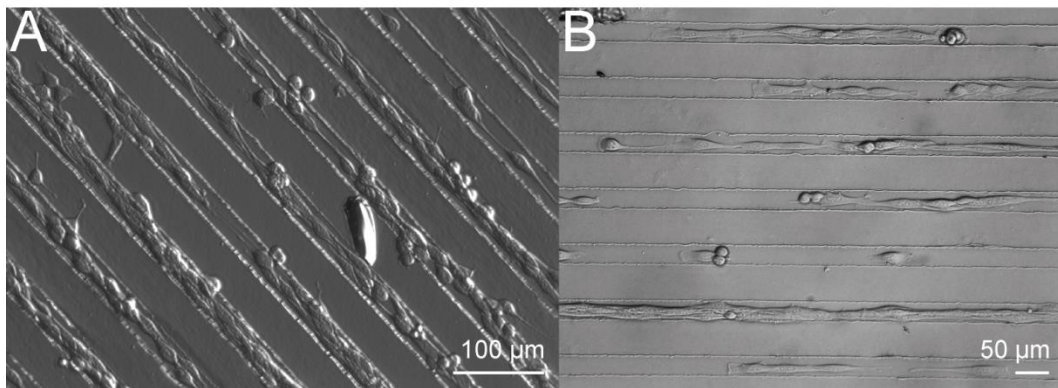


Figure 24: A: BALB/3T3 fibroblasts grown on structured films using eADF4(C16) as ground layer and N[AS]₈C as ridges after 96 hours of incubation; B: C2C12 myoblasts grown on eADF4(C16)/N[AS]₈C films after 48 hours of incubation. Reproduced by permission of *The Royal Society of Chemistry*.

Such films might be used in/as scaffolds for tissue engineering of tissues, where an ordered structure of the cells and high selective cell density is of advantage. Skeletal muscles as well as bone or epithelial cultures might be possible applications.

4.8. Individual contributions to joint publications

Chapter 7

Chapter 6 is reprinted with permission from *Biomacromolecules* (2012, 13, 3730-5).
Copyright 2012 American Chemical Society.

“Dependence of Mechanical Properties of Lacewing Egg Stalks on Relative Humidity”

By Felix Bauer, Luca Bertinetti, Admir Masic, and Thomas Scheibel

I carried out all of the measurements except the RAMAN measurements. Luca Bertinetti and Admir Masic performed the RAMAN measurements and corrected the manuscript. Felix Bauer and Thomas Scheibel wrote the manuscript.

Chapter 8

Chapter 7 is reproduced with permission from *Angewandte Chemie* (2012, 51, 6521-4).
Copyright 2012 WILEY-VCH Verlag GmbH & Co. KGaA, Weinheim.

“Artificial Egg Stalks Made of a Recombinantly Produced Silk Protein”

By Felix Bauer and Thomas Scheibel

I carried out all the design, cloning, fermentation, purification and measurements. Felix Bauer and Thomas Scheibel wrote the manuscript.

Chapter 9

Chapter 8 is reproduced by permission of *The Royal Society of Chemistry*. This work is submitted for publication: *Biomaterials Science* (2013, 1,1244-9).

“Controllable cell adhesion, growth and orientation on layered silk protein films”

By Felix Bauer, Stefanie Wohlrab, and Thomas Scheibel.

I developed the technique to fabricate the striped protein films, and carried out the image analysis after cell culture. Stefanie Wohlrab carried out the cell culture experiments. Felix Bauer, Stefanie Wohlrab and Thomas Scheibel wrote the manuscript.

5. Literature

1. Sutherland, T. D.; Young, J. H.; Weisman, S.; Hayashi, C. Y.; Merritt, D. J., Insect silk: One name, many materials. *Annual Review of Entomology* 2010, 55, 171-188.
2. Aprhisiart, A.; Vollrath, F., Design-Features of the Orb Web of the Spider, *Araneus-Diadematus*. *Behavioral Ecology* 1994, 5, (3), 280-287.
3. Vollrath, F., General-Properties of Some Spider Silks. *Silk Polymers* 1994, 544, 17-28.
4. Zschokke, S.; Vollrath, F., Web Construction Patterns in a Range of Orb-Weaving Spiders (Araneae). *European Journal of Entomology* 1995, 92, (3), 523-541.
5. Vollrath, F.; Holtet, T.; Thogersen, H. C.; Frische, S., Structural organization of spider silk. *Proceedings of the Royal Society of London Series B-Biological Sciences* 1996, 263, (1367), 147-151.
6. Yang, Y. M.; Chen, X. M.; Ding, F.; Zhang, P. Y.; Liu, J.; Go, X. S., Biocompatibility evaluation of silk fibroin with peripheral nerve tissues and cells in vitro. *Biomaterials* 2007, 28, (9), 1643-1652.
7. Hardy, J. G.; Romer, L. M.; Scheibel, T. R., Polymeric materials based on silk proteins. *Polymer* 2008, 49, (20), 4309-4327.
8. Leal-Egana, A.; Scheibel, T., Silk-based materials for biomedical applications. *Biotechnology and Applied Biochemistry* 2010, 55, 155-167.
9. Weisman, S.; Okada, S.; Mudie, S. T.; Huson, M. G.; Trueman, H. E.; Srisantha, A.; Haritos, V. S.; Sutherland, T. D., Fifty years later: The sequence, structure and function of lacewing cross-beta silk. *Journal of Structural Biology* 2009, 168, (3), 467-475.
10. Craig, C. L., Evolution of arthropod silks. *Annual Review of Entomology* 1997, 42, 231-67.
11. Vollrath, F.; Porter, D., Spider silk as archetypal protein elastomer. *Soft Matter* 2006, 2, (5), 377-385.
12. Allmeling, C.; Jokuszies, A.; Reimers, K.; Kall, S.; Vogt, P. M., Use of spider silk fibres as an innovative material in a biocompatible artificial nerve conduit. *Journal of Cellular and Molecular Medicine* 2006, 10, (3), 770-777.
13. Vollrath, F.; Edmonds, D. T., Modulation of the mechanical properties of spider silk by coating with water. *Nature* 1989, 340, (6231), 305-307.

14. Vollrath, F.; Madsen, B.; Shao, Z. Z., The effect of spinning conditions on the mechanics of a spider's dragline silk. *Proceedings of the Royal Society of London Series B-Biological Sciences* 2001, 268, (1483), 2339-2346.
15. Gerritsen, V. B., The tiptoe of an airbus. *Protein Spotlight, Swiss Prot* 2002, 24, 1-2.
16. Foelix, R. F., *The Biology of spiders*. Harvard Univ. Press: Cambridge, MA, 1982.
17. Alstad, D. N., Particle-Size, Resource Concentration, and the Distribution of Net-Spinning Caddisflies. *Oecologia* 1987, 71, (4), 525-531.
18. Stehr, F. W., *Immature Insects*. Kendall/Hunt: Dubuque, IA, 1987; Vol. 1, 2.
19. Craig, C. L., Predator Foraging Behavior in Response to Perception and Learning by Its Prey - Interactions between Orb-Spinning Spiders and Stingless Bees. *Behavioral Ecology and Sociobiology* 1994, 35, (1), 45-52.
20. Yonemura, N.; Sehnal, F.; Mita, K.; Tamura, T., Protein composition of silk filaments spun under water by caddisfly larvae. *Biomacromolecules* 2006, 7, (12), 3370-8.
21. Weisman, S.; Trueman, H. E.; Mudie, S. T.; Church, J. S.; Sutherland, T. D.; Haritos, V. S., An Unlikely Silk: The Composite Material of Green Lacewing Cocoons. *Biomacromolecules* 2008, 9, (11), 3065-3069.
22. Greenstone, M. H., Ballooning Frequency and Habitat Predictability in 2 Wolf Spider Species (Lycosidae, Pardosa). *Florida Entomologist* 1982, 65, (1), 83-89.
23. Kovoov, J., Comparative structure and histochemistry of silk-producing organs in arachnids. In *Ecophysiology of spiders*, Nentwig, W., Ed. Springer-Verlag: New York, 1987; pp 160-186.
24. Nentwig, W.; Heimers, S., Ecological aspects of spider webs. In *Ecophysiology of spiders*, Nentwig, W., Ed. Springer-Verlag: New York, 1987; pp 211-225.
25. Smith, G. B.; Watson, J. A. L., *Thysanura zygantoma* (Silverfish). In *Insects of australia*, Naumann, I. D.; Carne, P. B.; Lawrence, J. F.; Nielsen, E. S.; Spradbery, J. P., Eds. Cornell Univ. Press: Ithaca, NY, 1991; Vol. 1, 2.
26. Lucas, F.; Rudall, K. M., Extracellular fibrous proteins: the silks. In *Comprehensive Biochemistry*, Florkin, M.; Stotz, E. H., Eds. Elsevier: Amsterdam, 1968; pp 475-558.
27. Rudall, K. M., Silk and other cocoon proteins In *Comparative Biochemistry*, Florkin, M.; Mason, H. S., Eds. Academic: New York, 1962; Vol. IV, pp 397-433.
28. Rudall, K. M.; Kenching, W., Arthropod Silks - Problem of Fibrous Proteins in Animal Tissues. *Annual Review of Entomology* 1971, 16, 73-97.

29. Voet, D.; Voet, J. G., *Biochemistry*. 2nd ed.; Wiley & Sons: New York, 1995; p 1361.
30. Chothia, C.; Levitt, M.; Richardson, D., Helix to helix packing in proteins. *Journal of Molecular Biology* 1981, 145, (1), 215-50.
31. Woolfson, D. N., The design of coiled-coil structures and assemblies. *Fibrous Proteins: Coiled-Coils, Collagen and Elastomers* 2005, 70, 79-112.
32. Lawrence, W.; Foil, L. D., The effects of diet upon pupal development and cocoon formation by the cat flea (Siphonaptera: Pulicidae). *Journal of vector ecology : journal of the Society for Vector Ecology* 2002, 27, (1), 39-43.
33. Silverman, J.; Rust, M. K.; Reiersen, D. A., Influence of Temperature and Humidity on Survival and Development of the Cat Flea, *Ctenocephalides-Felis* (Siphonaptera, Pulicidae). *Journal of Medical Entomology* 1981, 18, (1), 78-83.
34. Sezutsu, H.; Kajiwarra, H.; Kojima, K.; Mita, K.; Tamura, T.; Tamada, Y.; Kameda, T., Identification of four major hornet silk genes with a complex of alanine-rich and serine-rich sequences in *Vespa simillima xanthoptera cameron*. *Bioscience Biotechnology and Biochemistry* 2007, 71, (11), 2725-2734.
35. Sutherland, T. D.; Campbell, P. M.; Weisman, S.; Trueman, H. E.; Sriskantha, A.; Wanjura, W. J.; Haritos, V. S., A highly divergent gene cluster in honey bees encodes a novel silk family. *Genome Research* 2006, 16, (11), 1414-1421.
36. Sutherland, T. D.; Weisman, S.; Trueman, H. E.; Sriskantha, A.; Trueman, J. W.; Haritos, V. S., Conservation of essential design features in coiled coil silks. *Molecular biology and evolution* 2007, 24, (11), 2424-32.
37. Lucas, F.; Shaw, J. T.; Smith, S. G., Comparative studies of fibroins. I. The amino acid composition of various fibroins and its significance in relation to their crystal structure and taxonomy. *Journal of Molecular Biology* 1960, 2, 339-49.
38. Warwicker, J. O., Comparative studies of fibroins. II. The crystal structures of various fibroins. *Journal of Molecular Biology* 1960, 2, 350-62.
39. Mita, K.; Ichimura, S.; James, T. C., Highly Repetitive Structure and Its Organization of the Silk Fibroin Gene. *Journal of Molecular Evolution* 1994, 38, (6), 583-592.
40. Tanaka, K.; Inoue, S.; Mizuno, S., Hydrophobic interaction of P25, containing Asn-linked oligosaccharide chains, with the H-L complex of silk fibroin produced by *Bombyx mori*. *Insect Biochemistry and Molecular Biology* 1999, 29, (3), 269-276.
41. Tanaka, K.; Kajiyama, N.; Ishikura, K.; Waga, S.; Kikuchi, A.; Ohtomo, K.; Takagi, T.; Mizuno, S., Determination of the site of disulfide linkage between heavy and light chains of

silk fibroin produced by *Bombyx mori*. *Biochimica Et Biophysica Acta* 1999, 1432, (1), 92-103.

42. Tanaka, K.; Mizuno, S., Homologues of fibroin L-chain and P25 of *Bombyx mori* are present in *Dendrolimus spectabilis* and *Papilio xuthus* but not detectable in *Antheraea yamamai*. *Insect Biochemistry and Molecular Biology* 2001, 31, (6-7), 665-77.

43. Yonemura, N.; Sehna, F., The design of silk fiber composition in moths has been conserved for more than 150 million years. *Journal of Molecular Evolution* 2006, 63, (1), 42-53.

44. Zhou, C. Z.; Confalonieri, F.; Medina, N.; Zivanovic, Y.; Esnault, C.; Yang, T.; Jacquet, M.; Janin, J.; Duguet, M.; Perasso, R.; Li, Z. G., Fine organization of *Bombyx mori* fibroin heavy chain gene. *Nucleic acids research* 2000, 28, (12), 2413-9.

45. Chang, J. C.; Gurr, G. M.; Fletcher, M. J.; Gilbert, R. G., Structure-property and structure-function relations of leafhopper (*Kahaono montana*) silk. *Australian Journal of Chemistry* 2006, 59, (8), 579-585.

46. Fletcher, M. J.; Kent, D. S., Feeding by *Kahaono* leafhoppers in silken shelters (Hemiptera: Cicadellidae: Typhlocybinae: Dikraneurini). *Aust. Entomol.* 2002, 29, 115-118.

47. Geddes, A. J.; Parker, K. D.; Atkins, E. D.; Beighton, E., "Cross-beta" conformation in proteins. *Journal of Molecular Biology* 1968, 32, (2), 343-58.

48. Kenchington, W., The Larval Silk of *Hypera* Spp (Coleoptera, Curculionidae) - a New Example of the Cross-Beta Protein Conformation in an Insect Silk. *Journal of Insect Physiology* 1983, 29, (4), 355-361.

49. Turner, C. H., Notes on the behavior of the ant-lion with emphasis on the feeding activities and letisimulation. *Biol. Bull.* 1915, 29, 277-307.

50. Wright, J. C., Myriapoda (Including Centipedes and Millipedes). In *eLS*, John Wiley & Sons, Ltd: 2012.

51. Hu, X.; Vasanthavada, K.; Kohler, K.; McNary, S.; Moore, A. M.; Vierra, C. A., Molecular mechanisms of spider silk. *Cell Mol Life Sci* 2006, 63, (17), 1986-99.

52. Römer, L.; Scheibel, T., The Elaborate Structure of Spider Silk: Structure and Function of a Natural High Performance Fiber. In *Fibrous Proteins*, 1 ed.; Scheibel, T., Ed. Landis Bioscience: Austin, Texas, USA, 2008.

53. Gosline, J. M.; Guerette, P. A.; Ortlepp, C. S.; Savage, K. N., The mechanical design of spider silks: from fibroin sequence to mechanical function. *The Journal of experimental biology* 1999, 202, (Pt 23), 3295-303.

54. Vollrath, F.; Knight, D. P., Structure and function of the silk production pathway in the spider *Nephila edulis*. *International Journal of Biological Macromolecules* 1999, 24, (2-3), 243-249.
55. Winkler, S.; Kaplan, D. L., Molecular biology of spider silk. *Journal of Biotechnology* 2000, 74, (2), 85-93.
56. Hagn, F.; Eisoldt, L.; Hardy, J. G.; Vendrely, C.; Coles, M.; Scheibel, T.; Kessler, H., A conserved spider silk domain acts as a molecular switch that controls fibre assembly. *Nature* 2010, 465, (7295), 239-242.
57. Hagn, F.; Thamm, C.; Scheibel, T.; Kessler, H., pH-dependent dimerization and salt-dependent stabilization of the N-terminal domain of spider dragline silk – implications for fiber formation. *Angewandte Chemie International Edition* 2010.
58. Landreh, M.; Askarieh, G.; Nordling, K.; Hedhammar, M.; Rising, A.; Casals, C.; Astorga-Wells, J.; Alvelius, G.; Knight, S. D.; Johansson, J.; Jörnvall, H.; Bergman, T., A pH-dependent dimer lock in spider silk protein. *Journal of Molecular Biology* 2010, 404, (2), 328-336.
59. Fox, L. R., Cannibalism in Natural-Populations. *Annual Review of Ecology and Systematics* 1975, 6, 87-106.
60. Sehnaal, F.; Akai, H., Insect Silk Glands - Their Types, Development and Function, and Effects of Environmental-Factors and Morphogenetic Hormones on Them. *International Journal of Insect Morphology & Embryology* 1990, 19, (2), 79-132.
61. Adachi, T.; Tomita, M.; Shimizu, K.; Ogawa, S.; Yoshizato, K., Generation of hybrid transgenic silkworms that express Bombyx mori prolyl-hydroxylase alpha-subunits and human collagens in posterior silk glands: Production of cocoons that contained collagens with hydroxylated proline residues. *Journal of Biotechnology* 2006, 126, (2), 205-219.
62. Iizuka, E.; Hachimori, A.; Abe, K.; Sunohara, M.; Hiraide, Y.; Ueyama, A.; Kamo, K.; Fujiwara, T.; Nakamura, F.; Uno, T., Comparative-Study on the Mechanical Property of Silk Thread from Cocoons of Bombyx-Mori-L. *Biorheology* 1983, 20, (5), 459-470.
63. Zhao, H. P.; Feng, X. Q.; Cui, W. Z.; Zou, F. Z., Mechanical properties of silkworm cocoon pelades. *Engineering Fracture Mechanics* 2007, 74, (12), 1953-1962.
64. Zhao, H.-P.; Feng, X.-Q.; Yu, S.-W.; Cui, W.-Z.; Zou, F.-Z., Mechanical properties of silkworm cocoons. *Polymer* 2005, 46, (21), 9192-9201.
65. Shukla, S. R.; Mathur, M.; Narayan, A.; Saligram, A. N., Efficiencies of Silk Degumming Process. *Colourage* 1992, 39, (4), 31-33.

66. Prabhu, J.; Sreesha, S.; Somashekar, T. H., Partial degumming of raw mulberry silkndasha novel approach in achieving quality and economics in dyeing. *Journal of the Society of Dyers and Colourists* 1995, 111, (7-8), 245-247.
67. Gulrajani, M. L.; Arora, S.; Aggarwal, S., Degummase treatment of spun silk fabric. *Indian Journal of Fibre & Textile Research* 1997, 22, (2), 119-123.
68. Freddi, G.; Mossotti, R.; Innocenti, R., Degumming of silk fabric with several proteases. *Journal of Biotechnology* 2003, 106, (1), 101-112.
69. R. Mossotti, R. I. M. Z. A. A. G. F., The degumming of silk fabrics: a preliminary near infrared spectroscopy study. *Journal of Near Infrared Spectroscopy* 2006, 14, (3), 201-208.
70. Inoue, S.; Tanaka, K.; Arisaka, F.; Kimura, S.; Ohtomo, K.; Mizuno, S., Silk fibroin of Bombyx mori is secreted, assembling a high molecular mass elementary unit consisting of H-chain, L-chain, and P25, with a 6 : 6 : 1 molar ratio. *Journal of Biological Chemistry* 2000, 275, (51), 40517-40528.
71. Sehna, F.; Zurovec, M., Construction of silk fiber core in lepidoptera. *Biomacromolecules* 2004, 5, (3), 666-74.
72. Perez-Rigueiro, J.; Viney, C.; Llorca, J.; Elices, M., Mechanical properties of single-brin silkworm silk. *Journal of Applied Polymer Science* 2000, 75, (10), 1270-1277.
73. Iizuka, E., Conformation of Silk Sericine in Solution, Bombyx Mori L. *Biochimica Et Biophysica Acta* 1969, 181, (2), 477-479.
74. Akai, H., Electron-Microscopic Observations on Secretions of Sericins in Silk Gland in Bombyx-Mori. *Journal of Electron Microscopy* 1977, 26, (3), 226-227.
75. Tsukada, M.; Komoto, T.; Kawai, T., Conformation of Liquid Silk Sericin. *Polymer Journal* 1979, 11, (6), 503-505.
76. Kaplan, D.; Adams, W. W.; Farmer, B.; Viney, C., Silk - Biology, Structure, Properties, and Genetics. *Silk Polymers* 1994, 544, 2-16.
77. Weisman, S.; Haritos, V. S.; Church, J. S.; Huson, M. G.; Mudie, S. T.; Rodgers, A. J.; Dumsday, G. J.; Sutherland, T. D., Honeybee silk: recombinant protein production, assembly and fiber spinning. *Biomaterials* 2010, 31, (9), 2695-700.
78. Daly, H. V.; Doyen, J. T.; Purcell III, A. H., 45. Trichoptera (caddisflies). In *Introduction to Insect Biology and Diversity*, 2. ed.; Oxford University Press: New York, 1998; pp 559-569.

79. Mey, W., Ordnung Trichoptera, Köcherfliegen. In *Lehrbuch der Speziellen Zoologie*, Dathe, H. H., Ed. Spektrum Akademischer Verlag Heidelberg: Berlin, 2003; Vol. 1.
80. Engster, M. S., Studies on silk secretion in the Trichoptera (F. Limmephilidae). II. Structure and amino acid composition of the silk. *Cell and tissue research* 1976, 169, (1), 77-92.
81. Wang, Y.; Sanai, K.; Wen, H.; Zhao, T.; Nakagaki, M., Characterization of unique heavy chain fibroin filaments spun underwater by the caddisfly *Stenopsyche marmorata* (Trichoptera; Stenopsychidae). *Molecular biology reports* 2010, 37, (6), 2885-92.
82. Stewart, R. J.; Wang, C. S., Adaptation of caddisfly larval silks to aquatic habitats by phosphorylation of h-fibroin serines. *Biomacromolecules* 2010, 11, (4), 969-74.
83. Smith, S. V.; Correia, J. J.; Case, S. T., Disulfide bonds in a recombinant protein modeled after a core repeat in an aquatic insect's silk protein. *Protein science : a publication of the Protein Society* 1995, 4, (5), 945-54.
84. Wellman, S. E.; Case, S. T., Disassembly and reassembly in vitro of complexes of secretory proteins from *Chironomus tentans* salivary glands. *The Journal of biological chemistry* 1989, 264, (18), 10878-83.
85. Duelli, P., A Missing Link in the Evolution of the Egg Pedicel in Lacewings. *Experientia* 1986, 42, (6), 624-624.
86. Eisner, T.; Attygalle, A. B.; Conner, W. E.; Eisner, M.; MacLeod, E.; Meinwald, J., Chemical egg defense in a green lacewing (*Ceraeochrysa smithi*). *Proceedings of the National Academy of Sciences of the United States of America* 1996, 93, (8), 3280-3283.
87. Ruzicka, Z., Protective role of the egg stalk in Chrysopidae (Neuroptera). *European Journal of Entomology* 1997, 94, (1), 111-114.
88. La Munyon, C., Hindgut changes preceding pupation and related cocoon structure in *Chrysoperla comanche* Banks (Neuroptera, Chrysopidae). *Psyche* 1988, 95, 203-209.
89. Lucas, F.; Shaw, J. T. B.; Smith, S. G., Amino-Acid Composition of the Silk of *Chrysopa* Egg-Stalks. *Nature* 1957, 179, (4566), 906-907.
90. Parker, K. D.; Rudall, K. M., Structure of the silk of *chrysopa* egg-stalks. *Nature* 1957, 179, (4566), 905-906.
91. Exler, J. H.; Hummerich, D.; Scheibel, T., The amphiphilic properties of spider silks are important for spinning. *Angewandte Chemie-International Edition* 2007, 46, (19), 3559-3562.

92. Rammensee, S.; Slotta, U.; Scheibel, T.; Bausch, A. R., Assembly mechanism of recombinant spider silk proteins. *Proceedings of the National Academy of Sciences of the United States of America* 2008, 105, (18), 6590-6595.
93. Vollrath, F.; Knight, D. P.; Hu, X. W., Silk production in a spider involves acid bath treatment. *Proceedings of the Royal Society of London Series B-Biological Sciences* 1998, 265, (1398), 817-820.
94. Dicko, C.; Kenney, J. M.; Knight, D.; Vollrath, F., Transition to a beta-sheet-rich structure in spidroin in vitro: The effects of pH and cations. *Biochemistry* 2004, 43, (44), 14080-14087.
95. Dicko, C.; Vollrath, F.; Kenney, J. M., Spider silk protein refolding is controlled by changing pH. *Biomacromolecules* 2004, 5, (3), 704-710.
96. Knight, D. P.; Vollrath, F., Changes in element composition along the spinning duct in a *Nephila* spider. *Naturwissenschaften* 2001, 88, (4), 179-82.
97. Knight, D. P.; Vollrath, F., Liquid crystals and flow elongation in a spider's silk production line. *Proceedings of the Royal Society of London Series B-Biological Sciences* 1999, 266, (1418), 519-523.
98. Perez-Rigueiro, J.; Elices, M.; Llorca, J.; Viney, C., Tensile properties of silkworm silk obtained by forced silking. *Journal of Applied Polymer Science* 2001, 82, (8), 1928-1935.
99. Perez-Riguero, J.; Elices, M.; Llorca, J.; Viney, C., Tensile properties of *Argiope trifasciata* drag line silk obtained from the spider's web. *Journal of Applied Polymer Science* 2001, 82, (9), 2245-2251.
100. Tillinghast, E. K.; Chase, S. F.; Townley, M. A., Water Extraction by the Major Ampullate Duct during Silk Formation in the Spider, *Argiope-Aurantia* Lucas. *Journal of Insect Physiology* 1984, 30, (7), 591-596.
101. Panzitta, D. Charakterisierung des Eistiels und der Eiablage von *Chrysoperla carnea* (Stephens). Technische Universität, München, 2009.
102. Bitsch, J., Anatomy of Adult Chrysopidae. In *Biology of Chrysopidae*, Canard, M.; Séméria, Y., Eds. Dr W. Junk Publisher: The Hague, 1984; pp 29-35.
103. Hepburn, H. R.; Chandler, H. D.; Davidoff, M. R., Extensomeric properties of insect fibroins: The green lacewing cross- β , honeybee α -helical and greater waxmoth parallel- β conformations. *Insect Biochemistry* 1979, 9, 69-77.

104. Nordlund, D. A.; Cohen, A. C.; Smith, R. A., Mass-rearing, release techniques, and augmentation. In *Lacewing in the crop environment*, McEwen, P.; New, T.; Whittington, A., Eds. Cambridge University Press: Cambridge 2007.
105. Wohlrab, S.; Muller, S.; Schmidt, A.; Neubauer, S.; Kessler, H.; Leal-Egana, A.; Scheibel, T., Cell adhesion and proliferation on RGD-modified recombinant spider silk proteins. *Biomaterials* 2012, 33, (28), 6650-9.
106. Bini, E.; Foo, C. W. P.; Huang, J.; Karageorgiou, V.; Kitchel, B.; Kaplan, D. L., RGD-functionalized bioengineered spider dragline silk biomaterial. *Biomacromolecules* 2006, 7, (11), 3139-3145.
107. Yao, J. M.; Zhu, Y. Q.; Li, Y.; Li, L., Solid-state structure of Bombyx mori silk fibroin-RGD fusion proteins and their cell adhesive ability. *Acta Chimica Sinica* 2006, 64, (12), 1273-1278.
108. Fahnestock, S. R.; Irwin, S. L., Synthetic spider dragline silk proteins and their production in Escherichia coli. *Applied Microbiology and Biotechnology* 1997, 47, (1), 23-32.
109. Huemmerich, D. Design, Synthese und Analyse von Spinnenseidenproteinen. TU München, München, 2004.
110. Xia, X. X.; Qian, Z. G.; Ki, C. S.; Park, Y. H.; Kaplan, D. L.; Lee, S. Y., Native-sized recombinant spider silk protein produced in metabolically engineered Escherichia coli results in a strong fiber. *Proceedings of the National Academy of Sciences of the United States of America* 2010, 107, (32), 14059-14063.
111. Lewis, R. V.; Hinman, M.; Kothakota, S.; Fournier, M. J., Expression and purification of a spider silk protein: A new strategy for producing repetitive proteins. *Protein Expression and Purification* 1996, 7, (4), 400-406.
112. Hedhammar, M.; Rising, A.; Grip, S.; Martinez, A. S.; Nordling, K.; Casals, C.; Stark, M.; Johansson, J., Structural properties of recombinant nonrepetitive and repetitive parts of major ampullate spidroin 1 from *Euprosthenois australis*: Implications for fiber formation. *Biochemistry* 2008, 47, (11), 3407-3417.
113. Arcidiacono, S.; Mello, C.; Kaplan, D.; Cheley, S.; Bayley, H., Purification and characterization of recombinant spider silk expressed in *Escherichia coli*. *Applied Microbiology and Biotechnology* 1998, 49, (1), 31-38.
114. Rising, A.; Widhe, M.; Johansson, J.; Hedhammar, M., Spider silk proteins: recent advances in recombinant production, structure–function relationships and biomedical applications. *Cellular and Molecular Life Sciences* 2011, 68, (2), 169-184.

115. Rosenberg, A. H.; Goldman, E.; Dunn, J. J.; Studier, F. W.; Zubay, G., Effects of consecutive AGG codons on translation in *Escherichia coli*, demonstrated with a versatile codon test system. *J. Bacteriol.* 1993, 175, 716-722.
116. Lock, R. L. Process for making silk fibroin fibers. 1993.
117. Trabbic, K. A.; Yager, P., Comparative structural characterization of naturally- and synthetically-spun fibers of *Bombyx mori* fibroin. *Macromolecules* 1998, 31, (2), 462-471.
118. Yao, J. M.; Masuda, H.; Zhao, C. H.; Asakura, T., Artificial spinning and characterization of silk fiber from *Bombyx mori* silk fibroin in hexafluoroacetone hydrate. *Macromolecules* 2002, 35, (1), 6-9.
119. Phillips, D. M.; Drummy, L. F.; Conrady, D. G.; Fox, D. M.; Naik, R. R.; Stone, M. O.; Trulove, P. C.; De Long, H. C.; Mantz, R. A., Dissolution and regeneration of *Bombyx mori* silk fibroin using ionic liquids. *Journal of the American Chemical Society* 2004, 126, (44), 14350-14351.
120. Phillips, D. M.; Drummy, L. F.; Naik, R. R.; De Long, H. C.; Fox, D. M.; Trulove, P. C.; Mantz, R. A., Regenerated silk fiber wet spinning from an ionic liquid solution. *Journal of Materials Chemistry* 2005, 15, (39), 4206-4208.
121. Seidel, A.; Liivak, O.; Jelinski, L. W., Artificial spinning of spider silk. *Macromolecules* 1998, 31, (19), 6733-6736.
122. Seidel, A.; Liivak, O.; Calve, S.; Adaska, J.; Ji, G. D.; Yang, Z. T.; Grubb, D.; Zax, D. B.; Jelinski, L. W., Regenerated spider silk: Processing, properties, and structure. *Macromolecules* 2000, 33, (3), 775-780.
123. Islam, S.; Karatzas, C.; Rodenhiser, A.; Alwattari, A.; Huang, Y.; Turcotte, C. Methods and apparatus for spinning spider silk protein. 2006.
124. Arcidiacono, S.; Mello, C. M.; Butler, M.; Welsh, E.; Soares, J. W.; Allen, A.; Ziegler, D.; Laue, T.; Chase, S., Aqueous processing and fiber spinning of recombinant spider silks. *Macromolecules* 2002, 35, (4), 1262-1266.
125. Lazaris, A.; Arcidiacono, S.; Huang, Y.; Zhou, J. F.; Duguay, F.; Chretien, N.; Welsh, E. A.; Soares, J. W.; Karatzas, C. N., Spider silk fibers spun from soluble recombinant silk produced in mammalian cells. *Science* 2002, 295, (5554), 472-476.
126. Kinahan, M. E.; Filippidi, E.; Koster, S.; Hu, X.; Evans, H. M.; Pfohl, T.; Kaplan, D. L.; Wong, J., Tunable silk: using microfluidics to fabricate silk fibers with controllable properties. *Biomacromolecules* 2011, 12, (5), 1504-11.

127. Wang, H.; Zhang, Y. P.; Shao, H. L.; Hu, X. C., Electrospun ultra-fine silk fibroin fibers from aqueous solutions. *Journal of Materials Science* 2005, 40, (20), 5359-5363.
128. Wang, H.; Shao, H. L.; Hu, X. C., Structure of silk fibroin fibers made by an electrospinning process from a silk fibroin aqueous solution. *Journal of Applied Polymer Science* 2006, 101, (2), 961-968.
129. Zarkoob, S.; Reneker, D. H.; Ertley, D.; Eby, R. K.; D., H. S. Synthetically spun silk nanofibers and a process for making the same. 2000.
130. Ohgo, K.; Zhao, C. H.; Kobayashi, M.; Asakura, T., Preparation of non-woven nanofibers of Bombyx mori silk, Samia cynthia ricini silk and recombinant hybrid silk with electrospinning method. *Polymer* 2003, 44, (3), 841-846.
131. Leal-Egana, A.; Lang, G.; Mauerer, C.; Wickinghoff, J.; Weber, M.; Geimer, S.; Scheibel, T., Interactions of Fibroblasts with Different Morphologies Made of an Engineered Spider Silk Protein. *Advanced Engineering Materials* 2012, 14, (3), B67-B75.
132. Cappello, J.; Mcgrath, K. P., Spinning of Protein Polymer Fibers. *Silk Polymers* 1994, 544, 311-327.
133. Teule, F.; Furin, W. A.; Cooper, A. R.; Duncan, J. R.; Lewis, R. V., Modifications of spider silk sequences in an attempt to control the mechanical properties of the synthetic fibers. *Journal of Materials Science* 2007, 42, (21), 8974-8985.
134. Keerl, D.; Scheibel, T., Characterization of natural and biomimetic spider silk fibers. *Bioinspired, Biomimetic and Nanobiomaterials* 2012, 1, (2), 83-94.
135. Peng, H.; Zhou, S.; Jiang, J.; Guo, T.; Zheng, X.; Yu, X., Pressure-induced crystal memory effect of spider silk proteins. *The journal of physical chemistry. B* 2009, 113, (14), 4636-41.
136. Zhang, X.; Reagan, M. R.; Kaplan, D. L., Electrospun silk biomaterial scaffolds for regenerative medicine. *Adv Drug Deliv Rev* 2009, 61, (12), 988-1006.
137. Shchepelina, O.; Drachuk, I.; Gupta, M. K.; Lin, J.; Tsukruk, V. V., Silk-on-silk layer-by-layer microcapsules. *Advanced Materials* 2011, 23, (40), 4655-60.
138. Hermanson, K. D.; Huemmerich, D.; Scheibel, T.; Bausch, A. R., Engineered microcapsules fabricated from reconstituted spider silk. *Advanced Materials* 2007, 19, (14), 1810-1815.
139. Hermanson, K. D.; Harasim, M. B.; Scheibel, T.; Bausch, A. R., Permeability of silk microcapsules made by the interfacial adsorption of protein. *Physical Chemistry Chemical Physics* 2007, 9, (48), 6442-6446.

140. Pritchard, E. M.; Dennis, P. B.; Omenetto, F.; Naik, R. R.; Kaplan, D. L., Review physical and chemical aspects of stabilization of compounds in silk. *Biopolymers* 2012, 97, (6), 479-98.
141. Zhang, J.; Pritchard, E.; Hu, X.; Valentin, T.; Panilaitis, B.; Omenetto, F. G.; Kaplan, D. L., Stabilization of vaccines and antibiotics in silk and eliminating the cold chain. *Proceedings of the National Academy of Sciences of the United States of America* 2012, 109, (30), 11981-6.
142. Megeed, Z.; Cappello, J.; Ghandehari, H., Genetically engineered silk-elastinlike protein polymers for controlled drug delivery. *Advanced Drug Delivery Reviews* 2002, 54, (8), 1075-1091.
143. Dinerman, A. A.; Cappello, J.; Ghandehari, H.; Hoag, S. W., Solute diffusion in genetically engineered silk-elastinlike protein polymer hydrogels. *Journal of Controlled Release* 2002, 82, (2-3), 277-287.
144. Dinerman, A. A.; Cappello, J.; Ghandehari, H.; Hoag, S. W., Swelling behavior of a genetically engineered silk-elastinlike protein polymer hydrogel. *Biomaterials* 2002, 23, (21), 4203-4210.
145. Nagarsekar, A.; Crissman, J.; Crissman, M.; Ferrari, F.; Cappello, J.; Ghandehari, H., Genetic engineering of stimuli-sensitive silk-elastin-like protein block copolymers. *Biomacromolecules* 2003, 4, (3), 602-7.
146. Megeed, Z.; Cappello, J.; Ghandehari, H., Thermal analysis of water in silk-elastinlike hydrogels by differential scanning calorimetry. *Biomacromolecules* 2004, 5, (3), 793-7.
147. Megeed, Z.; Haider, M.; Li, D.; O'Malley, B. W., Jr.; Cappello, J.; Ghandehari, H., In vitro and in vivo evaluation of recombinant silk-elastinlike hydrogels for cancer gene therapy. *Journal of controlled release : official journal of the Controlled Release Society* 2004, 94, (2-3), 433-45.
148. Dandu, R.; Megeed, Z.; Haider, M.; Cappello, J.; Ghandehari, H., Silk-elastinlike hydrogels: Thermal characterization and gene delivery. *Polymeric Drug Delivery II: Polymeric Matrices and Drug Particle Engineering* 2006, 924, 150-168.
149. Hatefi, A.; Cappello, J.; Ghandehari, H., Adenoviral gene delivery to solid tumors by recombinant silk-elastinlike protein polymers. *Pharmaceutical Research* 2007, 24, (4), 773-779.
150. Dandu, R.; Ghandehari, H.; Cappello, J., Characterization of structurally related adenovirus-laden silk-elastinlike hydrogels. *Journal of Bioactive and Compatible Polymers* 2008, 23, (1), 5-19.

151. Rammensee, S.; Huemmerich, D.; Hermanson, K. D.; Scheibel, T.; Bausch, A. R., Rheological characterization of hydrogels formed by recombinantly produced spider silk. *Applied Physics a-Materials Science & Processing* 2006, 82, (2), 261-264.
152. Slotta, U.; Hess, S.; Spiess, K.; Stromer, T.; Serpell, L.; Scheibel, T., Spider silk and amyloid fibrils: A structural comparison. *Macromolecular Bioscience* 2007, 7, (2), 183-188.
153. Yamaura, K.; Tanigami, T.; Matsuzawa, S., A Single Large Bubble Consisting of a Very Thin-Film of Native Aqueous Silk. *Journal of Colloid and Interface Science* 1985, 106, (2), 565-566.
154. Valluzzi, R.; Gido, S. P.; Zhang, W. P.; Muller, W. S.; Kaplan, D. L., Trigonal crystal structure of Bombyx mori silk incorporating a threefold helical chain conformation found at the air-water interface. *Macromolecules* 1996, 29, (27), 8606-8614.
155. Valluzzi, R.; Gido, S. P., The crystal structure of Bombyx mori silk fibroin at the air-water interface. *Biopolymers* 1997, 42, (6), 705-717.
156. Valluzzi, R.; Atvges, P.; Winkler, S.; Szela, S.; He, S. J.; Gido, S. P.; Kaplan, D. L., Pattern generation and morphology control in thin films of fibrous proteins. *Abstracts of Papers of the American Chemical Society* 1998, 216, U266-U266.
157. Gido, S. P.; Valluzzi, R.; He, S. J., Silk protein structure in thin films grown at interfaces. *Abstracts of Papers of the American Chemical Society* 1998, 216, U795-U795.
158. He, S. J.; Valluzzi, R.; Gido, S. P., Silk I structure in Bombyx mori silk foams. *International Journal of Biological Macromolecules* 1999, 24, (2-3), 187-195.
159. Valluzzi, R.; Gido, S. P.; Muller, W.; Kaplan, D. L., Orientation of silk III at the air-water interface. *International Journal of Biological Macromolecules* 1999, 24, (2-3), 237-242.
160. Kim, U.-J.; Park, J.; Joo Kim, H.; Wada, M.; Kaplan, D. L., Three-dimensional aqueous-derived biomaterial scaffolds from silk fibroin. *Biomaterials* 2005, 26, (15), 2775-2785.
161. Tamada, Y., New process to form a silk fibroin porous 3-D structure. *Biomacromolecules* 2005, 6, (6), 3100-6.
162. Nazarov, R.; Jin, H. J.; Kaplan, D. L., Porous 3-D scaffolds from regenerated silk fibroin. *Biomacromolecules* 2004, 5, (3), 718-726.
163. Mandal, B. B.; Gil, E. S.; Panilaitis, B.; Kaplan, D. L., Laminar Silk Scaffolds for Aligned Tissue Fabrication. *Macromolecular Bioscience* 2012.

164. Um, I. C.; Kweon, H. Y.; Lee, K. G.; Park, Y. H., The role of formic acid in solution stability and crystallization of silk protein polymer. *International Journal of Biological Macromolecules* 2003, 33, (4-5), 203-213.
165. Wang, X. Y.; Hu, X.; Daley, A.; Rabotyagova, O.; Cebe, P.; Kaplan, D. L., Nanolayer biomaterial coatings of silk fibroin for controlled release. *Journal of Controlled Release* 2007, 121, (3), 190-199.
166. Hines, D. J.; Kaplan, D. L., Mechanisms of controlled release from silk fibroin films. *Biomacromolecules* 2011, 12, (3), 804-12.
167. Liu, T. L.; Miao, J. C.; Sheng, W. H.; Xie, Y. F.; Huang, Q.; Shan, Y. B.; Yang, J. C., Cytocompatibility of regenerated silk fibroin film: a medical biomaterial applicable to wound healing. *Journal of Zhejiang University. Science. B* 2010, 11, (1), 10-6.
168. Cassinelli, C.; Cascardo, G.; Morra, M.; Draghi, L.; Motta, A.; Catapano, G., Physical-chemical and biological characterization of silk fibroin-coated porous membranes for medical applications. *International Journal of Artificial Organs* 2006, 29, (9), 881-892.
169. Zhu, H. L.; Wu, B. W.; Feng, X. X.; Chen, J. Y., Preparation and characterization of bioactive mesoporous calcium silicate-silk fibroin composite films. *Journal of Biomedical Materials Research Part B-Applied Biomaterials* 2011, 98B, (2), 330-341.
170. Sofia, S.; McCarthy, M. B.; Gronowicz, G.; Kaplan, D. L., Functionalized silk-based biomaterials for bone formation. *Journal of biomedical materials research* 2001, 54, (1), 139-48.
171. Uebersax, L.; Merkle, H. P.; Meinel, L., Insulin-like growth factor I releasing silk fibroin scaffolds induce chondrogenic differentiation of human mesenchymal stem cells. *Journal of controlled release : official journal of the Controlled Release Society* 2008, 127, (1), 12-21.
172. Magoshi, J.; Nakamura, S., Studies on physical properties and structure of silk - Glass-transition and crystallization of silk fibroin. *Journal of Applied Polymer Science* 1975, 19, (4), 1013-1015.
173. Magoshi, J.; Magoshi, Y.; Nakamura, S., Physical-Properties and Structure of Silk .7. Crystallization of Amorphous Silk Fibroin Induced by Immersion in Methanol. *Journal of Polymer Science Part B-Polymer Physics* 1981, 19, (1), 185-186.
174. Minoura, N.; Tsukada, M.; Nagura, M., Physico-chemical properties of silk fibroin membrane as a biomaterial. *Biomaterials* 1990, 11, (6), 430-4.

175. Spiess, K.; Ene, R.; Keenan, C. D.; Senker, J.; Kremer, F.; Scheibel, T., Impact of initial solvent on thermal stability and mechanical properties of recombinant spider silk films. *Journal of Materials Chemistry* 2011, 21, (35), 13594-13604.
176. Wohlrab, S.; Spiess, K.; Scheibel, T., Varying surface hydrophobicities of coatings made of recombinant spider silk proteins. *Journal of Materials Chemistry* 2012, 22, (41), 22050-22054.
177. Demura, M.; Asakura, T., Immobilization of Glucose-Oxidase with Bombyx-Mori Silk Fibroin by Only Stretching Treatment and Its Application to Glucose Sensor. *Biotechnology and Bioengineering* 1989, 33, (5), 598-603.
178. Bhat, N. V.; Ahirrao, S. M., Investigation of the Structure of Silk Film Regenerated with Lithium Thiocyanate Solution. *Journal of Polymer Science Part a-Polymer Chemistry* 1983, 21, (5), 1273-1280.
179. Gupta, M. K.; Khokhar, S. K.; Phillips, D. M.; Sowards, L. A.; Drummy, L. F.; Kadakia, M. P.; Naik, R. R., Patterned silk films cast from ionic liquid solubilized fibroin as scaffolds for cell growth. *Langmuir* 2007, 23, (3), 1315-1319.
180. Tao, H.; Kaplan, D. L.; Omenetto, F. G., Silk materials--a road to sustainable high technology. *Advanced Materials* 2012, 24, (21), 2824-37.
181. Parker, S. T.; Domachuk, P.; Amsden, J.; Bressner, J.; Lewis, J. A.; Kaplan, D. L.; Omenetto, F. G., Biocompatible Silk Printed Optical Waveguides. *Advanced Materials* 2009, 21, (23), 2411-2415.
182. Agarwal, N.; Hoagland, D. A.; Farris, R. J., Effect of moisture absorption on the thermal properties of Bombyx mori silk fibroin films. *Journal of Applied Polymer Science* 1997, 63, (3), 401-410.
183. Kluge, J. A.; Rabotyagova, O.; Leisk, G. G.; Kaplan, D. L., Spider silks and their applications. *Trends in biotechnology* 2008, 26, (5), 244-51.
184. Altman, G. H.; Diaz, F.; Jakuba, C.; Calabro, T.; Horan, R. L.; Chen, J. S.; Lu, H.; Richmond, J.; Kaplan, D. L., Silk-based biomaterials. *Biomaterials* 2003, 24, (3), 401-416.
185. Omenetto, F. G.; Kaplan, D. L., A new route for silk. *Nature Photonics* 2008, 2, (11), 641-643.
186. Plaza, G. R.; Guinea, G. V.; Perez-Rigueiro, J.; Elices, M., Thermo-hygro-mechanical behavior of spider dragline silk: Glassy and rubbery states. *Journal of Polymer Science Part B-Polymer Physics* 2006, 44, (6), 994-999.

187. Keten, S.; Xu, Z. P.; Ihle, B.; Buehler, M. J., Nanoconfinement controls stiffness, strength and mechanical toughness of beta-sheet crystals in silk. *Nature Materials* 2010, 9, (4), 359-367.
188. Kyte, J.; Doolittle, R. F., A simple method for displaying the hydropathic character of a protein. *Journal of Molecular Biology* 1982, 157, (1), 105-32.
189. Scheibel, T.; Bloom, J.; Lindquist, S. L., The elongation of yeast prion fibers involves separable steps of association and conversion. *Proceedings of the National Academy of Sciences of the United States of America* 2004, 101, (8), 2287-92.
190. Urry, D. W.; Pattanaik, A., Elastic protein-based materials in tissue reconstruction. *Annals of the New York Academy of Sciences* 1997, 831, 32-46.

6. List of abbreviations

| | |
|----------------------|---|
| <i>A. diadematus</i> | <i>Araneus diadematus</i> |
| a.u. | Arbitrary unit |
| <i>B. mori</i> | <i>Bombyx mori</i> |
| <i>C. carnea</i> | <i>Chrysopa carnea</i> |
| Da | Dalton |
| <i>E. coli</i> | <i>Escherichia coli</i> |
| FTIR | Fourier transform infrared spectroscopy |
| HEPES | 4-(2-hydroxyethyl)-1-piperazineethanesulfonic acid |
| HFA | Hexafluoroacetone trihydrate |
| HFIP | Hexafluoroisopropanol |
| <i>M. signata</i> | <i>Mallada signata</i> |
| MeOH | Methanol |
| PDMS | Polydimethylsiloxane |
| RGD | Arginine-glycine-aspartic acid |
| RH | Relative humidity |
| SDS-PAGE | Sodium dodecyl sulfate polyacrylamide gel electrophoresis |
| SEM | Scanning electron microscopy |
| TEM | Transmission electron microscope |
| Tris | 2-Amino-2-(hydroxymethyl)-propan-1,3-diol |
| w/v | Mass/volume |

7. Dependence of Mechanical Properties of Lacewing Egg Stalks on Relative Humidity



Article

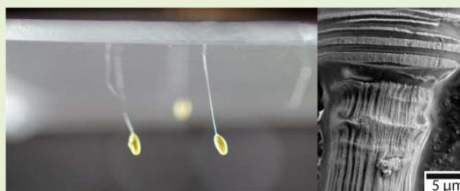
pubs.acs.org/Biomac

Dependence of Mechanical Properties of Lacewing Egg Stalks on Relative Humidity

Felix Bauer,[†] Luca Bertinetti,[‡] Admir Masic,^{*,‡} and Thomas Scheibel^{*,†}[†]Lehrstuhl Biomaterialien, Universität Bayreuth, Universitätsstrasse 30, 95440 Bayreuth, Germany[‡]Department of Biomaterials, Max Planck Institute of Colloids and Interfaces, Research Campus Golm, 14424 Potsdam, Germany

Supporting Information

ABSTRACT: Silk fibers are well known for their mechanical properties such as strength and toughness and are lightweight, making them an interesting material for a variety of applications. Silk mechanics mainly rely on the secondary structure of the underlying proteins. Lacewing egg stalk silk proteins obtain a cross- β structure with individual β strands aligned perpendicular to the fiber axis. This structure is in contrast with that of silks of spiders or silkworms with β strands parallel to the fiber axis and to that of silks of honeybees with α helices arranged in coiled coils. On the basis of the cross- β structure the mechanical properties of egg stalks are different from those of other silks concerning extensibility, toughness, and bending stiffness. Here we show the influence of relative humidity on the mechanical behavior of lacewing egg stalks and propose a model based on secondary structure changes to explain the differences on a molecular level. At low relative humidity, the stalks rupture at an extension of 3%, whereas at high relative humidity the stalks rupture at 434%. This dramatic increase corresponds to breakage of hydrogen bonds between the β strands and a rearrangement thereof in a parallel- β structure.



INTRODUCTION

Egg stalks of lacewings (Figure 1) comprise two or more proteins that adopt a cross- β structure in the stalk.^{1–4} The



Figure 1. Left: a green lacewing (*Chrysopa carnea*); right: an egg stalk with an egg attached.

primary structure of two previously identified proteins consists of a motif comprising 16 amino acids, which is repeated 51 times in MalXB1 and 29 times in MalXB2.¹ Both proteins have two nonrepetitive termini, whereas MalXB1 has additionally one nonrepetitive region in the middle. MalXB1 and MalXB2 contain 7 and 5 cysteines, respectively, mostly situated in terminal domains. It is speculated that these cysteine residues play a role in stiffness of the stalks by cross-linking the proteins through intramolecular disulfide bonds.¹ It is further predicted that stretches of eight amino acid residues within the repetitive core domain form β strands folded back on each other (supported by X-ray diffraction pattern of the stalk).³ In consequence, these sheets are stacked and form a ribbon-like

structure, with an intersheet spacing of 15 nm and with the termini of the proteins likely being situated in the interspace.³

Mechanical analysis of natural egg stalks revealed high extensibility of up to 600%.^{1,2,5} The ultimate elongation correlated with the extension one would estimate at breakage of all hydrogen bonds involved in the cross- β sheets, followed by the alignment of the β strands in parallel to the fiber axis. The latter was confirmed by X-ray diffraction showing β sheets in parallel to the fiber axis in the case of stretching a stalk (500%).³

Here we analyzed the mechanical properties of lacewing egg stalks with a focus on the transition from cross- β to parallel- β structures, which is highly dependent on relative humidity (RH).

EXPERIMENTAL SECTION

Fly Care. Green lacewings of the species *Chrysopa carnea* were obtained from Sauter & Stepper (Ammerbuch-Altingen Germany). Batches containing 1 male and 10 female lacewings were kept at room temperature in polystyrene dishes in the presence of a moist paper towel and a food mixture provided by Sauter & Stepper. The females regularly deposited eggs on stalks at the sealing of the container. The stalks were cylindrical (Figure S1 of the Supporting Information) and had nearly a constant diameter in their middle section. Twice a week, the lacewings were transferred to a new container, and the stalks were gently harvested with tweezers for further analysis.

Received: July 30, 2012

Revised: September 17, 2012

Published: October 7, 2012

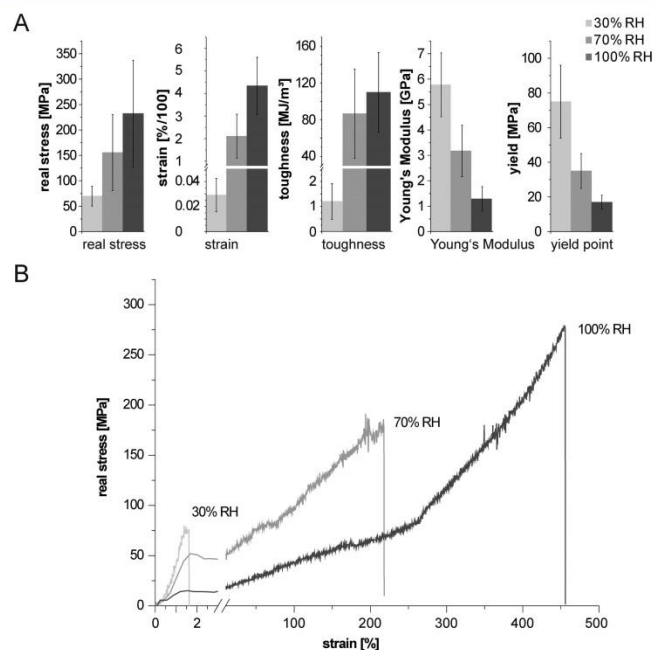


Figure 2. (A) Mechanical properties of lacewing egg stalks at different relative humidity (30% RH: $n = 50$; 70% RH: $n = 51$; 100% RH $n = 55$; all measurements differ significantly ($p = 99.99\%$), except the toughness modulus between 70% RH and 100% RH). (B) Exemplary true stress–strain curves at relative humidity of 30, 70, and 100%, respectively.

Tensile Testing. To determine their mechanical properties, we glued egg stalks on plastic card frames having a gauge length of 2 mm. After drying the samples, diameters were measured using a microscope (Leica DMI 3000B), and the cross-sectional area was calculated, which is easy due to the round shape of the stalks (Figure S1 of the Supporting Information). Next, the samples were incubated in a climate chamber under the accordant conditions (30, 70, and 100% RH) for at least 30 min. The samples were mounted on clamps, and the card frames were gently cut to not destroy the stalk. The stalks were stretched with a speed of 0.01 mm/s using a Bose Electroforce 3220 tensile tester equipped with a 2.5 N load cell. In sum, 50 to 55 stress strain curves were measured for each individual condition.

Six material properties were gained from the measurements. Strain at breakage and the stress at the yield point were measured, and true and engineered stress at rupture were calculated as previously described.⁵ For calculation of the Young's modulus, the first linear stretch was fitted using a regression line. The toughness modulus was calculated as the area below the stress–strain curve.

Raman Measurements. After stretching a stalk to a defined strain, it was unmounted from the tensile tester and placed under a confocal Raman microscope. The confocal Raman microscope (alpha300, WITec, Ulm, Germany) was equipped with a frequency-doubled Nd:YAG laser (532 nm) and piezoscanner (P-500, Physik Instrumente, Karlsruhe, Germany). The spectra were acquired with a thermoelectrically cooled CCD detector (DU401A-BV, Andor, U.K.) placed behind the spectrometer (UHTS 300; WITec) with a spectral resolution of 3 cm^{-1} . The ScanCtrlSpectroscopyPlus software (version 1.38, WITec) was used for measurements and WITec Project Plus (version 2.02, WITec) for spectra processing. Chemical images were achieved by integration over defined Raman shift regions in the spectrum using a sum filter. The amide I intensity was obtained by

integrating the total intensity of the amide I band (1600–1700 cm^{-1}). $P2$ and $P4$ values and the most probable distribution function were determined following the procedures described elsewhere^{6–8} using $R_{90} = 0.2$.⁹ In particular, the Lagrange multipliers can be calculated numerically considering that the average values of each Legendre polynomial weighted with the most probable distribution function must be equal to the corresponding order parameter obtained by the polarized Raman measurements.

SEM Pictures. For scanning electron microscopy, stalks were glued on SEM aluminum stubs using carbon adhesive tape. Samples were sputter-coated with platinum (2 nm thickness), and images were obtained with a Zeiss 1530 using the in-lens detector.

THEORETICAL CALCULATIONS

Theoretical Toughness in Longitudinal Direction. A theoretical toughness was calculated using the assumption that all hydrogen bonds in the β sheets break at a RH of 100%. The energy of a hydrogen bond was assumed to be 11.85 kJ/mol,¹⁰ and the size of a crystal cell was estimated as $a = 0.47$ nm, $b = 40$ nm (25 nm crystal + 15 nm between the columns), and $c = 0.5634$ nm comprising six hydrogen bonds.³ The number of hydrogen bonds was calculated per one m^3 and multiplied by the energy of one bond. This rough calculation solely includes the energy absorbed by the fiber during breakage of the involved hydrogen bonds of the cross- β sheets.

RESULTS AND DISCUSSION

Stress–Strain Properties of Egg Stalks. Stress–strain measurements of natural egg stalks from *C. carnea* indicate that

the stalks become more extensible with increasing humidity, with 3% extensibility at 30% RH and 434% at 100% RH (Figure 2). At low RH, the sum of individual hydrogen bonds within the stalk is high, as indicated by a high strength of the stalk. In consequence, the disulfide bonds in the stalk rupture before all hydrogen bonds break, as seen by the respective yield point of 75 MPa and the low rupture strain at 30% RH (Figure 2 A). Obviously, no structural transition from cross- β to parallel- β occurs before rupture. At 100% RH, the yield point is 17 MPa, accompanied by a decrease in Young's modulus from 5.8 (30% RH) to 1.3 GPa (100% RH) (Figure 2 A).

The engineered stress at rupture decreases from 68 MPa at 30% RH to 42 MPa (100% RH). In contrast, true stress at rupture increases from 70 (30% RH) to 232 MPa at 100% RH, which is strongly influenced by the increasing extensibility and therefore reduced cross-sectional area.

Egg stalks on average can absorb little energy at 30% RH (1 MJ/m³), a property that is highly improved at 100% RH with an energy absorption of 110 MJ/m³ (Figure 2 A). Strikingly, single samples can reach up to 194 MJ/m³ at a strain of 597%. The increase in extensibility and toughness modulus arises from hydrogen bond breakage and rearrangement of the amino acid side chains. At 100% RH, almost all hydrogen bonds break under strain within the cross- β sheets due to the presence of water molecules representing additional H donors/acceptors. The breakage of H bonds contributes strongly to the uptake of energy. A rough theoretical calculation of the toughness yields 111 MJ/m³ under the assumption that all hydrogen bonds break at 100% RH, being in the range of the measured value of 110 MJ/m³. In contrast, at 30% RH most hydrogen bonds keep intact until fracture.

Longitudinal Stress Induces Structural Changes in the Underlying Proteins. To gain a better insight into the molecular basis of toughness and extensibility, the secondary structure content of the egg stalk proteins was investigated before and after tensile testing using polarized Raman spectroscopy (Figure 3). Characteristic protein signals were observed, and the detailed assignment of bands is reported in the Supporting Information. Bands at 1167, 1660, 3050, and 3250 cm⁻¹, assigned to C⁼H bending and amide I C–H stretching and N–H stretching, show strong and equivalent polarization dependency. This latter aspect is consistent with the protein being organized in a β -sheet structure, because in this conformation the oscillators involved in the aforementioned vibrations should be almost in parallel to each other. Furthermore, the higher intensity of those bands in the ZZ spectra indicates that the backbone of the protein is perpendicular to the fiber axis before stretching. Raman imaging of the amide I region (C=O) along individual fibers showed that this orientation is homogeneous (Figure 3 top).

During stretching of the egg stalks (at 100% RH), most of the Raman bands undergo changes in their polarization behavior (Figure 3 and Figure 2 of the Supporting Information). To quantify these changes, we calculated the orientation parameters for the amide I band and the related most probable distribution function (Table 1 and Figure 4).

The calculated distribution functions for the CO oscillators clearly indicate a progressive rearrangement of the vibrational units from a Z-axis alignment in the unstretched state to X axis alignment after rupture. Samples stretched to ~100% show two different morphologies (Figure 2 of the Supporting Information and Figure 5): one similar to an unstretched fiber and the other one significantly thinner. Orientation parameters of both

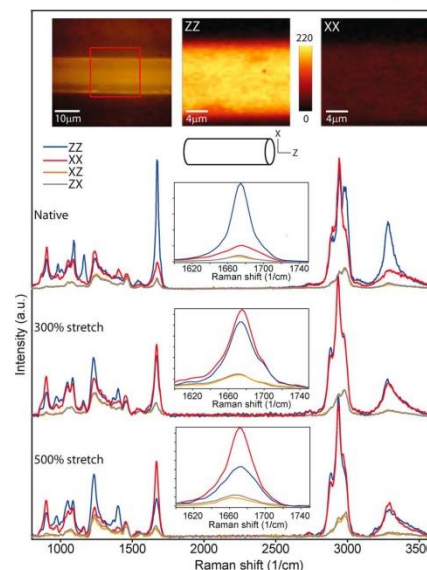


Figure 3. Polarized Raman spectra of native and stretched (300 and 500%) egg stalks at 100% RH. Insets show enlargements of the amide I regions. Top: microscopic picture and Raman imaging obtained by integrating the amide I spectral region (1600–1720 cm⁻¹), showing higher intensity when the polarization of the incident light is parallel to the fiber axis.

Table 1. Orientation Parameters Calculated for the Amide I Band from the Polarized Raman Spectra of Unstretched and Stretched (at 100% RH) egg stalks

| sample | P2 | P4 | I2 | I4 |
|----------------------------|--------------|-------------|--------|--------|
| native | 0.54 ± 0.03 | 0.33 ± 0.03 | 1.764 | 1.213 |
| 50% stretch | 0.55 ± 0.01 | 0.21 ± 0.01 | 2.546 | 0.092 |
| 100% stretch (not thinned) | 0.47 ± 0.02 | 0.05 ± 0.03 | 2.803 | -0.914 |
| 100% stretch (thinned) | 0.05 ± 0.03 | 0.08 ± 0.03 | 0.175 | 0.640 |
| 300% stretch | 0.06 ± 0.01 | 0.00 ± 0.01 | -0.314 | -0.024 |
| 500% stretch | -0.29 ± 0.05 | 0.10 ± 0.05 | -1.935 | 0.456 |

regions were calculated (Table 1), and a radical change in the necked region was observed. The shape of the distribution functions calculated for the necked regions indicates the coexistence of CO groups oriented along and perpendicular to the fiber axis. This latter evidence suggests that the transformation does not result from a continuous rotation of CO oscillators but from a direct conversion of cross- β into parallel- β sheets. This model is also supported by the fact that the shape of the amide I band does not change through the entire transformation.

Scanning electron microscopy of stretched and unstretched egg stalks showed a thinning of the stalks at individual portions (Figure 5). Such thinned parts are not stiff, and the thinning is irreversible even under water (Figure 4 of the Supporting Information), further confirming that the conversion from

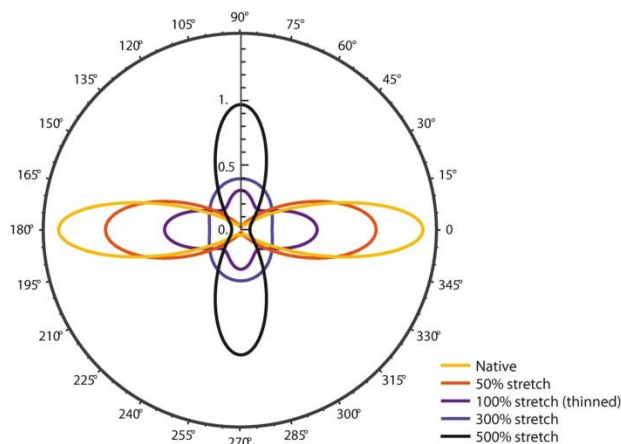


Figure 4. Orientation parameters and most probable distribution functions for amide I bands calculated from the values of P2 and P4 reported in Table 1. The 0° of the polar plot coincides with the fiber direction.

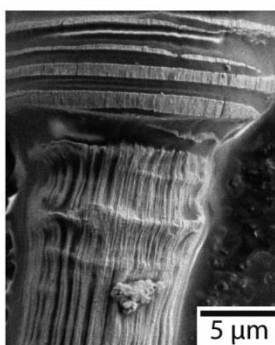


Figure 5. Scanning electron micrograph of a partially stretched lacewing egg stalk.

cross- β to parallel- β occurs in the respective region of the stalk.¹¹

Structural Model of Egg Stalks. On the basis of our results, we propose that the intramolecular hydrogen bonds break between individual β strands within cross- β sheets under tension due to H-donor/acceptor exchange with water molecules at high RH. Such water-assisted H-bond breakage allows the realignment of strands to form H-bonded β sheets parallel to the fiber axis without affecting β -sheet content (Figure 6).

The conformational transition from cross- β to parallel- β sheet occurs only in the presence of water (high RH (70% or 100% RH) or in liquid water). In a first step, externally applied force is distributed over the entire length of the stalk under any condition, and the hydrogen bonds in parallel to the fiber axis are stretched (tear forces) (Figure 6A1/B1). At low RH, the hydrogen bonds simultaneously break in one layer upon a yield strain (three layers of hydrogen bonds due to mechanical/sterical reasons), followed by a concomitant break of hydrogen

bonds in the neighboring layers of the same protein (Figure 6A2). At the terminal domains, load is applied to the disulfide bonds cross-linking the termini of proteins from different layers.

At low RH, the bonding energy of the sum of hydrogen bonds (11.83 kJ/mol for a single hydrogen bond) is strong in comparison with those of individual disulfide bonds (251 kJ/mol). Therefore, the disulfide bonds likely break first, followed by adjacent β sheets in the same layer. Finally, all columns are broken and the stalk ruptures (Figure 6A3).

At high RH, the hydrogen bonds within the cross- β sheets can interchange with residual water molecules; therefore, β sheets unpack into strands at much lower stress values (indicated by a lower stress at the yield point) (Figure 2). In contrast to low humidity, the bonding energy of the sum of hydrogen bonds in one layer, stabilizing the structure, is comparable to that of the disulfide bonds therein, prevalently resulting in a sustained break of hydrogen bonds in the adjacent proteins in fiber direction accompanied by disulfide breakage. The breakage of disulfide bonds was seen by Raman spectroscopy at stalks stretched further than 300% (Figure 3 of the Supporting Information).

One visible effect of the rearrangement of the protein backbone is thinning of the stalks (Figure 5); another one is the constant force needed to elongate the stalk (Figure 6B2). Thinning of the stalk is caused by reorienting the β strands (and protein backbones) along the fiber axis, as indicated by the parallel- β structure seen by X-ray diffraction and Raman spectroscopy at extensions above 300%.³ Interestingly, the overall β -sheet content of thinned regions is not significantly different in comparison with not-converted parts of the stalk. After complete rearrangement of the β strands (between approximately 200 and 400% strain (average 308% strain)), shear forces replace the tear forces, resulting in cooperative effects among hydrogen bonds;¹² therefore, higher forces are needed to elongate the stalk. The latter can be seen as strain hardening in the stress strain curve (Figure 6B). Further stretching of the stalk leads to breakage of hydrogen bonds and slippage of β strands in the load direction (Figure 6B3).¹³ This

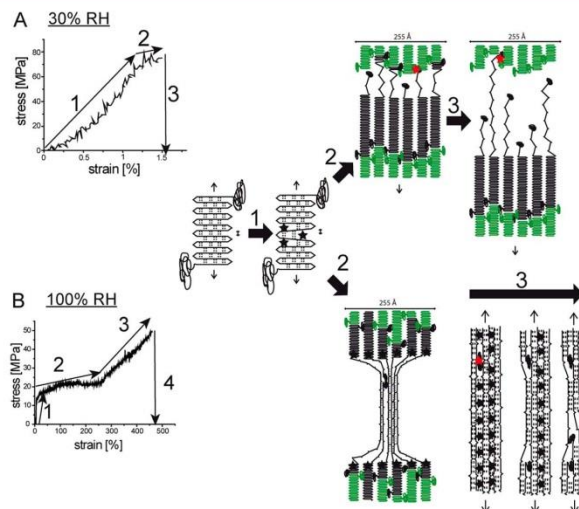


Figure 6. Rupture of egg stalks at low and high relative humidity. (Black stars: hydrogen bonds break; red stars: disulfide bonds break; black protein backbone: involved in rearrangement; green protein backbone: unaffected).

is accompanied by breakage of disulfide bonds and further thinning of the stalk (more homogeneous over the entire length of the stalk) (Figure 6B3). In case too many ends of the proteins slip apart and the stalks get too thin, they rupture (Figure 6B3).

CONCLUSIONS

The extensibility of lacewing egg stalk silk is highly influenced by RH. This is due to the fact that the strength of hydrogen bonds depends on the H-donor/acceptor exchange with residual water. Together with the disulfide bonds (bonding strength is independent of water), which are cross-linking the proteins of different layers, humidity is the major factor to control the mechanical properties of lacewing egg stalks. At low RH, the strength of the sum of hydrogen bonds in one layer of the stalk is higher than the strength of the sum of disulfide bonds. As a result, the disulfide bonds break at a low strain, and the stalk can absorb little energy. The situation is different at higher RH. The hydrogen bonds are weakened due to H-donor/acceptor exchange with present water molecules. The disulfide bonds of one layer in sum are now comparably strong, leading to a breakage of the hydrogen bonds between the β sheets conformations, followed by slippage of the β sheets and disulfide bond breakage. As a consequence, the stalks extend up to 600% before rupture, and they can absorb much more energy.

ASSOCIATED CONTENT

Supporting Information

Tentative assignment of Raman bands. SEM picture of an egg stalk cross-section. Raman spectra of a stretched (100%) egg stalk (thinned and not thinned regions). Raman spectra of stretched (500%) egg stalks ($400\text{--}600\text{ cm}^{-1}$) showing disulfide

bond breakage. Pulling and release of an egg stalk. This material is available free of charge via the Internet at <http://pubs.acs.org>.

AUTHOR INFORMATION

Corresponding Author

*Tel: +49921-55 7361. Fax: (+49921-557346). E-mail: thomas.scheibel@uni-bayreuth.de; Admir.Masic@mpikg.mpg.de.

Notes

The authors declare no competing financial interest.

ACKNOWLEDGMENTS

We thank Claudia Blüm and Johannes Diehl for assistance with the SEM pictures.

REFERENCES

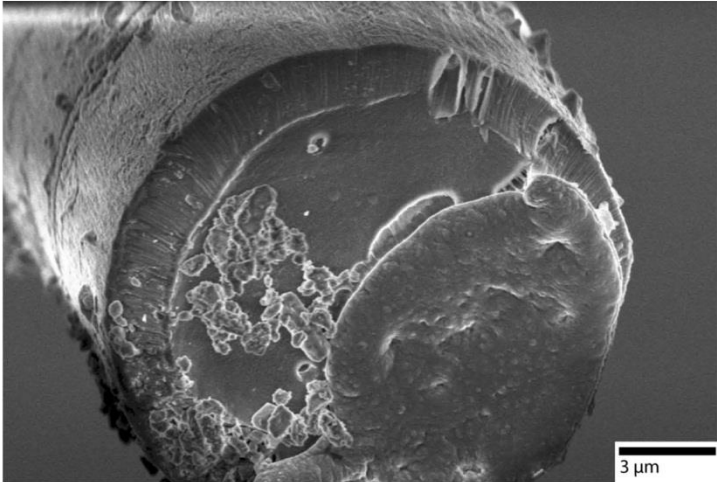
- (1) Weisman, S.; Okada, S.; Mudie, S. T.; Huson, M. G.; Trueman, H. E.; Srikantha, A.; Haritos, V. S.; Sutherland, T. D. *J. Struct. Biol.* **2009**, *168*, 467–475.
- (2) Bauer, F.; Scheibel, T. *Angew. Chem., Int. Ed.* **2012**, *51*, 6521–6524.
- (3) Geddes, A. J.; Parker, K. D.; Atkins, E. D.; Beighton, E. *J. Mol. Biol.* **1968**, *32*, 343–358.
- (4) Parker, K. D.; Rudall, K. M. *Nature* **1957**, *179*, 905–906.
- (5) Hepburn, H. R.; Chandler, H. D.; Davidoff, M. R. *Insect Biochem* **1979**, *9*, 69–77.
- (6) Masic, A.; Bertinetti, L.; Schuetz, R.; Galvis, L.; Timofeeva, N.; Dunlop, J. W.; Seto, J.; Hartmann, M. A.; Fratzl, P. *Biomacromolecules* **2011**, *12*, 3989–3996.
- (7) Rousseau, M. E.; Lefevre, T.; Beaulieu, L.; Asakura, T.; Pezolet, M. *Biomacromolecules* **2004**, *5*, 2247–2257.
- (8) Tsuboi, M.; Kubo, Y.; Akahane, K.; Pezolet, M.; Lefevre, T.; Thomas, G. J. *Biophys. J.* **2005**, *88*, 559a.
- (9) Rousseau, M. E.; Beaulieu, L.; Lefevre, T.; Paradis, J.; Asakura, T.; Pezolet, M. *Biomacromolecules* **2006**, *7*, 2512–2521.
- (10) Buehler, M. J.; Keten, S.; Ackbarow, T. *Prog Mater Sci* **2008**, *53*, 1101–1241.
- (11) Craig, C. L. *Annu. Rev. Entomol.* **1997**, *42*, 231–267.

- (12) Keten, S.; Buehler, M. J. *Nano Lett.* **2008**, *8*, 743–748.
- (13) Keten, S.; Xu, Z. P.; Ihle, B.; Buehler, M. J. *Nat. Mater.* **2010**, *9*, 359–367.

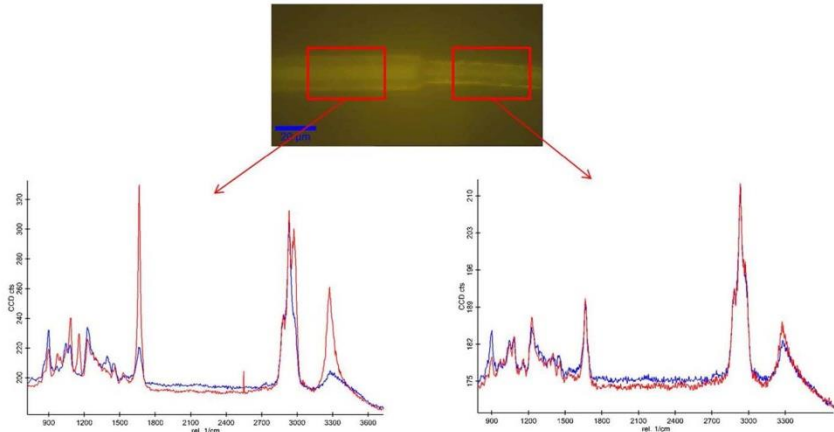
SUPPORTING INFORMATION PARAGRAPH

Supplementary Table 1: Tentative assignment of RAMAN bands

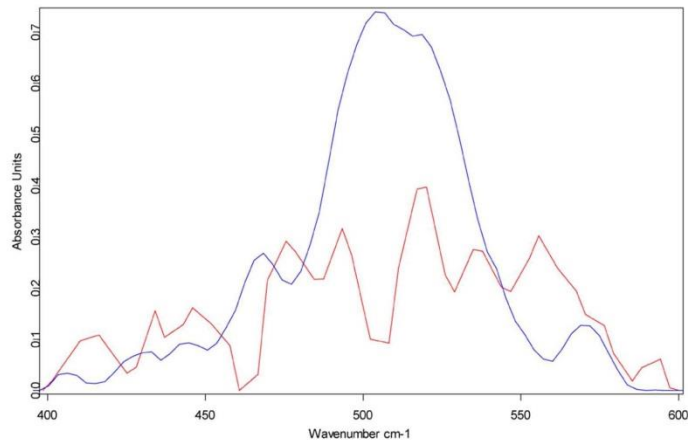
- 505/8 cm^{-1} C-OH torsion of methoxy
- 509 cm^{-1} S-S disulfide stretching band n(S-S) gauche-gauche-gauche (amino acid cysteine)
- 524 cm^{-1} S-S disulfide stretching in proteins n(S-S) gauche-gauche-trans (amino acid cysteine)
- 540 cm^{-1} n(S-S) trans-gauche-trans (amino acid cysteine)
- 869 cm^{-1} Proline
- 980 cm^{-1} C-C stretching b-sheet (proteins)
- 1053 cm^{-1} C-O stretching, C-N stretching (protein)
- 1099 cm^{-1} n(C-N)
- 1165 cm^{-1} C-H banding in alpha C of Gly
- 1240 cm^{-1} Amide III (beta-sheet and random coils)
- 1401 cm^{-1} Bending modes of methyl groups
- 1460 cm^{-1} CH₂/CH₃ deformation of lipids & collagen
- 1655 cm^{-1} Amide I alpha
- 1675 cm^{-1} Amide I (b-sheet)
- 1685 cm^{-1} Amide I (disordered structure; non hydrogen bonded)
- 1697 cm^{-1} Amide I (turns and bands)
- 2886 2883 cm^{-1} CH₂ asymmetric stretch of proteins; 2885 cm^{-1} ns CH₃; 2886 cm^{-1} Fermi resonance CH₂ stretch
- 2889–2908 cm^{-1} CH₂ asymmetric stretch of proteins
- 2940 cm^{-1} C-H vibrations in lipids & proteins, nas CH₂, lipids, fatty acids
- 2970 cm^{-1} nas CH₃,
- 2975-2985 2971/3 cm^{-1} Asymmetric stretching of methoxy
- 3284 3232 cm^{-1} O-H & N-H stretching vibrations (hydrogen bonding network; 3300 cm^{-1} Attributed to OH stretch; 3329 cm^{-1} N-H vibration of proteins; 3350–550 cm^{-1} OH stretching



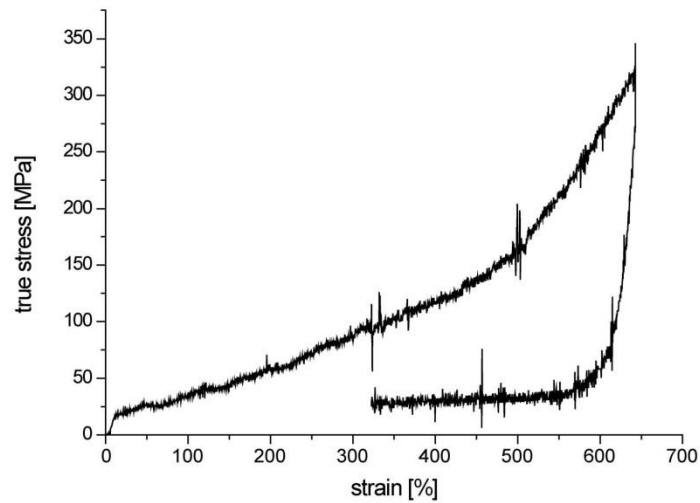
Supplementary Figure 1: SEM picture of a cross-section of a lacewing egg stalk, prepared by cutting with a focused ion beam.



Supplementary Figure 2: Polarized Raman spectra of a stretched (100%) lacewing egg stalk (at a relative humidity of 100%). Raman spectra could be obtained at thinned and not-thinned regions. The cross-beta structure changes into a more disordered structure.



Supplementary Figure 3: Raman spectra from 400 - 600 cm^{-1} ; blue: unstretched egg stalk; red: stretched (500%) egg stalk.



Supplementary Figure 4: Pulling and release of an egg stalk at a relative humidity of 100%.

PAGE analysis revealed an apparently higher molecular weight for N[AS]₈C than calculated, the correct mass of the protein was confirmed by mass spectrometry (Supporting Information, Figure S2).

Owing to the low solubility of N[AS]₈C in aqueous solutions, we dissolved the protein (10% w/v) in hexafluoroacetone (HFA). In general, HFA induces an α -helical structure in dissolved proteins,^[14] and in case of N[AS]₈C this secondary structure was confirmed by circular dichroism (CD) spectroscopy (Supporting Information, Figure S3). Mimicking the silk stalk formation of lacewings, tweezers were dipped in a droplet of N[AS]₈C solution and a fiber was withdrawn. The end of the resulting stalk was transferred to a tinfoil support followed by drying (Figure 2A). For post-treatment, stalks were placed in a climate chamber at 60°C and 70% relative humidity overnight. Other possibilities for post treatment of the stalks would be the use of cosmotropic salt solutions, ethanol, methanol, isopropanol, or high pressure.^[15,16]

The artificial stalks have a smooth surface that is similar to natural stalks (Supporting Information, Figure S4). However, necking occurs in natural stalks, which is related to stressing the stalk at high humidity (>30%) or under water. This phenomenon leads to a loss of rigidity in the necked parts accompanied by a transition from a cross- β -sheet to a parallel- β -sheet structure.^[9] Such necking was not observed for artificial stalks.

Accordingly, both artificial and natural stalks were structurally analyzed using FTIR spectroscopy (Figure 3). For secondary structure analysis, Fourier self-deconvolution

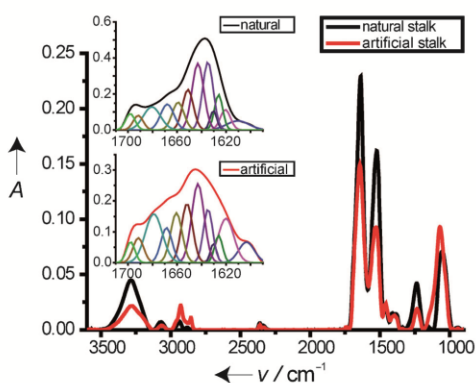


Figure 3. FTIR absorbance spectra of natural and artificial stalks before tensile testing. Insets show the Fourier self-deconvoluted amide I region of natural and artificial stalks.

of the amide I region^[17] was performed indicating a lower β -sheet content in artificial stalks in comparison to natural stalks (Table 1). Measuring FTIR spectra before and after stretching of natural and artificial stalks revealed no changes for natural stalks and a slight increase in β -sheet content with a reduced turn content for stretched artificial stalks. The α -helical content in both stalks is quite low at 6–9%. Strikingly,

Table 1. Calculated secondary structure of natural and artificial egg stalks measured before (btt) and after (att) individual tensile testing using FTIR spectroscopy and Fourier self-deconvolution of the amide I band.^[17]

| Secondary structure | Natural egg stalk | | Artificial egg stalk | |
|---------------------|-------------------|---------|----------------------|---------|
| | btt [%] | att [%] | btt [%] | att [%] |
| β sheets | 40 ± 6 | 39 ± 5 | 32 ± 3 | 39 ± 4 |
| α helices | 6 ± 4 | 7 ± 1 | 9 ± 2 | 7 ± 1 |
| turns | 24 ± 3 | 22 ± 1 | 30 ± 3 | 24 ± 1 |
| random coils | 30 ± 4 | 32 ± 2 | 29 ± 1 | 30 ± 2 |

the helical content was also similar before and after stretching. The poly(L-alanine) NC α stretching vibration^[18] of natural egg stalks at 1167 cm⁻¹, as detected by polarized FTIR spectra measured at 0° and 90° of the stalk axis, indicates a strong orientation of poly(Ala) β sheets perpendicular to the stalk axis (molecular order parameter: $S^{\text{mol}} = -0.44$,^[25] Supporting Information, Figure S5). The engineered protein does not contain poly(alanine) sequences, and therefore no orientation could be observed. This indicates that as yet undetected poly(alanine)-rich proteins, probably amongst the three additional proteins detected in *C. carnea* (Figure 1B), could be critically involved in protein alignment in natural stalks. Therefore, our present approach is not suited to fully mimic the natural egg stalk properties.

Both the natural as well as the artificial stalks show birefringence (Figure 4) that is based on structural anisotropy. The birefringence has a high intensity in natural stalks based

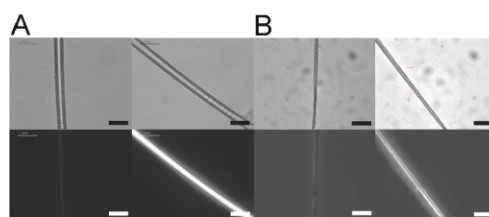


Figure 4. Comparison of birefringence of natural and artificial stalks. A) Microscope images of a natural lacewing egg stalk. B) Microscope images of an artificial egg stalk. Top: bright field; bottom: with crossed polarizers. Scale bars: 50 μm .

on highly ordered crystalline regions with β sheets ordered perpendicular to the stalk axis, while the artificial stalks show weaker birefringence, indicating less but still ordered structures in the stalks.

The artificial stalks have similar diameters (10 μm) as the natural stalks and they reveal a similar apparent rigidity (Figure 2B). Mechanical properties were analyzed at a relative humidity (RH) of 30% and 70% at 22°C. Controlled humidity is highly important for tensile testing of silk.^[19–21] The strength of the natural egg stalks (*C. carnea*) is quite low with values of 68 MPa (30% RH) and 155 MPa (70% RH) measured under the chosen conditions, if compared to the published values of 186–375 MPa measured at 65% RH (*Mallada signata* and *Chrysopa spec.*,^[11,22] Table 2). At 30%

Table 2: Tensile testing of natural (*C. carnea*) and artificial egg stalks.^[a]

| | Extensibility [%] | Strength σ_{max} [MPa] | Young's modulus [MPa] | Toughness [MJ m^{-3}] |
|-----------------------------------|-------------------|--------------------------------------|-----------------------|----------------------------------|
| literature values: ^[b] | | | | |
| 65% RH ^[11] | 381 | 310 | | |
| 65% RH ^[22] | 249 | ca. 375 | | |
| natural egg stalk: | | | | |
| 30% RH | 2 ± 1 | 68 ± 19 | 5777 ± 1257 | 1.2 ± 0.72 |
| 70% RH | 210 ± 100 | 155 ± 75 | 3175 ± 1016 | 87 ± 49 |
| artificial egg stalk: | | | | |
| 30% RH | 5 ± 2 | 55 ± 14 | 2330 ± 850 | 1.76 ± 0.9 |
| 70% RH | 6 ± 3 | 25 ± 11 | 1012 ± 252 | 1.09 ± 0.59 |

[a] Experiments were carried out at 30% and 70% relative humidity at 22 °C. [b] For *M. signata* and *C. spec.*

RH, the stalks rupture at a strain of about 2%, while at 70% RH they rupture at a strain of 211% (Figure 5 and Table 2). The Young's modulus of natural egg stalks at 30% RH is 5.7 GPa, while the artificial egg stalks have about 40% of the stiffness (2.3 GPa). The tensile strength of the natural stalks is 68 MPa and that of the artificial stalks is 55 MPa (Table 2). Thus, taking the porosity of the artificial stalks into account, a tensile strength of about 63 MPa was calculated (30% RH). Interestingly, the toughness of the artificial stalks at 30% RH is 1.76 MJ m^{-3} and is slightly higher than that of the natural stalks (1.2 MJ m^{-3}).

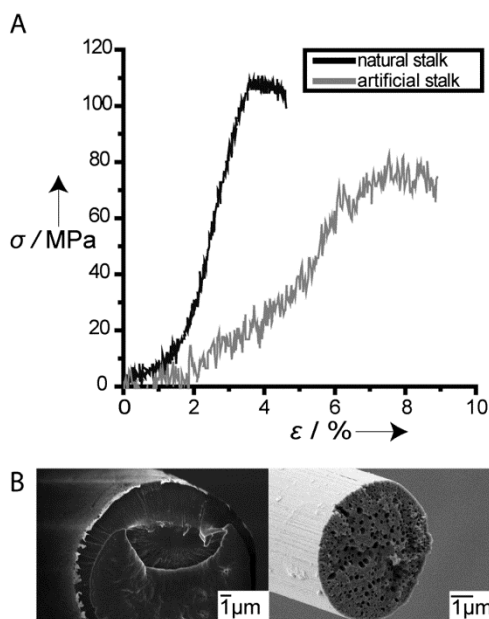


Figure 5. A) Stress–strain curves of the best-performing natural and artificial stalks measured at 30% relative humidity. Differences in noise level are due to smaller stalk diameters in the case of artificial stalks. B) SEM images of cross-sections of a natural stalk (left) and an artificial stalk (right).

The designed and recombinantly produced lacewing egg stalk protein could be processed into artificial stalks with similar properties in relation to natural stalks at 30% RH. The stalks show bending properties that are very similar to the natural stalks, which may open applications for protein fibers, where rigidity in the transversal direction is of interest. Furthermore, the recombinant approach allows the molecular structure–function relationship in egg stalk proteins to be better understood. It

will therefore be of importance to identify poly(alanine)-containing eggstalk proteins and to obtain aqueous spinning dopes, which will be necessary to obtain initial structure formation. A pre-structured dope solution will be the key to obtain fibers with cross β structures.

Experimental Section

All of the gene modules (N, [AS], and C) were designed with a 5'-*Bam*HI and a 3'-*Hind*III restriction site and obtained from Geneart. Modules were cloned using the enzymes *Bsa*I, *Bsg*I, and *Bse*RI followed by ligation.^[12] The complete N[AS]₈C construct was transferred to a pET28 vector using *Bam*HI and *Hind*III.

BL21 (DE3) cells were transformed with pET28 N[AS]₈C and grown in a fermenter (Infors Minifors 2.5 L) using a procedure described previously.^[23] At an OD₆₀₀ of 72, the bacteria were induced with 1 mM isopropyl β -D-thiogalactopyranoside (IPTG) for 3 h. Cells were harvested and washed three times.

Purification was performed following a procedure described for other recombinant silk proteins.^[24] After cell lysis, acidification, and centrifugation, the supernatant was fractionally precipitated using ammonium sulfate (1.5 M and 2.5 M). The precipitated protein was washed with water and lyophilized.

To analyze the produced protein, N[AS]₈C (3 mg mL^{-1}) was dissolved in 6 M guanidinium thiocyanate and diluted to a final concentration of 2 M guanidinium thiocyanate. Before spotting, samples were desalted by ZipTip C4 pipette tips and eluted by matrix solution. MALDI-TOF mass spectrometry was performed on a Bruker Reflex III equipped with a 337 nm N₂ laser in the linear mode and a 20 kV acceleration voltage. Sinapinic acid (20 mg mL^{-1}) was used as the matrix in 50% CH₃CN and 0.1% trifluoroacetic acid in H₂O.

The stalks were pulled out of a droplet of N[AS]₈C (10% w/v) in HFA and dried at room temperature. Afterwards, tension was removed from the stalk by moving the contact points closer, and the samples were placed overnight in a climate chamber at 60 °C and 70% RH.

For scanning electron microscopy, samples were sputter-coated with platinum (thickness 2 nm). SEM images were obtained with a Zeiss 1530 using the inlens detector.

FTIR spectroscopy was performed using a Bruker tensor 27/pike MIRacle using a Hyperion unit. Data processing and Fourier self-deconvolution of the amide I region was performed using the Opus 6.5 software.^[17] Polarized FTIR measurements and processing of the data was done according to Hagenau et al.^[25]

Microscope images were obtained using a Leica DMI 3000B microscope equipped with polarizers.

Samples for tensile testing were glued with plastic glue onto plastic frames having a gauge length of 2 mm. Stress–strain curves

were recorded on a tensile tester (Bose Electroforce 3220) equipped with a 0.5N load cell using a climate chamber to adjust the relative humidity. The stalks were extended with a rate of 0.01 mm s⁻¹ until they ruptured.

Circular dichroism spectra were recorded from 250 nm to 195 nm using a Jasco J-815 CD spectrometer measuring with an interval of 0.1 nm, a bandwidth of 1 nm, a scanning speed of 50 nm min⁻¹, a digital integration time (D.I.T.) of 1 s, and three accumulations.

Received: January 20, 2012

Revised: April 10, 2012

Published online: May 16, 2012

Keywords: β sheets · biomimetic systems · fiber proteins · lacewing · silk

- [1] J. G. Hardy, T. R. Scheibel, *Prog. Polym. Sci.* **2010**, *35*, 1093–1115.
- [2] A. Leal-Egana, T. Scheibel, *Biotechnol. Appl. Biochem.* **2010**, *55*, 155–167.
- [3] A. Lammel, M. Schwab, M. Hofer, G. Winter, T. Scheibel, *Biomaterials* **2011**, *32*, 2233–2240.
- [4] C. Allmeling, A. Jokuszies, K. Reimers, S. Kall, C. Y. Choi, G. Brandes, C. Kasper, T. Scheper, M. Guggenheim, P. M. Vogt, *Cell Proliferation* **2008**, *41*, 408–420.
- [5] C. Allmeling, A. Jokuszies, K. Reimers, S. Kall, P. M. Vogt, *J. Cell. Mol. Med.* **2006**, *10*, 770–777.
- [6] K. Spiess, A. Lammel, T. Scheibel, *Macromol. Biosci.* **2010**, *10*, 998–1007.
- [7] S. Weisman, V. S. Haritos, J. S. Church, M. G. Huson, S. T. Mudie, A. J. Rodgers, G. J. Dumsday, T. D. Sutherland, *Biomaterials* **2010**, *31*, 2695–2700.
- [8] J. G. Hardy, L. M. Romer, T. R. Scheibel, *Polymer* **2008**, *49*, 4309–4327.
- [9] K. D. Parker, K. M. Rudall, *Nature* **1957**, *179*, 905–906.
- [10] C. L. Craig, *Annu. Rev. Entomol.* **1997**, *42*, 231–267.
- [11] S. Weisman, S. Okada, S. T. Mudie, M. G. Huson, H. E. Trueman, A. Sriskantha, V. S. Haritos, T. D. Sutherland, *J. Struct. Biol.* **2009**, *168*, 467–475.
- [12] D. Huemmerich, C. W. Helsen, S. Quedzuweit, J. Oschmann, R. Rudolph, T. Scheibel, *Biochemistry* **2004**, *43*, 13604–13612.
- [13] C. Vendrely, T. Scheibel, *Macromol. Biosci.* **2007**, *7*, 401–409.
- [14] J. M. Yao, H. Masuda, C. H. Zhao, T. Asakura, *Macromolecules* **2002**, *35*, 6–9.
- [15] H. Peng, S. Zhou, J. Jiang, T. Guo, X. Zheng, X. Yu, *J. Phys. Chem. B* **2009**, *113*, 4636–4641.
- [16] X. Zhang, M. R. Reagan, D. L. Kaplan, *Adv. Drug Delivery Rev.* **2009**, *61*, 988–1006.
- [17] X. Hu, D. Kaplan, P. Cebe, *Macromolecules* **2006**, *39*, 6161–6170.
- [18] W. H. Moore, S. Krimm, *Biopolymers* **1976**, *15*, 2465–2483.
- [19] A. Schäfer, T. Vehoff, A. Glisovic, T. Salditt, *Eur. Biophys. J. Biophys. Lett.* **2008**, *37*, 197–204.
- [20] T. Vehoff, A. Glisovic, H. Schollmeyer, A. Zippelius, T. Salditt, *Biophys. J.* **2007**, *93*, 4425–4432.
- [21] G. R. Plaza, G. V. Guinea, J. Perez-Rigueiro, M. Elices, *J. Polym. Sci. Part B* **2006**, *44*, 994–999.
- [22] H. R. Hepburn, H. D. Chandler, M. R. Davidoff, *Insect Biochem.* **1979**, *9*, 69–77.
- [23] D. J. Korz, U. Rinas, K. Hellmuth, E. A. Sanders, W. D. Deckwer, *J. Biotechnol.* **1995**, *39*, 59–65.
- [24] X.-X. Xia, Z.-G. Qian, C. S. Ki, Y. H. Park, D. L. Kaplan, S. Y. Lee, *Proc. Natl. Acad. Sci. USA* **2010**, *107*, 14059–14063.
- [25] A. Hagenau, P. Papadopoulos, F. Kremer, T. Scheibel, *J. Struct. Biol.* **2011**, *175*, 339–347.



Supporting Information

© Wiley-VCH 2012

69451 Weinheim, Germany

Artificial Egg Stalks Made of a Recombinantly Produced Lacewing Silk Protein**

*Felix Bauer and Thomas Scheibel**

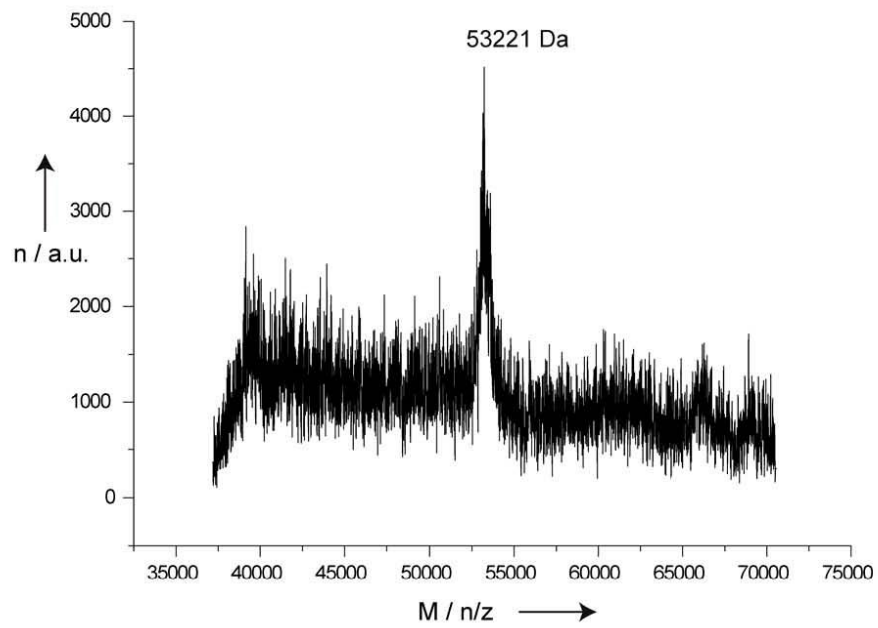
ange_201200591_sm_miscellaneous_information.pdf

Supporting Information

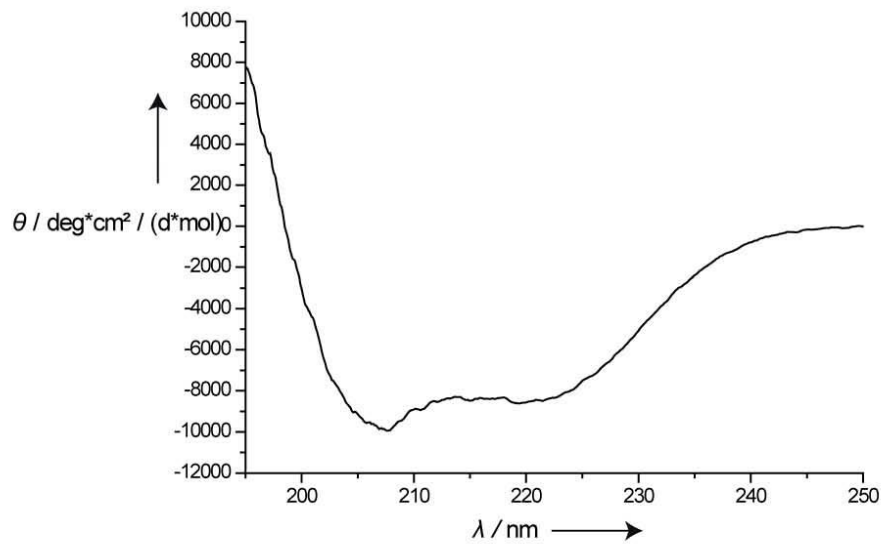
| Position | Original sequence of the repetitive part of MALXB2 | Consensus sequence | % of most frequently used amino acid | AS module |
|----------|--|--------------------|--------------------------------------|-----------|
| 1 | G G G G G G G G G G | G | 100 | G |
| 2 | S S S S S S S S S S | S | 100 | S |
| 3 | A A A S S A A A A A | A | 80 | A |
| 4 | G G G S S G G G G G | G | 80 | G |
| 5 | A A A A A A A A A A | A | 100 | A |
| 6 | S S S S S S S S S S | S | 100 | S |
| 7 | S S S S S S S S S S | S | 100 | S |
| 8 | N N Q N N N N N D G | N | 70 | N |
| 9 | G G G G G G G G G G | G | 100 | G |
| 10 | S S S S S S S S S S | S | 100 | S |
| 11 | V S S S S S S S S T | S | 80 | S |
| 12 | A A A A A A A A A A | A | 100 | A |
| 13 | G S S G T T T T S A | T | 40 | T |
| 14 | A A A A A A A A A A | A | 100 | A |
| 15 | S T T S S T T S S S | S | 60 | S |
| 16 | K K K K K K K K K K | K | 100 | K |
| 17 | G G G D G G G G G G | G | 89 | G |
| 18 | A S S G S S S S S S | S | 78 | S |
| 19 | A A A A A A A A A A | A | 100 | A |
| 20 | G G G G G G G G G G | G | 100 | G |
| 21 | A A A A A A A A A A | A | 100 | A |
| 22 | S S T A T T T T T T | T | 67 | T |
| 23 | S S S S S S S S S S | S | 100 | S |
| 24 | N G N N N N N N N N | N | 89 | N |
| 25 | G N G G G G G G G G | G | 89 | G |
| 26 | S S S S S S S S S S | S | 100 | S |
| 27 | S T S T S S S S S S | S | 78 | T |
| 28 | A A A A A A A A A A | A | 100 | A |
| 29 | S V V V V V V V V V | V | 89 | V |
| 30 | A A A A A A A A A A | A | 100 | A |
| 31 | S S S S S S S S S S | S | 100 | S |
| 32 | K K K K K K K K K K | K | 100 | K |
| 33 | G G G G G G G G G G | G | 100 | G |
| 34 | S S S S S S S S S S | S | 100 | S |
| 35 | A A A A A A A A A A | A | 100 | A |
| 36 | S G G G G G G G G G | G | 90 | G |
| 37 | G A A A A A A A A A | A | 90 | A |
| 38 | S S S S A S S S S S | S | 90 | S |
| 39 | S S S S S S S S S S | S | 100 | S |
| 40 | G G N G G G G G G G | G | 90 | G |
| 41 | G S G N N N N N N N | N | 70 | N |
| 42 | S S S S S S S S S S | S | 100 | S |
| 43 | S T S T T T T T T T | T | 80 | T |
| 44 | A A A A A A A A A A | A | 100 | A |
| 45 | S T S S S S S S S S | S | 90 | S |
| 46 | A A A A A A A A A A | A | 100 | A |
| 47 | S S S T T S S S S S | S | 80 | T |
| 48 | K K K K K K K K K K | K | 100 | K |

Supplementary Figure 1: Sequence of the repetitive part of MalXB2. Shown are as well the consensus sequence (with the frequencies of the most abundant amino acids) and the designed [AS] module. Blue highlighted areas comprise the amino acids predicted to form turns.

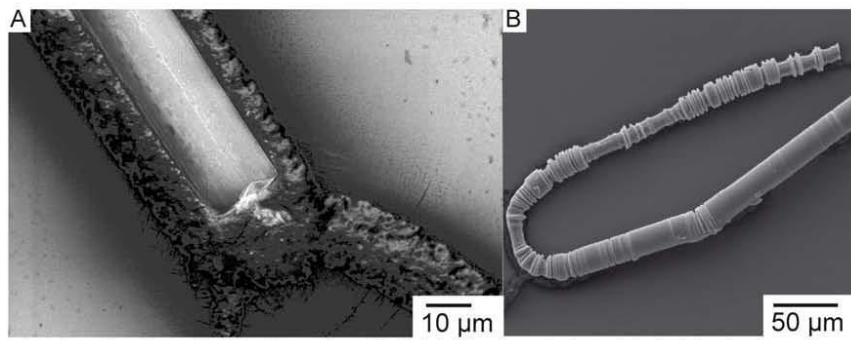




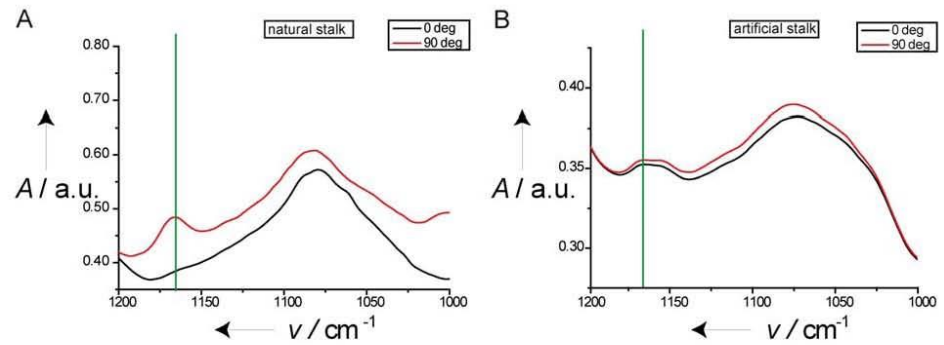
Supplementary Figure 2: MALDI-TOF spectrum of N[AS]₉C.



Supplementary Figure 3: CD spectrum of N[AS]₉C solubilised in HFA.



Supplementary Figure 4: SEM pictures of an artificial stalk (A) and a natural egg stalk, the later showing necking due to mechanical stress (B).



Supplementary Figure 5: Polarised FTIR spectra of natural and artificial stalks. A) natural stalk; B) artificial stalk; green line: 1167 cm⁻¹ (poly(L-Alanine) NCα stretching vibration).

9. Controllable cell adhesion, growth and orientation on layered silk protein films

Biomaterials
Science

RSCPublishing

PAPER

Controllable cell adhesion, growth and orientation on layered silk protein films†

Cite this: *Biomater. Sci.*, 2013, **1**, 1244

Felix Bauer,‡ Stefanie Wohlrab‡ and Thomas Scheibel*

Received 2nd May 2013,
Accepted 9th July 2013
DOI: 10.1039/c3bm60114e

www.rsc.org/biomaterialsscience

Due to their mechanical stability, biocompatibility and biodegradability, silks are promising materials for various biomedical applications including tissue engineering. Since the shape and the organisation of cells in and on scaffolds both affect their function, we tested patterned silk scaffolds made of three different silk proteins concerning their influence on cell adhesion, growth and orientation. Two different cell lines, BALB/3T3 fibroblasts and C2C12 myoblasts, showed controllable cell adhesion as well as orientation dependent on the silk proteins used and patterns made. Surprisingly, the presence of the integrin binding motif RGD did not influence cell adhesion and orientation on structured silk films, although it did so significantly on flat films.

Introduction

Silks are protein-based fibres produced by various arthropods including spiders and insects. They are well known for their mechanical stability, biocompatibility and biodegradability, which allow their use in biomedical applications.¹ In contrast to obtaining silk proteins from natural sources, recombinantly produced silk proteins have the advantages of a defined composition, constantly high purity, and quality.² Further, recombinant silk proteins can be processed into different morphologies such as fibres, nonwoven-meshes, capsules, particles, hydrogels, foams, and films.^{3,4}

Previously it has been shown that BALB/3T3 fibroblast adhesion is weak on flat eADF4(C16) (a recombinantly produced engineered spider silk protein) films,⁵ based on the lack of specific motifs for cell attachment in the protein's primary structure. Introduction of such motifs can improve cell adhesion on flat silk films.^{6–9} eADF4(C16) modified with the integrin binding motif RGD yielded significantly improved cell adhesion and proliferation.⁸

In tissue engineering it is further essential to restore the tissue structure and organisation. In most organs the cells and the extracellular matrix (ECM) are aligned, being essential for their cellular function and mechanical properties.^{10–12}

The surface topography of a substrate is known to influence the adhesion and polarisation of cells. In order to align

different cell types, various scaffolds are currently in use, such as contact guidance materials like micro-/nanogrooved scaffolds or fiber mesh matrices made of polymeric fibers.^{13–17} Most promising for tissue engineering applications are adhesive micro patterns produced by micro contact printing or other photolithographic methods. Parallel grooves for example promote topographical anchorage and orientation of the cells, which is important e.g. for bone implants, skin transplants, or artificial nerve tubes.^{13,14,16} Patterned structures allow to align different cell types such as osteoblasts, cardiac cells, muscle cells, corneal epithelial cells, and fibroblasts.^{10,18–20}

Here, we used structured films made of two different silk proteins (Fig. 1) to test the influence of chosen proteins and morphology on BALB/3T3 fibroblasts. As a second model, mouse myoblast cells from muscle were tested, which fuse to myotubes at high cell densities and need alignment to generate strength and tension.^{20,21}

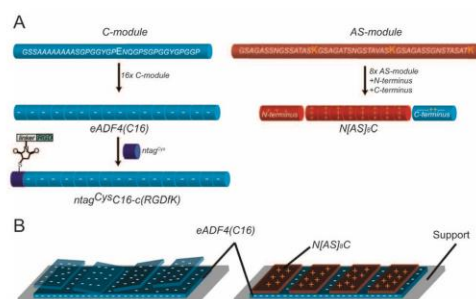


Fig. 1 Schematic diagram of eADF4(C16), ntag^{Cys}C16-c(RGDFK), and N[AS]₂C (A) and of films cast from proteins with identical and opposite charges (B).

Lehrstuhl Biomaterialien, Universität Bayreuth, Universitätsstraße 30,
95440 Bayreuth, Germany. E-mail: Thomas.scheibel@uni-bayreuth.de;
Fax: +49 921 557346; Tel: +49 921 557361

† Electronic supplementary information (ESI) available. See DOI: 10.1039/c3bm60114e

‡ These authors contributed equally to this work.

Materials and methods

Protein production

The spider silk protein eADF4(C16) was produced and purified as described by Huemmerich *et al.*²⁶ Chemical coupling of synthesized cyclic RGD to ntag^{Cys}C16-c(RGDfK) was performed as described previously.⁸ The production of the recombinant lacewing egg stalk protein N[AS]₈C was described by Bauer and Scheibel.²⁷

Coupling of NHS-fluorescein to N[AS]₈C

1 mg of lyophilised N[AS]₈C was dissolved in 6 M GdmSCN and dialysed against 20 mM HEPES (pH 7). For coupling, a 5-fold molar excess of NHS-fluorescein was added to the protein solution. After two hours of incubation at room temperature N[AS]₈C was precipitated with ammonium sulphate, subsequently washed with distilled water, and lyophilised.

Production of films

For production of unstructured films as well as for the ground layer films, lyophilised proteins were dissolved in formic acid and cast onto glass slides (1% (w/v), 0.15 mg cm⁻²) followed by evaporation of the solvent. Since spider silk films made from formic acid are water-insoluble, no post-treatment was necessary.²⁴

To prove the water stability of films made of the recombinant lacewing egg stalk protein, 1% (w/v) N[AS]₈C was dissolved in formic acid and cast into a 48 well plate. After drying, the films were incubated in water for 24 hours. Afterwards, wells with films and blank wells were stained with Coomassie Brilliant Blue, and the presence of films was inspected visually.

Production of patterned two protein films

The patterns were made using photolithographically produced templates to generate PDMS (polydimethylsiloxane) negatives. First, silicon wafers were spin coated with a photoresist resulting in a 25 μm thick layer. After curing, the wafer was exposed with the desired mask and subsequently treated with gamma-(4-fluorophenyl)-gamma-butyrolactone to remove the photoresist from the undesired areas. As a result, grooves with a width

of 50 μm and ridges with a width of 20 μm with a height difference of 25 μm were retained (Fig. 2A).

Then, polydimethylsiloxane (PDMS) moulds were created by using a 10 : 1 mixture of PDMS prepolymer and curing agent. The mixture was degassed for 20 minutes and afterwards poured onto the wafer. The moulds were cured for 90 minutes at 80 °C, peeled from the wafer, and cut into pieces (Fig. 2B).

A protein ground layer was cast on a glass slide (see Production of films). To deposit a protein stripe (ridge), the PDMS moulds were placed with their structured side downwards on the ground layer films (Fig. 2C and D). A droplet of a 1% (w/v) solution of the second protein in formic acid was deposited at the open side of the channels (the ground layer remains stable as seen when using the same protein as the ground layer and the ridges of the latter peel off (ESI Fig. 1†)). Based on capillary forces the channels were filled with the protein solution (Fig. 2E). After drying, the mould was gently removed (Fig. 2F) and the films were investigated microscopically.

Cell culture experiments

For cell culture experiments BALB/3T3 mouse fibroblasts and C2C12 mouse myoblasts (European Collection of Cell Cultures) were cultured in DMEM media (Biochrom, Berlin, Germany) supplemented with 10% foetal bovine serum (Biochrom, Berlin, Germany), 1% (v/v) GlutaMAX (Gibco, Grand Island, USA), and 0.1% (v/v) gentamicin sulphate (Sigma-Aldrich, Seelze, Germany). An incubator was used to control the atmosphere (5% CO₂, 95% humidity) to maintain the cells.

The glass slides containing the protein films were placed in six well plates, and 5000 cells per cm² were seeded per film. The medium was changed once a day. Cells were cultured for up to 96 hours.

Calcein-AM staining

BALB/3T3 fibroblasts were stained with 2 mM calcein acetoxy-methyl ester (calcein A/M) (Invitrogen, Eugene, Oregon, USA). Live cells were analyzed with a LeicaDMI3000 B fluorescence microscope after 15 min of incubation at 37 °C (Leica, Wetzlar, Germany).

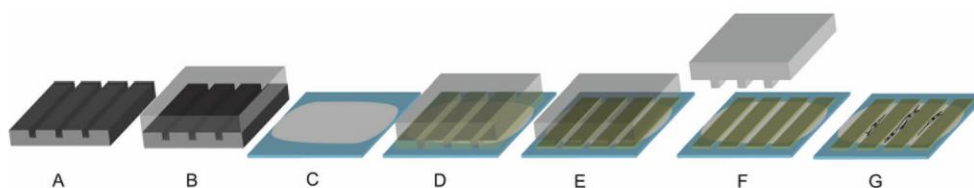


Fig. 2 Production of patterned films (the ridges have a width of 50 μm and a height of less than 1 μm, whereas the grooves (*i.e.* spacing between the ridges) have a width of 20 μm): A: a silicon wafer was used as a template to process a PDMS stamp (B); C: a film was cast on a glass slide to form a ground layer; D: a PDMS stamp was placed on the ground layer protein film; E: a protein solution with a second protein was soaked into the channels of the PDMS stamp by capillary forces; F: after drying, the PDMS stamp was removed, leaving ridges of the second protein; G: cells preferentially adhere and align on the ground layer but not on the ridges.

Microscopy

To confirm the existence of the protein ridges and to measure the height of the ridges, fluorescein was coupled to N[AS]₈C prior to inflating the mould. Subsequently, the films were observed in a confocal laser scanning microscope (DMI 6000 CS Leica).

Cell growth and alignment were observed with a Leica DMI 3000B microscope equipped with a camera. Images were made with and without cells at 48 h and at 96 h after fibroblast seeding.

Picture analysis

To analyse the preferences of the cells to bind to different regions of the protein films, all adhered cells were marked in Powerpoint software by a line across the longest axis of the spread cells symbolising their orientation (e.g. 267 fibroblasts were present on the surface, 218 were spread and marked with a line, ESI Fig. 3†). Afterwards, spread cells were counted on each protein type and the percentage of cells on the bottom layer was calculated.

The orientation of the marked cells was measured using ImageJ software. The angle of the cells was measured relative to the groove direction of the film and plotted in 5° steps. The distribution and orientation of the cells were calculated from a minimum of three pictures.

Results and discussion

Employed proteins

To produce stable silk films with distinct topographies, proteins were chosen with different net charges (Fig. 1). N[AS]₈C, an engineered protein based on the lacewing egg stalk protein MalXB2, was used as a polycationic silk protein and the spider silk protein eADF4(C16) with or without an RGD-modification as a polyanionic silk protein.^{5,8}

Production of flat silk surfaces

The preparation of silk films with a flat surface is straightforward and has been shown previously.²² Here, formic acid was chosen as a solvent for the proteins.^{23–25} Previously, it was shown that eADF4(C16) films made from formic acid solutions are water-insoluble due to a high β-sheet content enabling direct use in cell culture without further post treatment.²⁴ The water stability of N[AS]₈C films made from formic acid solution was confirmed by Coomassie staining of the films after intensive washing with water (data not shown).

Fibroblast and myoblast adhesion on flat silk surfaces

BALB/3T3 mouse fibroblasts were seeded on eADF4(C16), ntag^{Cys}C16-c(RGDfK), a variant of eADF4(C16) with a chemically coupled, cyclic RGD-peptide,⁸ and N[AS]₈C films respectively.

As shown previously, BALB/3T3 fibroblasts adhered weakly on flat eADF4(C16) films, resulting in clustering of the cells

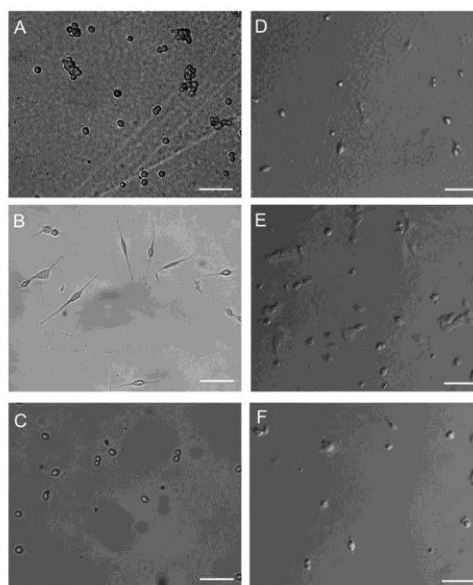


Fig. 3 A–C: BALB/3T3 mouse fibroblasts cultured on films made of eADF4(C16) (A), ntag^{Cys}C16-c(RGDfK) (B) or N[AS]₈C (C) with a cell seeding density of 5000 cells per cm² after 24 hours of incubation. D–F: C2C12 myoblasts cultured on films made of eADF4(C16) (D), ntag^{Cys}C16-c(RGDfK) (E) or N[AS]₈C (F) with a cell seeding density of 5000 cells per cm² after 24 hours of incubation. Scale bars: 100 μm.

(Fig. 3A),^{5,8} based on the low surface roughness and the lack of adhesion motifs in the primary structure of eADF4(C16).

Good adhesion of BALB/3T3 fibroblasts was achieved on flat films of RGD-modified eADF4(C16). On such ntag^{Cys}C16-c(RGDfK) films, BALB/3T3 fibroblasts showed a spread morphology (Fig. 3B), and the proliferation rate and doubling time were similar to those of the positive control (treated cell culture plates).⁸

Films made of the recombinant lacewing egg stalk protein N[AS]₈C showed a low surface roughness similar to films made of eADF4(C16), and fibroblast adhesion was very low on such films (Fig. 3C).

Concomitantly, C2C12 myoblasts showed a similar behaviour on all three film types (Fig. 3D–F). On eADF4(C16) films as well as on N[AS]₈C films, myoblasts revealed a spherical morphology and adhered weakly to the surface (Fig. 3D and F). The modification of eADF4(C16) with an RGD peptide resulted in spread morphology with improved cell adhesion (Fig. 3E).

Production of patterned films

To promote cell alignment on our silk film surfaces, patterned two-layer films made of various combinations of eADF4(C16), N[AS]₈C, and ntag^{Cys}C16-c(RGDfK) were processed.

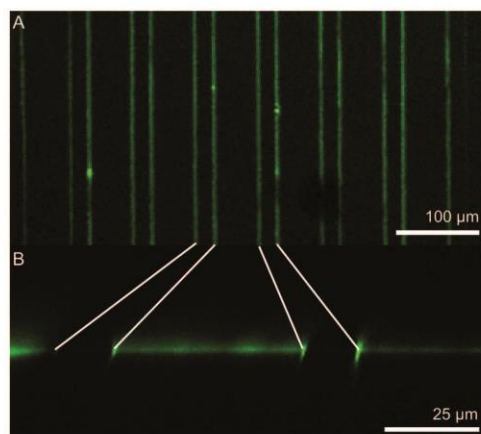


Fig. 4 Fluorescence microscopic images of a patterned film with fluorescein-coupled N[AS]₈C protein as ridges (A: top view; B: side view). The gaps between ridges are clearly visible in B.

The width between the ridges was adjusted to 20 μm, since widths between 10 μm and 20 μm were previously shown to be suitable for cell alignment, and the ridges had a width of 50 μm.¹⁵

In order to visualise the film patterns, N[AS]₈C was chemically labelled with fluorescein before film formation. Confocal laser scanning microscopy (CLSM) of structured films with the labelled protein revealed a precise alignment of the two protein layers (Fig. 4A) and a thickness of the N[AS]₈C layer (*i.e.* the height of the ridges) of less than one micron (Fig. 4B).

First a ground layer was made of ntag^{Cys}C16-c(RGDfK) with good cell adhesion properties, and ridges were processed thereon using N[AS]₈C with low adhesion properties. Next, films with eADF4(C16) as the ground layer and N[AS]₈C as ridges were produced (Fig. 1B).

Fibroblast growth on patterned films

Single protein films. BALB/3T3 fibroblasts were grown on patterned films made of eADF4(C16) (in ground and ridge layers) to confirm the influence of the structure on the adhesion and alignment of cells.

Cell adhesion was improved compared to unstructured films due to the rough edges of the structures. The orientation of the cells was measured after 48 hours and revealed a good alignment with the film structures (Fig. 5A). Cells adhered everywhere but with 63.2% of the cells in the grooves (Table 1).

Cell adhesion on N[AS]₈C films could not be quantified, since only a few cells adhered and were oriented with the axis of the ridges.

ntag^{Cys}C16-c(RGDfK) structured films showed no improved adhesion in comparison to unstructured ones due to the already high level of adhesion on the flat films.

Unfortunately, structured films made of one protein by this technique are highly unstable due to the identical charge of the proteins in both layers, and, therefore, the ridges peel off easily (ESI Fig. 1†).

Two protein films. Generating stable films was possible using two proteins with opposite charges. We used RGD modified silk (ntag^{Cys}C16-c(RGDfK)) promoting fibroblast attachment as a ground layer and positively charged N[AS]₈C prohibiting efficient fibroblast attachment for making the ridges (Fig. 5B).

On such films, 85.5% of the fibroblasts adhered on the ground layer (94.2% when standardised per area due to the

Table 1 Distribution of fibroblasts on patterned films, consisting of two independent proteins. Most cells spread within the grooves. The first protein reflects the ground layer and the second the ridge material.

| | ntag ^{Cys} C16-c (RGDfK)/N[AS] ₈ C | eADF4 (C16)/N [AS] ₈ C | eADF4 (C16)/ eADF4(C16) |
|--|--|-----------------------------------|-------------------------|
| Cells in the grooves | 85.5% | 78.8% | 63.2% |
| Cells standardised per area in the grooves | 94.2% | 91.5% | 85.3% |

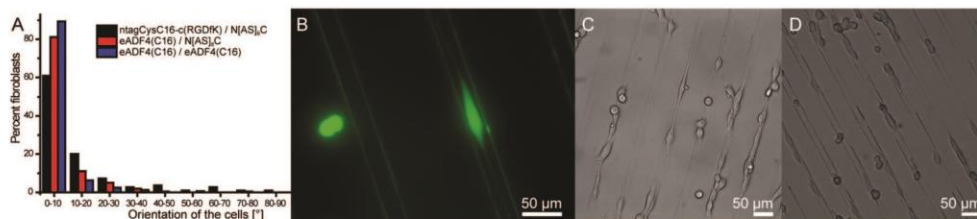


Fig. 5 BALB/3T3 fibroblasts grown on structured films. A: orientation of fibroblasts grown on patterned films made of different protein combinations (ground layer protein/ridge protein) as depicted by the colour code after 48 hours of incubation; B: fluorescence microscopy of calcein AM stained cells, grown on a film with ntag^{Cys}C16-c(RGDfK) as the ground layer and N[AS]₈C as ridges; C and D: light microscopic image after 48 hours of incubation using ntag^{Cys}C16-c(RGDfK) as the ground layer with N[AS]₈C as ridges (C) and eADF4(C16) as the ground layer with N[AS]₈C as ridges (D).

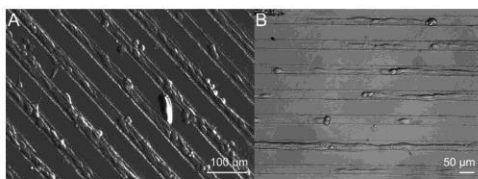


Fig. 6 A: BALB/3T3 fibroblasts grown on structured films using eADF4(C16) as the ground layer and N[AS]₈C as ridges after 96 hours of incubation; B: C2C12 myoblasts grown on eADF4(C16)/N[AS]₈C films after 48 hours of incubation.

2.5 times larger area of the top layer), and most of the cells aligned along the axis of the ridges (Table 1, Fig. 5A, 5C and ESI Fig. 2†). Even the few cells adhering to the N[AS]₈C ridges were mostly aligned.

Surprisingly, control experiments using eADF4(C16) instead of ntag^{Cys}C16-c(RGDfK) as the ground layer revealed similar results (Fig. 5D), with much higher cell adhesion numbers than for eADF4(C16)/eADF4(C16) films. The fibroblasts mostly grew on the eADF4(C16) area (78.8% of the fibroblasts (91.5% calculated per area)) and not on the N[AS]₈C ridges (Table 1). Cell alignment was pronounced as well (Fig. 5A) accentuating the importance of substrate morphology for cell attachment. The adhesion of fibroblasts on eADF4(C16) films is much better on structured films than on flat ones (Fig. 3A), probably due to the microstructure at the interface of the two layers, which results from drying effects. In contrast, N[AS]₈C seems to be a good ridge material as it is not a good substrate for cells, and, therefore, it directs cell adhesion to the desired ground layer areas. Images after 96 hours showed that cells proliferated well on the films and stayed on the ground protein layer as desired (Fig. 6A).

In summary, structures are important for orientation of cells even if they are less than 1 μm in height (Fig. 4B).

Myoblast growth on patterned films

C2C12 myoblasts grown on patterned films made of ntag^{Cys}C16-c(RGDfK)/N[AS]₈C and eADF4(C16)/N[AS]₈C behaved similar to fibroblasts (Fig. 6B). C2C12 myoblasts mostly grew on the spider silk ground layers and not on the N[AS]₈C ridges.

It was impossible to calculate the cell angle and distribution due to the high cell density after 48 hours and the formation of myotubes.

The formation of myotubes in an aligned manner, however, is an important step towards skeletal muscle regeneration.

Conclusion

The beneficial influence of patterned scaffolds on fibroblast and myoblast adhesion and alignment was shown by our experiments with patterned films using one single protein. Fibroblasts as well as myoblasts adhere and proliferate much

better on structured than on unstructured films made of the same protein. A width of 20 μm between ridges with a height of 1 μm is suitable to induce fibroblast as well as myoblast alignment in parallel to the grooved pattern (Fig. 5 and 6). On patterned eADF4(C16) films, fibroblasts grew on the ridges and in the grooves with slight preferences for the grooves. The deposition of N[AS]₈C as stripe protein (ridges) with low fibroblast and myoblast adhesion properties increased cell binding in the grooves. Surprisingly, ntag^{Cys}C16-c(RGDfK) as the ground layer did not result in a significantly better cell binding compared to an eADF4(C16) ground layer. The unspecific cell adhesion, induced by surface roughness and structure, leads to strong cell adhesion in the case of the polyanionic spider silk proteins, but not in the case of the polycationic egg stalk silk protein. Surprisingly, in this context the specific interaction of the cells with RGD did not show significant benefits for patterned spider silk films.

In the future, our results will have an impact on patterning of silk coatings *e.g.* for bone grafts, muscle cell cultures, or nerve guidance/regeneration.^{13,14}

Acknowledgements

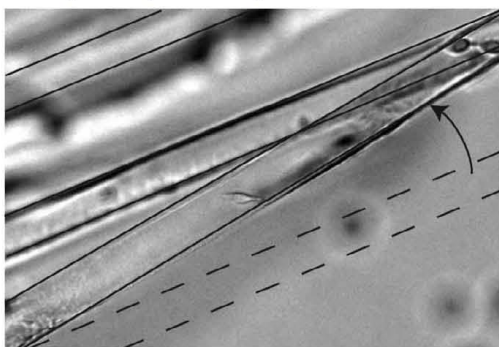
The authors thank Aniela Heidebrecht for the CLSM images, Martin Trebbin for the silicon wafer template and Martin Humenik for critically reading the manuscript. This work was supported by the DFG SCHE603/4 and the Bavarian State Ministry of the Environment and Public Health (U8793-2012/6-2).

Notes and references

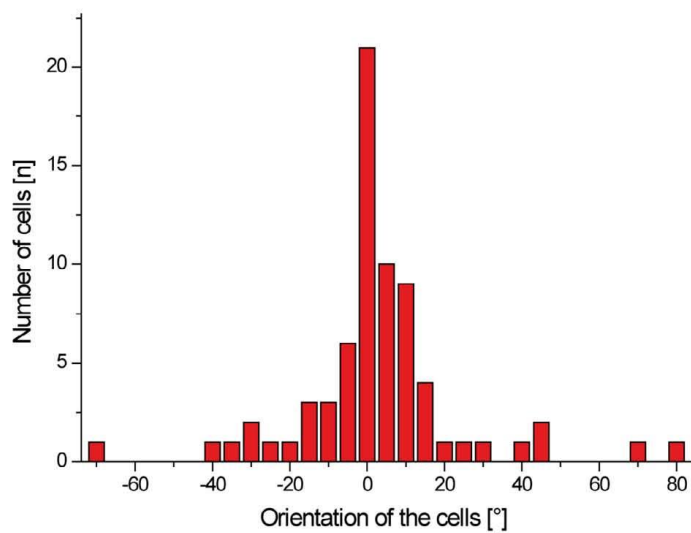
- 1 M. Heim, L. Romer and T. Scheibel, *Chem. Soc. Rev.*, 2010, **39**, 156–164.
- 2 A. Heidebrecht and T. Scheibel, *Adv. Appl. Microbiol.*, 2013, **82**, 115–153.
- 3 J. G. Hardy, L. M. Romer and T. R. Scheibel, *Polymer*, 2008, **49**, 4309–4327.
- 4 J. G. Hardy and T. R. Scheibel, *J. Polym. Sci., Polym. Chem.*, 2009, **47**, 3957–3963.
- 5 A. Leal-Egana, G. Lang, C. Mauerer, J. Wickinghoff, M. Weber, S. Geimer and T. Scheibel, *Adv. Eng. Mater.*, 2012, **14**, B67–B75.
- 6 E. S. Gil, B. B. Mandal, S. H. Park, J. K. Marchant, F. G. Omenetto and D. L. Kaplan, *Biomaterials*, 2010, **31**, 8953–8963.
- 7 E. Bini, C. W. Foo, J. Huang, V. Karageorgiou, B. Kitchel and D. L. Kaplan, *Biomacromolecules*, 2006, **7**, 3139–3145.
- 8 S. Wohlrab, S. Muller, A. Schmidt, S. Neubauer, H. Kessler, A. Leal-Egana and T. Scheibel, *Biomaterials*, 2012, **33**, 6650–6659.
- 9 A. Leal-Egana and T. Scheibel, *J. Mater. Chem.*, 2012, **22**, 14330–14336.

- 10 E. S. Gil, S. H. Park, J. Marchant, F. Omenetto and D. L. Kaplan, *Macromol. Biosci.*, 2010, **10**, 664–673.
- 11 J. Torbet, M. Malbouyres, N. Builles, V. Justin, M. Roulet, O. Damour, A. Oldberg, F. Ruggiero and D. J. Hulmes, *Biomaterials*, 2007, **28**, 4268–4276.
- 12 B. D. Lawrence, J. K. Marchant, M. A. Pindrus, F. G. Omenetto and D. L. Kaplan, *Biomaterials*, 2009, **30**, 1299–1308.
- 13 D. Yucel, G. T. Kose and V. Hasirci, *Biomacromolecules*, 2010, **11**, 3584–3591.
- 14 D. Yucel, G. T. Kose and V. Hasirci, *Biomaterials*, 2010, **31**, 1596–1603.
- 15 J. L. Charest, A. J. Garcia and W. P. King, *Biomaterials*, 2007, **28**, 2202–2210.
- 16 J. T. Zhang, J. Q. Nie, M. Muhlstadt, H. Gallagher, O. Pullig and K. D. Jandt, *Adv. Funct. Mater.*, 2011, **21**, 4079–4087.
- 17 S. Fujita, M. Ohshima and H. Iwata, *J. R. Soc. Interface*, 2009, **6**(Suppl 3), S269–S277.
- 18 B. Zhu, Q. Lu, J. Yin, J. Hu and Z. Wang, *Tissue Eng.*, 2005, **11**, 825–834.
- 19 T. C. McDevitt, K. A. Woodhouse, S. D. Hauschka, C. E. Murry and P. S. Stayton, *J. Biomed. Mater. Res. A*, 2003, **66**, 586–595.
- 20 A. W. Feinberg, A. Feigel, S. S. Shevkoplyas, S. Sheehy, G. M. Whitesides and K. K. Parker, *Science*, 2007, **317**, 1366–1370.
- 21 H. Fujita, K. Shimizu and E. Nagamori, *Biotechnol. Bioeng.*, 2009, **103**, 1034–1041.
- 22 D. Huebnerich, U. Slotta and T. Scheibel, *Appl. Phys. A: Mater.*, 2006, **82**, 219–222.
- 23 K. Spiess, S. Wohlrab and T. Scheibel, *Soft Matter*, 2010, **6**, 4168–4174.
- 24 K. Spiess, R. Ene, C. D. Keenan, J. Senker, F. Kremer and T. Scheibel, *J. Mater. Chem.*, 2011, **21**, 13594–13604.
- 25 S. Wohlrab, K. Spiess and T. Scheibel, *J. Mater. Chem.*, 2012, **22**, 22050–22054.
- 26 D. Huebnerich, C. W. Helsen, S. Quedzuweit, J. Oschmann, R. Rudolph and T. Scheibel, *Biochemistry*, 2004, **43**, 13604–13612.
- 27 F. Bauer and T. Scheibel, *Angew. Chem., Int. Ed.*, 2012, **51**, 6521–6524.

Electronic Supplementary Material (ESI) for Biomaterials Science
This journal is © The Royal Society of Chemistry 2013

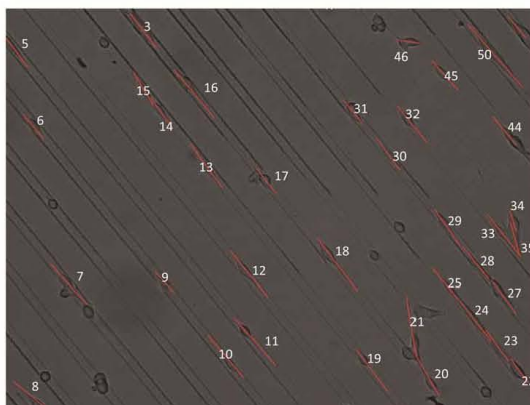


Supplemental Figure 1: Stripes easily peel off eADF4(C16)/eADF4(C16) structured films. The arrow is indicating the movement of the stripe.



Supplemental Figure 2: Distribution of the cell alignment of fibroblasts on a ntag^{C98}C16-c(RGDfK)/N[AS]₈C film.

Electronic Supplementary Material (ESI) for Biomaterials Science
This journal is © The Royal Society of Chemistry 2013



Supplemental Figure 3: Picture analysis of a eADF4(C16)/N[AS]₈C (ground layer protein/ ridge protein) patterned film to calculate the orientation and distribution of the cells. All adhered cells were marked along the longest axis of the spread cells indicative of their orientation.

10. List of publications and patents

Bauer, F., Bertinetti, L., Masic, A., and Scheibel, T.; Dependence of Mechanical Properties of Lacewing Egg Stalks on Relative Humidity. *Biomacromolecules* **2012**, 13 (11), 3730-3735.

Bauer, F. and Scheibel, T.; Artificial Egg Stalk Made of a Recombinantly Produced Lacewing Silk Protein. *Angewandte Chemie* **2012**, 51, 6521-6524.

Bauer, F., Wohlrab, S., and Scheibel, T.; Controllable cell adhesion, growth and orientation on layered silk protein films. *Biomaterials Science* **2013**, 1, 1244-1249.

Bauer, F. and Scheibel, T.; A novel biopolymer having excellent tensile strength, extensibility and toughness. International Patent PCT / EP12 15 1315.4; **2012** (submitted)

11. Acknowledgement

Danksagung

Diese Arbeit wurde von Juli 2008 bis Mai 2013 am Lehrstuhl Biomaterialien der Universität Bayreuth unter Betreuung von Prof. Dr. Thomas Scheibel durchgeführt. Ihm möchte ich ganz herzlich für die Möglichkeit danken, dieses spannende Thema mit vielen Freiheiten und Möglichkeiten zu bearbeiten.

Prof. Dr. Thomas Scheibel, Prof. Dr. –Ing. Volker Altstät und Dr. Stefan Geimer danke ich für die Übernahme meines Mentorats.

Für die Einweisung und Hilfen sowie Aufnahmen am REM und TEM danke ich Dr. Rainer Detsch, Johannes Diehl, Claudia Blüm, sowie Dr. Stefan Geimer und Kristin Schacht.

Admir Masic und Luca Bertinetti danke ich für die Zusammenarbeit bei der Publikation und die Messungen am Raman. Stefanie Wohlrab will ich für die gute Kooperation bei der Arbeit für unsere Veröffentlichung danken.

Prof. Louise Serpell und Kyle Morris gilt mein Dank für ihre Bemühungen mit der Aufnahme von Röntgenbeugungsspektren, auch wenn diese nicht den Weg in diese Dissertation gefunden haben.

Ute Kuhn danke ich für die TGA und DSC Messungen.

Annemarie Heiduk danke ich für die Unterstützung bei den Zugmessungen an Köcherfliegen-seide im Rahmen ihrer Projektarbeit.

Natürlich möchte ich mich auch bei meinen Kollegen bedanken:

- Susanne Schramm für ihre immer freundliche und aufmunternde Art.
- John für die Hilfestellungen in der Anfangszeit und die lustigen Abende nach dem Kondi-Training mit isotonischem Sportgetränk.
- Lukas, Martin, Andrew für das Korrekturlesen der Paper und Diskussionen und Tipps wenn mal Probleme auftraten.
- Klomaster Anderl für die Ausbildung als sein Padawan.
- Anderl und Johnobo für ihre Hilfe und Unterstützung beim Fermentieren.
- Den Stammkunden im BBB.

- Den Fußballern für die lustige Ablenkung auch in stressigen Zeiten.
- Den Kellerkindern.
- Bei meinen Bürokollegen David, Gregor, Kristina, Anja, Markus, Aniela, Elena und Claudia dafür, dass sie mich und meine Launen ertragen haben und wir immer eine lustige Zeit miteinander hatten.

Zu guter Letzt möchte ich meinen Eltern danken, dass sie mich über all die Zeit unterstützt haben und mit immer den Rücken frei gehalten haben.

12. Erklärung:

Hiermit erkläre ich eidesstattlich, dass ich die vorliegende Arbeit selbständig verfasst, und keine anderen als die angegebenen Quellen und Hilfsmittel benutzt habe.

Ferner erkläre ich, dass ich weder an der Universität Bayreuth noch anderweitig mit oder ohne Erfolg versucht habe, eine Dissertation einzureichen oder eine Doktorprüfung abzulegen. Des Weiteren erkläre ich, dass ich weder bisher noch in Zukunft Hilfe von gewerblichen Promotionsberatern bzw. -vermittlern in Anspruch genommen habe bzw. nehmen werde.

Bayreuth im Mai 2013

.....
Felix Bauer